FOSSIL

DOE/PC/79816-T3
(DE92011275)

AN INNOVATIVE CATALYST SYSTEM FOR SLURRY-PHASE FISCHER-TROPSCH SYNTHESIS: COBALT PLUS A WATER-GAS-SHIFT CATALYST

Final Technical Report

By
Charles N. Satterfield
Ian C. Yates
Claire Chanenchuk

July 1991

Work Performed Under Contract No. AC22-87PC79816

For
U.S. Department of Energy
Pittsburgh Energy Technology Center
Pittsburgh, Pennsylvania

By
Massachusetts Institute of Technology
Cambridge, Massachusetts

DISCLAIMER

Printed in the United States of America, Office of Scientific and Technical Information, Oak Ridge , Tennessee

DOE/PC/79816--T3

DE92 011275

AN INNOVATIVE CATALYST SYSTEM FOR SLURRY-PHASE FISCHER-TROPSCH SYNTHESIS: COBALT PLUS A WATER-GAS-SHIFT CATALYST

Final Technical Report

Charles N. Satterfield

Ian C. Yates

Claire Chanenchuk

Department of Chemical Engineering

Massachusetts Institute of Technology

Cambridge, Massachusetts 02139

July, 1991

Prepared for the

U.S. Department of Energy

under

Contract No. DE-AC22-87PC79816

TABLE OF CONTENTS

Executive Summary

The feasibility of using a mechanical mixture of a $Co/MgO/SiO_2$ Fischer-Tropsch catalyst and a $Cu\text{-}ZnO/Al_2O_3$ water-gas-shift (WGS) catalyst for hydrocarbon synthesis in a slurry reactor has been established. Such a mixture can combine the superior product distribution from cobalt with the high activity for the WGS reaction characteristic of iron. Weight ratios of $Co/MgO/SiO_2$ to $Cu\text{-}ZnO/Al_2O_3$ of 0.27 and 0.51 for the two catalysts were studied at 240°C, 0.79 MPa, and *in situ* H_2/CO ratios between 0.8 and 3.0. Each catalyst mixture showed stable Fischer-Tropsch activity for about 400 hours-on-stream at a level comparable to the cobalt catalyst operating alone. The $Cu\text{-}ZnO/Al_2O_3$ catalyst exhibited a very slow loss of activity under these conditions, but when operated alone it was stable in a slurry reactor at 200-220°C, 0.79-1.48 MPa, and H_2/CO *in situ* ratios between 1.0 and 2.0. The presence of the water-gas-shift catalyst did not affect the long-term stability of the primary Fischer-Tropsch selectivity, but did increase the extent of secondary reactions, such as l-alkene hydrogenation and isomerization.

The rate of synthesis gas consumption over the catalyst was measured at 220 to 240°C, 0.5 to 1.5 MPa, H_2/CO feed ratios of 1.5 to 3.5 and conversions of 6 to 68% of hydrogen and 11 to 73% of carbon monoxide. The inhibiting effect of carbon monoxide was determined quantitatively and a Langmuir-Hinshelwood-type equation of the following form was found to best represent the results:

$$-R_{H_2+CO} = \frac{a\, P_{CO} P_{H_2}}{(1 + b\, P_{CO})^2}$$

The apparent activation energy was 93 to 95 kJ/mol. Data from previous studies on cobalt-based Fischer-Tropsch catalysts are also well correlated with this rate expression.

Increasing space velocity (decreasing conversion) or decreasing reactor H_2/CO ratio decreased the yield of (undesired) C_1 products and increased the yield of (desired) $C_{10}+$ products. Reactor temperature and pressure had little effect on the carbon number distribution. These findings are interpreted in terms of the extent of the readsorption of 1-alkenes into growing chains on the catalyst surface. The relative selectivity to 1-alkenes by the primary synthesis and secondary reaction of 1-alkenes to n-alkanes and 2-alkenes depends on reactor H_2/CO ratio and CO concentration.

The cobalt-catalyzed reactions of C_2H_4, C_3H_6, or 1-C_4H_8 added to synthesis gas in concentrations ranging from 0.5 to 1.2 mol.% of total feed were studied at 220°C, and 0.45 to 1.48 MPa. H_2/CO feed ratios were varied between 1.45 to 2.25 and H_2 + CO conversions between 5 and 30% were observed.

1-Alkenes incorporate into growing chains on the catalyst surface, probably by initiating and/or terminating the chain growth process. Only ethene may propagate chain growth significantly. The propensity of the 1-alkenes to incorporate decreases with increasing carbon number of the 1-alkene and is affected by the extent of competitive reactions, notably hydrogenation to the alkane and isomerization to the 2-alkene. Incorporation is most evident in products above about $C_{10}+$.

The double-α behavior exhibited by most Fischer-Tropsch catalysts can be interpreted as the sum of two growth processes, one a stepwise single-carbon growth process and the other a 1-alkene incorporation process. Many of the effects of process variables on the hydrocarbon selectivity of Fischer-Tropsch catalysts are consistent with this theory.

The results of the study are divided into four parts, as outlined in the Table of Contents.

I. The Fischer-Tropsch Synthesis with a Mechanical Mixture of a Cobalt Catalyst and a Copper-Based Water-Gas-Shift Catalyst

Abstract

The feasibility of using a mechanical mixture of a $Co/MgO/SiO_2$ Fischer-Tropsch catalyst and a $Cu\text{-}ZnO/Al_2O_3$ water-gas-shift (WGS) catalyst for hydrocarbon synthesis in a slurry reactor has been established. Such a mixture can combine the superior product distribution from cobalt with the high activity for the WGS reaction characteristic of iron. Weight ratios of $Co/MgO/SiO_2$ to $Cu\text{-}ZnO/Al_2O_3$ of 0.27 and 0.51 for the two catalysts were studied at 240°C, 0.79 MPa, and *in situ* H_2/CO ratios between 0.8 and 3.0. Each catalyst mixture showed stable Fischer-Tropsch activity for about 400 hours-on-stream at a level comparable to the cobalt catalyst operating alone. The $Cu\text{-}ZnO/Al_2O_3$ catalyst exhibited a very slow loss of activity under these conditions, but when operated alone it was stable in a slurry reactor at 200-220°C, 0.79-1.48 MPa, and H_2/CO *in situ* ratios between 1.0 and 2.0. The presence of the water-gas-shift catalyst did not affect the long-term stability of the primary Fischer-Tropsch selectivity, but did increase the extent of secondary reactions, such as l-alkene hydrogenation and isomerization.

I.A. Introduction

Cobalt-based Fischer-Tropsch catalysts exhibit many performance characteristics superior to those based on iron. Carbon formation on cobalt is minimal, which may increase catalyst life and facilitate purification of the product, and oxygenates such as aldehydes, ketones and alcohols are formed in much lower quantities, and make product workup easier. However an advantage of iron catalysts is that they are generally active for the water-gas shift reaction. Thus, Fischer-Tropsch reactors can be fed with the hydrogen-lean synthesis gas produced by modern coal gasifiers, and hydrogen can be generated *in situ* simultaneously with the synthesis reaction, via the water-gas shift reaction.

Cobalt catalysts lack water-gas-shift (WGS) activity at the optimum temperatures of the synthesis reaction. Thus, a mechanical mixture of a cobalt catalyst and a water-gas shift catalyst may make possible a combination of the product advantages of cobalt and the operating advantages of a slurry reactor.

Shell patents[1,2] indicate that a mechanical mixture of a $Co/ZrO_2/SiO_2$ Fischer-Tropsch catalyst and a $Cu/ZnO/Al_2O_3$ shift catalyst can be successfully used to carry out Fischer-Tropsch synthesis in a fixed-bed reactor. The cited preferred conditions are 175-275°C and 1 to 7.5 MPa. The ratio of cobalt to shift catalyst is adjusted depending on the H_2/CO feed ratio, with a higher portion of shift catalyst recommended for lower H_2/CO ratios.

Tominaga et al.[3] report results of studies with a fixed-bed at 0.3 MPa and between

220 and 280°C using a 10 wt.% Co on SiO_2 catalyst mixed with a Cu/Cr_2O_3 shift catalyst. The primary focus of their research was the Köelbel-Engelhardt synthesis, in which CO and H_2O, rather than synthesis gas, are fed to the reactor. However, they report some data on feeds containing only H_2 and CO with a H_2/CO ratio of 0.5. Two trends were observed. First, when the shift catalyst was added, the CO_2 in the products increased from 0.1 to 6.0 mol.%, indicating a large enhancement in shift activity. Second, the weight fraction of C_5+ products remained unaffected by addition of the shift catalyst to the system.

Post and co-workers give no information on possible change in activity and selectivity with time. Tominaga et al. report that the yield of CO_2 decreased to 50% of its initial value within the first 6 hours of operation, attributed to competitive inhibition of the shift reaction by hydrocarbons. They state that this decreased activity is the steady-state value, but present no data after 12 hours-on-stream.

Therefore, no data on the long-term stability of water-gas shift and a Fischer-Tropsch catalyst system are available. Further, the performance of such a system in a fixed-bed may be difficult to understand because of changing conditions along the bed. Poisons or reaction conditions may deactivate the shift catalyst or the Fischer-Tropsch catalyst in one region of the bed, while catalyst activity may be maintained in another region. In a well-mixed slurry reactor, as used here, operating conditions are the same throughout the vessel.

The primary objective of this work was to search for a combination of a shift catalyst and a cobalt Fischer-Tropsch catalyst that could operate simultaneously and efficiently in a slurry reactor. Ideally, the combined system should exhibit stable activity

and selectivity, with neither catalyst adversely affecting the other.

I.B. Experimental

Our approach was to study the Fischer-Tropsch synthesis and the water-gas-shift reaction independently before combining these catalysts. The experiments were performed in a continuous, mechanically-stirred, one-liter autoclave. The slurry reactor and ancillary equipment are described in detail elsewhere.[4,5,6] In all runs, an impeller speed of 800 RPM or higher was used, to eliminate possible mass transfer effects.

I.B.1. Water-Gas-Shift (WGS) Catalysts. Three commercially-available WGS catalysts were studied by themselves. Two Cu-Cr_2O_3 catalysts (52% CuO and 48% Cr_2O_3 or 50% CuO, 4% MnO and 46% Cr_2O_3) were found to have insufficient stability or activity and are not discussed further here (for details, see Yates[7]). Satisfactory performance was achieved with Katalco 52-2 (33% CuO, 33% ZnO and 33% Al_2O_3, surface area = 36 m^2/g, bulk density 62 lb/ft^3, as reported by the manufacturer).

The three shift catalysts were each ground and sieved to 50 to 90 μm and loaded into the reactor, which had been previously charged with recrystallized octacosane, the carrier used in our slurry Fischer-Tropsch experiments. The octacosane was recrystallized in HPLC grade tetrahydrofuran as recommended by Huff and Satterfield.[4] The catalysts were then reduced according to the manufacturers' guidelines (see Table I). For the studies reported here, which utilized the Cu/ZnO/Al_2O_3 catalyst, the reduction procedure was slightly modified as outlined in Table I-1.

Following completion of the reduction, flow of vapor comprising 42.9 mol.% CO, 21.4 mol.% H_2, and 35.7 mol.% H_2O at 0.019 Nl/min/g.cat. (unreduced basis) was

begun. The rate at which water was fed is approximately five times that which would be typically synthesized in our reactor with a cobalt Fischer-Tropsch catalyst.[7] For the initial stability testing, temperature and pressure were held constant at 200°C and 0.79 MPa. All data presented here on gas composition and gas flow rates are on a wet-gas basis.

Water was delivered by a Waters Associates, Inc., Model 6000A pump, which is accurate to $\pm$ 0.005 ml of liquid/min (1.12×10^{-4} Nl of water vapor/min). Before being charged, the water was purified in a two-step process. First, the water was passed through a reverse-osmosis Millipore HEMO-RO*60 filtration system which removes ions and produces water with a resistivity of greater than 10 MΩ/cm. The deionized water was then passed through a Millipore Milli-Q Reagent H_2O system with ion-exchange and activated carbon beds. The purified water was verified by HPLC to contain less than 1 ppm of total impurities.

The water was fed to the reactor through a 0.159 cm (1/16 inch) O.D. tube which was heated to 20°C above reactor temperature to vaporize the water. The outlet of the tube was at the same height as the reactor's impeller and was therefore submerged in slurry wax during operation. The temperature of the outlet line from the reactor was held at 250°C to minimize the possibility of reflux of water during operation.

Activity was monitored by calculating the percent approach to equilibrium, either from disappearance of CO or appearance of H_2 and CO_2. Based on CO, X_{CO} is given by:

$$-X_{CO} = 100\left[\frac{(\mu_{inlet} - \mu_{out})}{(\mu_{equilibrium} - \mu_{inlet})}\right] \quad (1)$$

As a cross-check for a material balance, the equivalent value based on the products, H_2 and CO_2, $X_{product}$ is defined as:

$$X_{product_k} = 100\left[\frac{(\mu_{out_k} - \mu_{inlet_k})}{(\mu_{equilibrium_k} - \mu_{inlet_k})}\right] \quad (2)$$

where, for component k

$\mu_{out,k}$ = measured flow rate at outlet [mmol/min]. (3)

$\mu_{inlet,k}$ = measured flow rate at inlet [mmol/min]. (4)

$\mu_{equilibrium,k}$ = outlet flow rate at equilibrium [mmol/min]. (5)

The inlet CO_2 is zero. Ranging from 0% at no activity to 100% at equilibrium conversion, equations 1 and 2 provide a convenient benchmark for comparison of different feed compositions and/or flow rates. All material balances on WGS-only data were required to close within 3% on carbon.

I.B.2. Fischer-Tropsch Catalyst. The cobalt Fischer-Tropsch catalyst was prepared by an outside supplier and is of the approximate composition of the cobalt catalysts used at Ruhrchemie.[8] The nominal composition of the catalyst, as reported to us by its manufacturer, is 21.4 wt.% Co (as Co), 3.9 wt.% Mg (as Mg), and the remainder diatomaceous earth.

Supplied as an extrudate, the catalyst was ground and sieved to 50 to 90 μm. Following sieving, the catalyst was placed in an external reduction vessel. It was held in this unit with a 7 μm frit while hydrogen (prepurified, MedTech Gases, Inc.) was brought

on stream at a flow of 1.36 Nl/min (approximately 10,000 V/V/hr). At this flow rate the pressure in the vessel was approximately 0.72 MPa. The temperature of the reduction tube was increased steadily from 25°C to 330°C over 4.75 hours while the inlet flow rate was held constant. The reduction unit was then held at 330°C for 0.75 hours and subsequently the unit was pressurized with helium and rapidly cooled.

I.B.3. Combined System. The reduced cobalt catalyst was transferred under helium to the autoclave reactor which contained the reduced water-gas-shift catalyst, also under helium. The reactor was brought on-stream at 0.79 MPa, 187°C, and $H_2/CO = 1.5$ at a flow rate of 1.0 Nl/min. The CO used in these experiments was CP grade (North East Airgas, Inc.) and the H_2 was prepurified grade (MedTech Gases, Inc.).

The reactor conditions were held constant for the first 66 hours and then the H_2/CO feed ratio was adjusted to about 1.0 with an inlet flow of 0.59 Nl/min and the temperature was increased to 240°C over a period of 8 hours. The following reactor conditions were then considered to be "standard" conditions: 0.79 MPa, 240°C, and inlet $H_2/CO = 1.0$ at a flow rate of about 0.60 Nl/min.

Two combined-system runs were performed. Run L was operated with 9.0 grams of $Co/MgO/SiO_2$ catalyst and 33 grams of $Cu\text{-}ZnO/Al_2O_3$ (both on an unreduced basis) for a weight ratio of 0.27; run H was operated with 17.0 grams of $Co/MgO/SiO_2$ catalyst and 33 grams of $Cu\text{-}ZnO/Al_2O_3$ catalyst for a weight ratio of 0.51. In run L, "standard" conditions were utilized for the entire run of about 400 hours-on-stream. Under these conditions, about 16.5% of the H_2+CO fed was converted to Fischer-Tropsch products.

In run H, "standard" conditions were held for the first 220 hours-on-stream. Subsequently, the feed to the reactor was varied systematically over a H_2/CO feed ratio

of 1 to 2, and at either of two flow rates, about 0.30 and 0.60 Nl/min. These conditions provided conversions of H_2+CO between 29 and 75%. At 350 hours-on-stream, operating conditions were returned to "standard" to verify catalyst stability, and the run was ended after about 400 hours on stream. All material balances reported on the combined Fischer-Tropsch/water-gas-shift system closed within 3% on oxygen. Oxygen was chosen as the material balance closure element because carbon and hydrogen accumulate in the reactor in the form of heavy waxes under Fischer-Tropsch synthesis conditions, which makes it more difficult to base material balances on these elements.

I.C. Results and Discussion: Water-Gas-Shift Catalyst Alone

A preliminary run with the $Cu/ZnO/Al_2O_3$ catalyst showed stable activity, but it appeared desirable to modify the reduction procedure (see Table I-1) by increasing the length of the helium purge and decreasing the severity of the final reduction period. This reduction procedure was found to be superior.

We present here the results of a single run that extended over about 1030 hours and is outlined in Table I-2. No process changes were made during the first 300 hours-on-stream. Then, either the pressure, temperature or feed composition was changed and the % of equilibrium conversion was monitored for an interval of 48 to 100 hours. The reactor was then returned to "base case" conditions which would in turn be monitored for 48 to 100 hours. Thus, we were able to monitor both the effect of the process change on activity and on catalyst stability.

I.C.1. Stability. Figure I-1 shows the % of equilibrium conversions for the "base case" conditions. As Figure I-1 illustrates, the catalyst deactivated very slowly with time-

on-stream.

I.C.2. Effect of Pressure. Total pressure does not affect the equilibrium of the shift reaction, so increasing pressure would be expected to change conversion only by its effect on the reaction rate, which in turn may change the concentrations of the components in the reactor. After 303 hours-on-stream, the pressure was increased from 0.79 to 1.48 MPa. Temperature, space velocity, and feed composition were held constant. After a further 55 hours, the reactor was returned to the "base case" conditions and held there for 67 hours.

Figure I-2 shows the conversion data for the time period before, during, and after the pressure change. Increased pressure has no significant effect on the rate of water-gas shift or the long-term stability of the catalyst.

I.C.3. Effect of Inlet H_2/CO Ratio. The H_2/CO ratio is an important consideration for evaluating the stability of a shift catalyst for the Fischer-Tropsch synthesis. A $(H_2/CO)_{in}$ ratio of 0.5 was chosen for the base case, because, after undergoing the shift reaction, it provided an *in situ* H_2/CO ratio of approximately two, the usage ratio for cobalt catalysts. To elucidate the effect of H_2/CO, two additional feed ratios, 0.7 and 1.0, were studied. These produced *in situ* H_2/CO ratios near 2.5 and 3, respectively. Higher H_2/CO ratios were examined because higher hydrogen partial pressures might increase the likelihood of sintering and higher CO partial pressures are reported not to have deleterious effects on low-temperature shift catalysts.[9,10]

Figure I-3 shows that the % of equilibrium fell about 3 to 5% upon increased reactor H_2/CO ratios. In order to simplify the figure, the component conversions are not shown. This decrease is consistent with a simple equilibrium-limited rate expression,

presented by Moe[9], of the form:

$$R_{\text{water-gas shift}} = k\left[P_{CO}P_{H_2O} - \frac{P_{H_2}P_{CO_2}}{K_p}\right] \qquad (6)$$

In equation 6, increasing P_{H_2} and decreasing P_{CO} would decrease the "driving force" for reaction, thereby slowing the rate of reaction.

I.C.4. Effect of Temperature. Because copper-based shift catalysts sinter readily[11], catalyst manufacturers recommend that these catalysts not be used above 250°C. For most of the run, the reactor was operated at 200°C, the lowest temperature at which $Cu/ZnO/Al_2O_3$ catalysts reportedly have appreciable activity.[10] Figure I-1, which presents the "base case" data, indicates that at 200°C the catalyst converted approximately 65-70% of the H_2O and CO fed. After 637 hours-on-stream, the reactor temperature was increased from 200 to 220°C, and at 693 hours-on-stream, the temperature was returned to 200°C. At 220°C, % of equilibrium conversion increased to around 80% (Figure I-4), but it reverted to its former performance when the temperature was returned to 200° C.

I.C.5. Effect of 1-Butene. It has been suggested that alkenes may adsorb on the surface of shift catalysts, inhibiting their activity. To test this possibility, 1-butene was added to the feed at 924 hours-on-stream, in the form of a mixture of 2 mol.% 1-butene in prepurified H_2 (Matheson Gases, Inc.). 1-Butene is representative of 1-alkenes from the Fischer-Tropsch reaction and is easy to study in our reactor system, as it is the highest molecular weight 1-alkene that is not condensed in the product traps.[12,13]

Figure I-5 shows that shift activity remains essentially unchanged by the addition

of the 1-butene at this concentration. The amount of hydrogen consumed by 1-butene hydrogenation was negligible. About 96% of the added 1-butene was either hydrogenated to butane or isomerized to *cis*-2-butene and *trans*-2-butene; no significant amount was cracked to smaller hydrocarbons. The product composition was about 4% l-butene, 53% n-butane, 29% trans-2 butene and 14% cis-2 butene. The hydrogenation probably occurs on reduced copper, a known hydrogenation catalyst, and the isomerization on acidic sites on the Al_2O_3 support. *Cis*-2-butene and *trans*-2-butene are formed in almost equilibrium ratios.

In summary, a reduction procedure was achieved that allowed stable water-gas-shift behavior for a Cu-ZnO/Al_2O_3 catalyst in a slurry reactor. Within the ranges studied, the catalyst was not adversely affected by increased temperature, pressure, *in situ* ratio of H_2/CO, or the presence of 1-butene.

I.D. Results and Discussion: Fischer-Tropsch plus Water-Gas-Shift Catalyst

Two weight ratios of [$Co/MgO/SiO_2$] to [$Cu\text{-}ZnO/Al_2O_3$] were studied, termed run L and run H, with results summarized in Table I-3 and displayed in Figures I-6 through I-16.

I.D.1. Fischer-Tropsch Activity. Figure I-6 shows that, for each run, the combined catalyst system retained steady-state Fischer-Tropsch activity for the entire time of about 400 hours-on-stream. The average rate of H_2+CO consumption was 0.53 mmol/min-g.Co-cat., on an unreduced basis, for run L and 0.55 mmol/min-g.Co-cat. for run H (both at "standard" conditions). The reactor gas compositions were different for the two runs, but the inherent Fischer-Tropsch activity can be compared to each other and to that of the $Co/MgO_2/SiO_2$ catalyst operating alone by the following rate expression developed for this cobalt catalyst.[14]

$$-R_{H_2+CO}=\frac{aP_{CO}P_{H_2}}{(1+bP_{CO})^2} \tag{7}$$

At 240°C, $a=75.76$ mmol/min-g.cat.-MPa^2 and $b=11.61$ MPa^{-1}.

Figure I-7 shows the average rate of H_2+CO consumption and the rate as predicted from equation 7 for the reactor conditions of run L. The activity of the combined system appears to be slightly higher than that predicted. This may represent additional hydrogen consumption by hydrogenation on the water-gas shift catalyst, or may have been caused by a slight variation in the reduction procedure of the cobalt catalyst. Within our ability to reproduce catalyst reduction procedures, the cobalt catalyst acting alone and the cobalt catalyst operating in conjunction with the water-gas

shift catalyst display similar activity.

Since operating conditions were varied during run H, comparisons can be made of not only the absolute Fischer-Tropsch activity, but also the form of the rate equation. Equation 7 can be linearized as follows:

$$\left[\frac{P_{H_2}P_{CO}}{-R_{H_2+CO}}\right]^{1/2} = \frac{1}{a^{1/2}} + \frac{b}{a^{1/2}}P_{CO} \qquad (8)$$

Figure I-8, a plot of the left side of equation 8 versus P_{CO} for run H, shows that the form of this equation is obeyed in the presence of the WGS catalyst as well as in its

absence. The parameter values for the combined system were non-linearly regressed and found to be $a = 81.7 \pm 9.7$ mmol/min-g.Co-cat.-MPa^2 and $b = 8.1 \pm 0.8$ MPa^{-1} at 240°C. These values are remarkably close to the values obtained with the Co-based Fischer-Tropsch catalyst acting alone.

Figures I-6 through I-8 show that neither the absolute activity nor the long-term stability of the cobalt Fischer-Tropsch catalyst was adversely affected by the presence of the copper WGS catalyst.

I.D.2. Water-Gas-Shift Activity. At the temperatures of interest for the Fischer-Tropsch synthesis, the equilibrium of the water-gas-shift reaction favors the production of H_2 and CO_2. Thus, a good measure of shift activity is the extent to which H_2O reacts to form CO_2 as measured by X_{WGS} where:

$$X_{WGS} = \frac{P_{CO_2}}{(P_{CO_2} + P_{H_2O})} \qquad (9)$$

X_{WGS} is independent of Fischer-Tropsch synthesis gas consumption, as it depends only on the relative rates of formation of CO_2 and H_2O. At 240°C, if the system achieved equilibrium conversion, X_{WGS} would exceed 0.99. For the fused iron ammonia synthesis catalyst used in a similar manner in many previous studies in our laboratories, X_{WGS} ranged from 0.8 at 232°C to 1.0 at 263°C.[15]

Figure I-9 shows the extent of water-gas shift, expressed as shown in equation 9, for runs L and H. In run L, an average of 94% of the water formed was converted to CO_2, indicating that the system approached equilibrium. The shift catalyst retained its activity, even in the presence of the cobalt catalyst and the Fischer-Tropsch synthesis

products. Cobalt has little shift activity[7,8,16] and, therefore, the shift activity shown in Figure I-9 must come from the shift catalyst. The extent of the water-gas shift decreased steadily with time-on-stream for run H, but did not correlate with percent synthesis gas conversion, eliminating alkene inhibition as a possible cause of the deactivation.

The combined catalyst system in run L produced higher yields of methanol than were produced in run H or when the cobalt catalyst was operated alone (see Figures I-15a,b, and c), although these decreased with time (Fig. I-10). The Cu-ZnO/Al_2O_3 catalyst is active for methanol synthesis as well as the water-gas-shift. Despite intensive study, there is still controversy over the chemical state of copper on the catalyst during methanol synthesis and the kinetics of the reaction are complex.[17] The relative activity for the two reactions must vary in response to different nuances of surface structure and gas composition, judging from some of the results here. In run L the rate of methanol production decreased with time-on-stream, whereas the WGS activity remained constant, as did reactor conditions (Figure I-10). In run H, however, WGS activity decreased steadily with time (Fig. I-9).

I.D.3. Product Selectivity. Figures I-11a and I-11b show Schulz-Flory overhead product distributions (oxygenates plus hydrocarbons) at several times during the entire run, for runs L and run H. The distribution is essentially invariant for run L, but there is a moderate increase in the heaviest products with time for run H. This is probably caused by the subtle interaction of several effects. 1-Alkenes, formed as a primary product, may undergo secondary reactions such as hydrogenation to n-paraffins or isomerization, predominantly to 2-alkenes. Figures I-12a and I-12b show the ratio of 1-butene/n-butane and 1-butene/2-butene versus time-on-stream. The lower these ratios,

the greater the extent of secondary reaction. In run L secondary reaction activity did not seem to vary significantly with time-on-stream. For run H, the degree of secondary reactions appeared to decrease moderately with time-on-stream. The resulting increase in l-alkene/alkane ratio would allow an increasing degree of alkene incorporation into growing chains (see below).

There are two possible explanations for the decrease in secondary reactions with time in run H. Catalyst sintering reduces the accessible surface area of the catalyst and would be expected to cause a decline in all three types of activity, hydrogenation on reduced Cu, isomerization on acidic Al_2O_3 sites, and water-gas shift. Young and Clark[11] recommend that low-temperature shift catalysts not be operated at temperatures above 250°C because of the low melting point of copper. Some sintering may have occurred at the temperature of 240°C used for the mixed catalyst runs, versus the WGS scouting experiments performed at slightly lower temperatures (200-220°C), which could explain the long-term stability of the catalyst then.

Alternatively, loss in hydrogenation and isomerization activity may have been caused by the loss in WGS activity. In run H, the extent of WGS activity decreased with time, causing the reactor H_2/CO to decrease as feed conditions were held constant (Fig. I-9). Hydrogenation is approximately first order in hydrogen partial pressure and inhibited by adsorbed CO.[7] Thus, as the data labels on figure I-12b show, the decrease in secondary reactions may not be an intrinsic characteristic of the catalyst system, but rather caused by a decreasing H_2/CO ratio.

Figure I-13 shows that the 1-alkene/n-alkane ratio of the Fischer-Tropsch products is indeed a strong function of the H_2/CO ratio in the reactor (run H). This

ratio was varied by feeding gas with three different H_2/CO ratios at each of two different space velocities. For any given reactor H_2/CO, a lower feed rate results in a lower 1-butene/n-butane ratio in the products. This shows that hydrogenation is occurring as a secondary reaction, which would increase as the residence time increases. Figure I-14 illustrates the effect of reactor H_2/CO on the hydrogenation activity of the cobalt catalyst studied alone.[7] Note that higher *in situ* H_2/CO values occurred here because the cobalt catalyst itself lacks WGS activity. For a specified reactor H_2/CO ratio, the ratio (1-butene/n-butane) was much higher, indicating less secondary hydrogenation. Apparently, much of the hydrogenation and isomerization activity of the mixed catalyst systems was derived from the WGS catalyst, making these runs more sensitive to changes in reactor conditions. Consistent with this hypothesis, the average 1-butene/n-butane ratio in run L was lower than that in run H (Figures I-12a and I-12b).

Figure I-15a is a representative component Schulz-Flory diagram from the Fischer-Tropsch cobalt catalyst studied alone[7], that may be compared to similar diagrams for the two mixed catalyst runs (Fig. I-15b and c). For similar operating conditions (Table I-3), the overall product distributions of the mixed catalyst systems are similar to that of the Co catalyst acting alone, with a few exceptions. In all cases, the predominant Fischer-Tropsch products are n-alkanes. Selectivity to 2-alkenes, 1-alkenes, and n-alcohols drops off sharply with increased C number. The presence of the WGS catalyst may increase the secondary reaction activity which impacts upon the component selectivity, and in turn, the overall molecular weight distributions.

Table I-3 gives the average selectivity to various product cuts for the three runs. The selectivity to fuel range products, C_5+, is approximately 50 wt.% for run L, 77% for

run H, and 76% for Co-only.

Recent work by Yates and Satterfield[18] suggests that yields of high molecular weight products on cobalt are significantly affected by the incorporation of low molecular weight alkenes into growing product chains. 1-Alkenes, the primary synthesis product, may undergo isomerization or hydrogenation, instead of incorporation into growing chains. Thus the low yield to heavy molecular weight products in run L may have been caused by a high degree of hydrogenation of l-alkenes. At low space velocities (high conversions) these secondary reactions become more noticeable, decreasing alkene concentrations and thus the probability of alkene incorporation.

Figures I-16a and b show analyses of the pot liquid at the end of runs L and H. The normalized Schulz-Flory plots, with the carrier, $C_{28}H_{58}$, subtracted from the distributions, both show α values of 0.83. These represent the high molecular weight products that have accumulated throughout the run. The end-of-run slurry from the cobalt catalyst alone, operated over a wide range of conditions, exhibited an α of 0.87.[7] These values of α are comparable.

I.E. Conclusions

A Cu-ZnO/Al_2O_3 water-gas-shift catalyst was found to exhibit stable activity in a slurry reactor under typical Fischer-Tropsch conditions. The stability of the catalyst was not adversely affected by increased pressure, temperature, variation in *in situ* H_2/CO ratio, or the addition of 1-butene, a representative Fischer-Tropsch product. l-Butene underwent considerable hydrogenation and isomerization, but did not crack.

A $Co/MgO/SiO_2$ Fischer-Tropsch catalyst was operated in conjunction with this shift catalyst at two different [$Co/MgO/SiO_2$]/[Cu-ZnO/Al_2O_3] weight ratios, 0.27 and

0.51. Operating conditions were 240°C, 0.79 MPa, and feed H_2/CO ratios from 1.0 to 2.0 at 0.3 to 0.6 Nl/min. In both runs, the Fischer-Tropsch catalyst maintained steady-state activity for the entire run of about 400 hours-on-stream at a level comparable to the cobalt catalyst operating alone. The rate of the Fischer-Tropsch reaction in the mixture followed a rate expression for the cobalt catalyst alone. The $Cu\text{-}ZnO/Al_2O_3$ WGS catalyst exhibited a very slow loss of its activity.

Each mixed catalyst system exhibited stable long-term Fischer-Tropsch selectivity, but the presence of the WGS catalyst increased the extent of the secondary reactions, thereby lowering the overall selectivity to fuel range products. The feasibility of a mechanical mixture of a cobalt-based Fischer-Tropsch catalyst and a Cu-ZnO WGS catalyst in a slurry reactor has been established.

I.F. References to Part I

(1) Post, M.F.M., and Sie, S.T., European Patent Application, Pub. No. 0153780, February 12, 1985a.

(2) Post, M.F.M., and Sie, S.T., European Patent Application, Pub. No. 0153781, February 12, 1985b.

(3) Tominaga, H., Miyachiharu, M. and Fujimoto, K., Bull. Chem. Soc. Jpn., **1987**, 60, 2310.

(4) Huff, G.A., Jr., and Satterfield, C.N., Ind. Eng. Chem. Fund., **1982**, 21, 479.

(5) Donnelly, T.J., and Satterfield, C.N., Appl. Catal., **1989**, 56, 231.

(6) Huff, G.A., Jr., Satterfield, C.N., and Wolf, M.H., Ind. Eng. Chem. Fund., **1983**, 22, 258.

(7) Yates, I.C., The Slurry-Phase Fischer-Tropsch Synthesis, Ph.D. Thesis, Massachusetts Institute of Technology, Cambridge, Massachusetts (1990).

(8) Storch, H.H., Golumbic, N., and Anderson, R.B., The Fischer Tropsch and Related Syntheses, John Wiley & Sons, New York, 1951.

(9) Moe, J.M., Chem. Eng. Prog., **1962**, 58(3), 33.

(10) Newsome, D.S., Catal. Rev.-Sci. Eng., **1980**, 21(2), 275.

(11) Young, P.W. and Clark, C.B., Chem. Eng. Prog., **1973**, 69 (5), 69.

(12) Hanlon, R.T., Catalyst Characterization and Secondary Reaction Effects in Iron-Catalyzed Fischer-Tropsch Synthesis, Sc.D. Thesis, Massachusetts Institute of Technology, Cambridge, Massachusetts, 1985.

(13) Matsumoto, D.K., The Effects of Selected Process Variables on the Performance of an Iron Fischer-Tropsch Catalyst, Sc.D. Thesis, Massachusetts Institute of Technology, Cambridge, Massachusetts 1985.

(14) Yates, I.C., and Satterfield, C.N., Energy and Fuels, **1991**, 5, 168.

(15) Huff, G.A., Jr., Fischer-Tropsch Synthesis in a Slurry Reactor, Sc.D. Thesis, Massachusetts Institute of Technology, Cambridge, Massachusetts, 1982.

(16) Anderson, R. B., The Fischer-Tropsch Synthesis, Harcourt, Brace & Jovanovich, New York, 1984.

(17) Satterfield, C.N., Heterogeneous Catalysis in Industrial Practice, second edition, McGraw-Hill, 1991, p. 453.

(18) Yates, I.C., and Satterfield, C.N., to be published.

TABLE I-1

REDUCTION PROCEDURE FOR WATER-GAS SHIFT CATALYSTS

Hours-on-stream	Temperature (°C)	Flow, (Nl/min/g.cat.)
		Initial Procedure
0 to 2	70 to 120	0.015 of gas C
2 to 2.5	120	0 to 0.015 gas A, 0.015 to 0 of gas C
2.5 to 6	120 to 200	0.015 of gas A
6 to 7	200	0 to 0.015 of gas B, 0.015 to 0 of gas A
7 to 20	200	0.015 of gas B
		Modified Procedure
0 to 16	70	0.015 of gas C
16 to 18	70 to 120	0.015 of gas C
18 to 19	120	0 to 0.015 of gas A, 0.015 to 0 of gas C
19 to 21.5	120 to 200	0.015 of gas A
21.5 to 24	200	0 to 0.015 of gas D, 0.015 to 0 of gas A
24 to 25	200	0.015 of gas D

TABLE I-1 (Continued)

Notes: Time and temperature periods shown indicate a smooth ramping of conditions. Typically, process changes were made every 15 minutes. The modified procedure was used for the data reported here.

Gas A was 1000 ppm prepurified H_2 in prepurified N_2 (Matheson Gases, Inc.).

Gas B was prepurified H_2 (MedTech Gases, Inc.).

Gas C was prepurified He (Colony, Inc.).

Gas D was 3 vol.% prepurified H_2 in prepurified N_2 (Matheson Gases, Inc.).

TABLE I-2

PROCESS CHANGES FOR $Cu/ZnO/Al_2O_3$ ALONE

Time-on-stream [hours]	Process Change
0	On-stream with base case conditions[a].
303	Base case except pressure = 1.48 MPa.
358	Returned to base case conditions.
425	Base case except H_2/CO feed ratio increased to 1.0.
473	Returned to base case conditions.
637	Base case except temperature increased to 220°C.
693	Returned to base case conditions.
783	Base case except H_2/CO feed ratio increased to 0.7.
830	Returned to base case conditions.
924	Base case except 2 mol.% 1-butene added to H_2 feed.
1030	Returned to base case conditions.

[a] "Base case" conditions are 200°C, 0.79 MPa, and a feed of 42.9 mol.% CO, 21.4 mol.% H_2, and 35.7 mol.% H_2O. Feed rate (includes water vapor) = 0.019 Nl/min/g.cat. (unreduced basis). 25 g. of catalyst (unreduced basis) were charged to the reactor containing 400 g. of recrystallized octacosane.

TABLE I-3

STANDARD OPERATING CONDITIONS AND PRODUCT DISTRIBUTIONS FOR COMBINED SYSTEMS AND COBALT CATALYST ALONE

	Run L [Co/MgO/SiO_2]/ [Cu-ZnO/Al_2O_3] = 0.27	Run H [Co/MgO/SiO_2]/ [Cu-ZnO/Al_2O_3] = 0.51	Cobalt-Catalyst Only[a]
Temperature (°C)	240	240	240
Pressure (MPa)	0.79	0.79	0.79
(H_2/CO) *In Situ*	1.02	0.98	1.52
Feed Flow Rate (Nl/min-g.Co-cat.)	0.065	0.035	0.026
Weight Fraction C_1	0.26	0.08	0.09
Weight Fraction C_{2-4}	0.24	0.14	0.15
Weight Fraction C_{5-9}	0.27	0.29	0.31
Weight Fraction C10+[b]	0.23	0.48	0.45

[a] Data of Yates.[7]

[b] Calculated for the C_{10}-C_{100} fraction by extrapolation, using overhead composition data for the C_3-C_{16} fraction.[7]

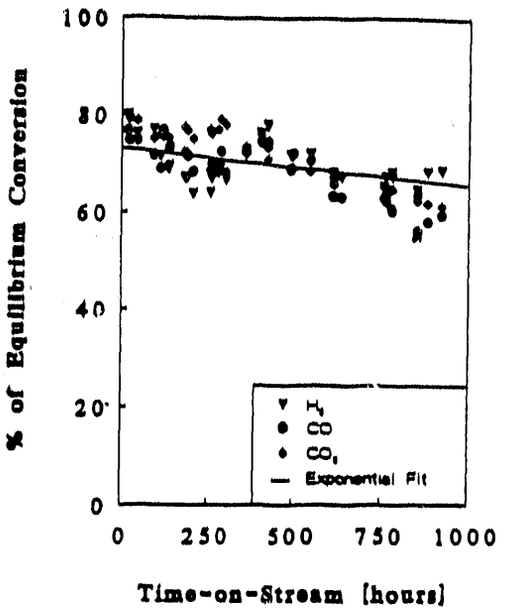

Fig.I-1 Stable activity of $Cu\text{-}ZnO/Al_2O_3$ at "base case" conditions (see note to Table 2).

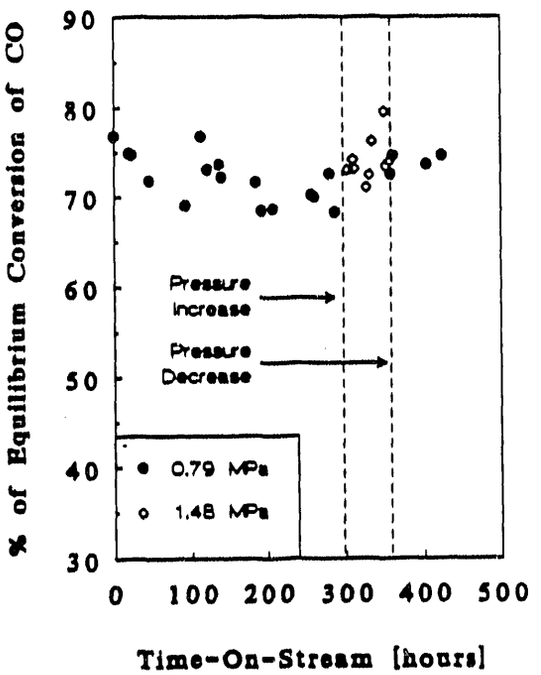

Fig.I-2 Pressure has no deleterious effect on the activity of the $Cu\text{-}ZnO/Al_2O_3$ shift catalyst.

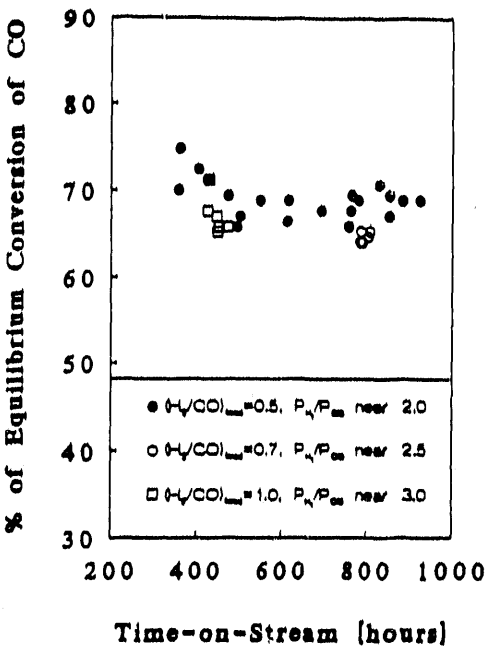

Fig.I-3 Increasing hydrogen-to-carbon monoxide ratio reduces rate, but intrinsic activity remains stable for the Cu-ZnO/Al_2O_3 shift catalyst (200°C, 0.79 MPa, $H_2 + CO = 0.0122$ Nl/min/g.cat., and H_2O at 0.0068 Nl/min/g.cat. (unreduced basis)).

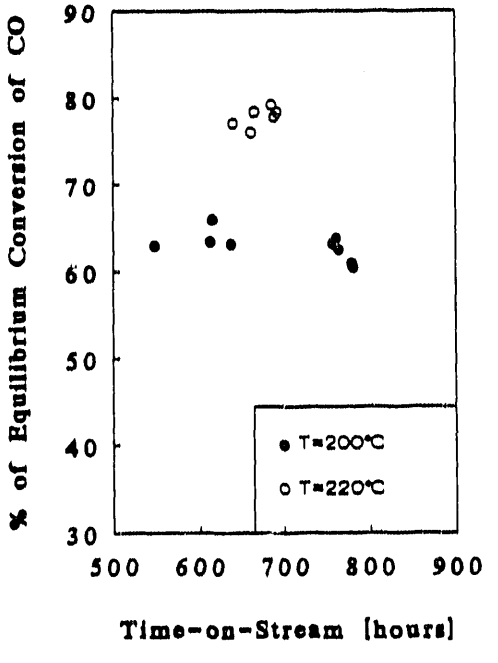

Fig.I-4 Temperature increases % of equilibrium conversion. Standard conditions.

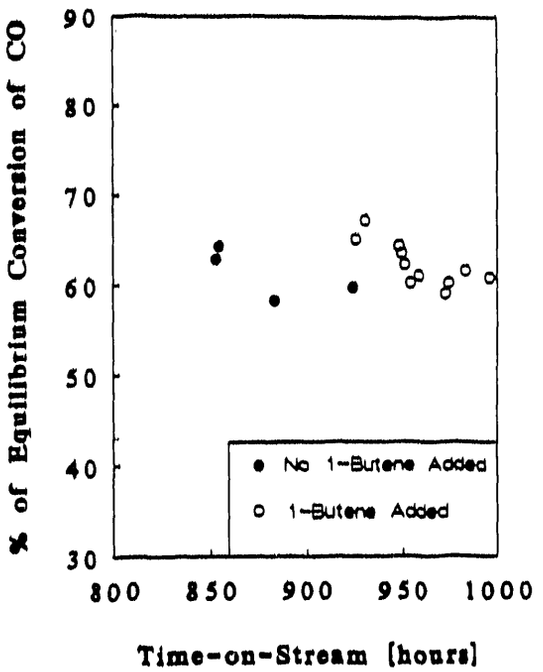

Fig. I-5 1-Butene has no significant inhibiting effect on the shift activity of the Cu-ZnO/Al_2O_3 shift catalyst. 1-butene added as 2 mol.% of H_2.

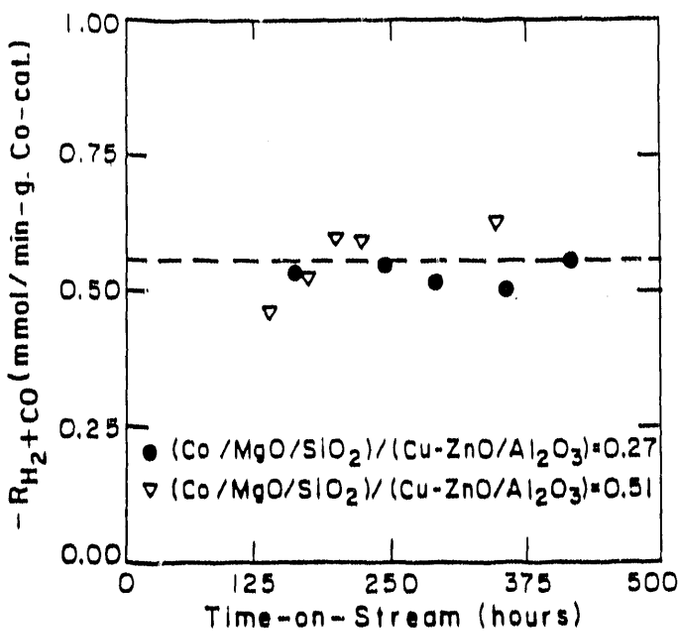

Fig. I-6 The Fischer-Tropsch activity of the catalysts in both run H and run L remained stable for the entire runs of about 400 hours-on-stream each. Feed rate about 0.60 Nl/min.

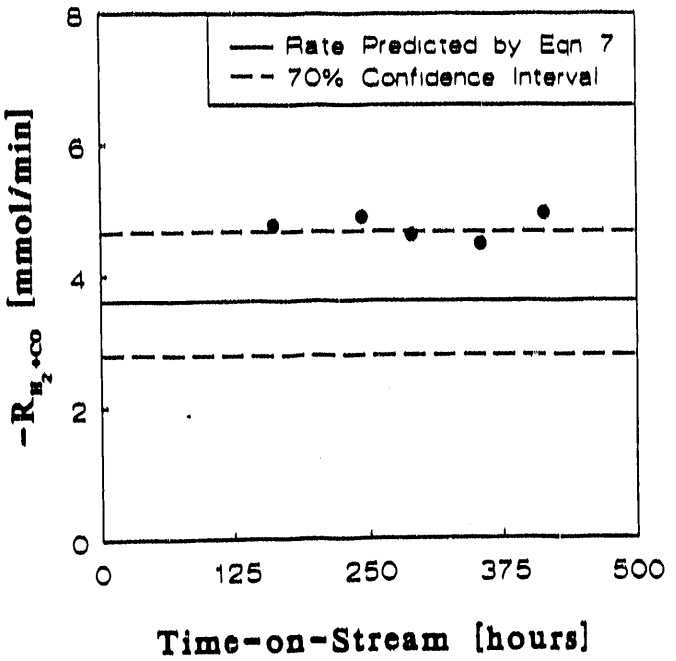

Fig. I-7 Activity of combined catalyst system run L ([Co/MgO/SiO_2]/[Cu-ZnO/Al_2O_3] = 0.27) matches that predicted by equation 7. (240°C, 0.79 MPa, *in situ* $H_2/CO = 1.02$, and fed 0.065 Nl/min-g.Co-cat).

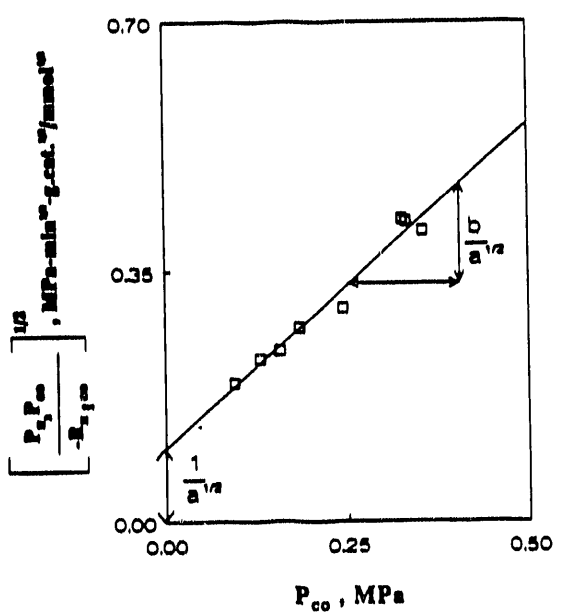

Fig. I-8 Data from combined catalyst system, run H, are well fit by linearized form of recommended rate equation (equation 8). Intercept = $1/a^{1/2}$, Slope = $b/a^{1/2}$.

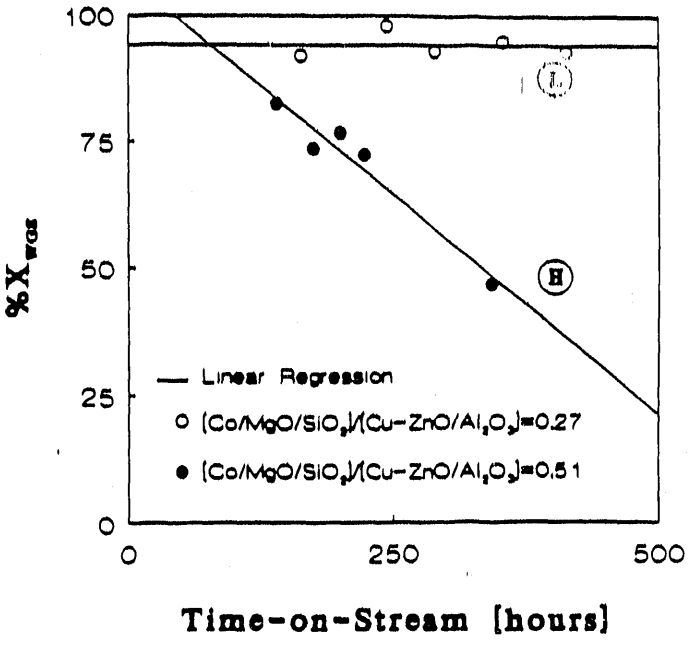

Fig. I-9 The water-gas-shift reaction approached equilibrium limitations for run L, while the activity declined for run H. Standard conditions.

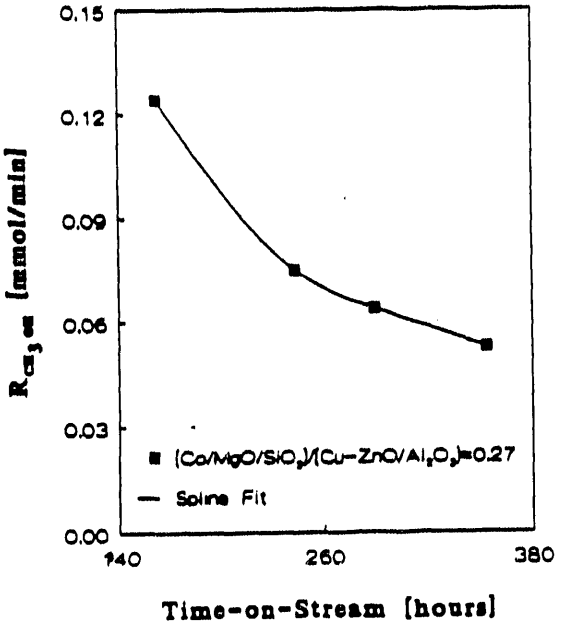

Fig. I-10 The rate of methanol synthesis decreased with time during run L. Standard conditions.

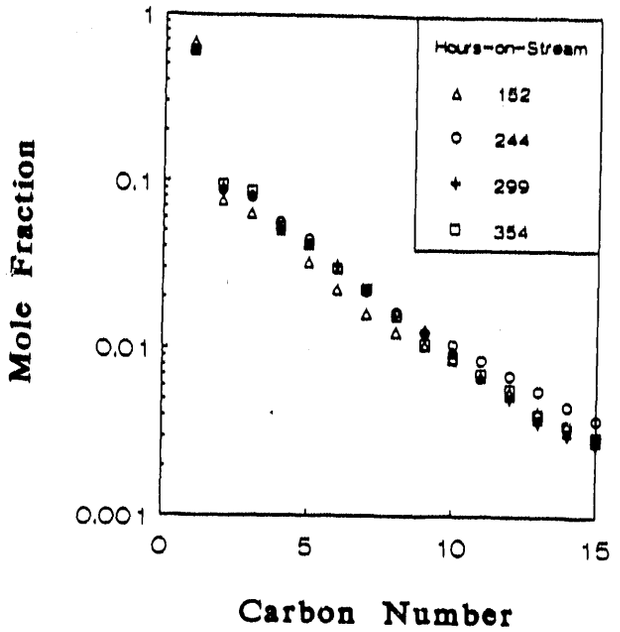

Fig. I-11a Schulz-Flory Diagrams obtained at various time periods show stable Fischer-Tropsch selectivity for run L. Standard conditions.

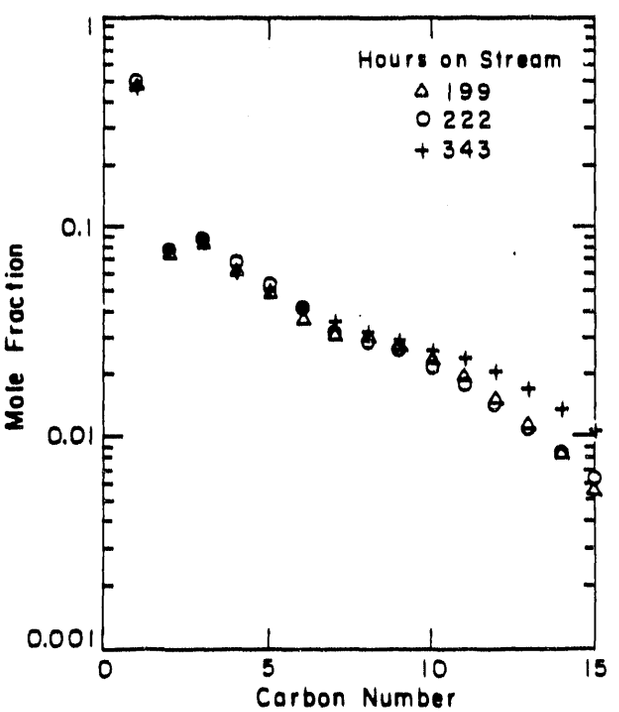

Fig. I-11b Schulz-Flory Diagrams obtained over a 400-hour time period show stable Fischer-Tropsch selectivity for run H. Standard feed conditions.

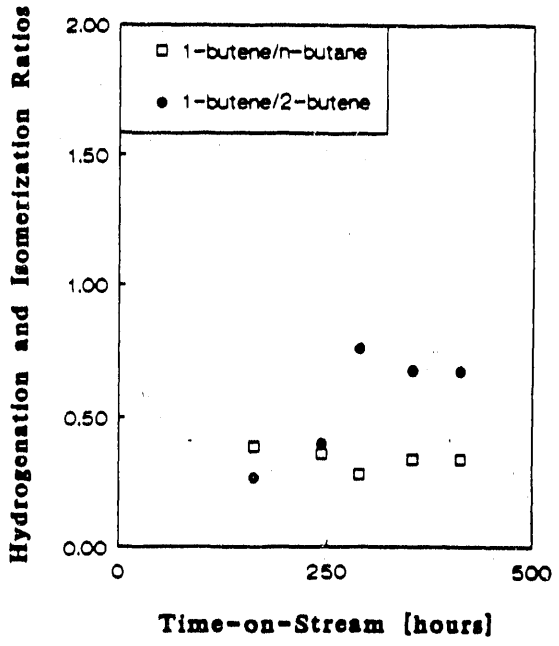

Fig. I-12a The secondary reaction activity of run L remained stable. Standard conditions.

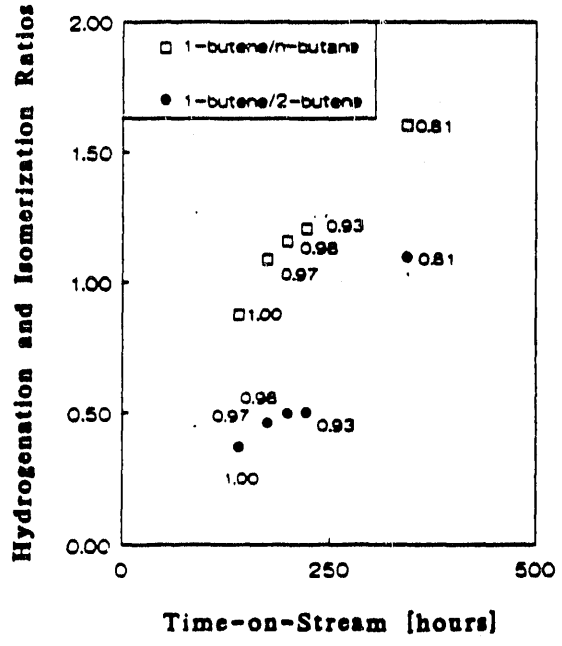

Fig. I-12b The secondary reaction activity of run H appeared to decline with time but may have been caused by decreasing *in situ* H_2/CO (See data labels). Standard feed conditions.

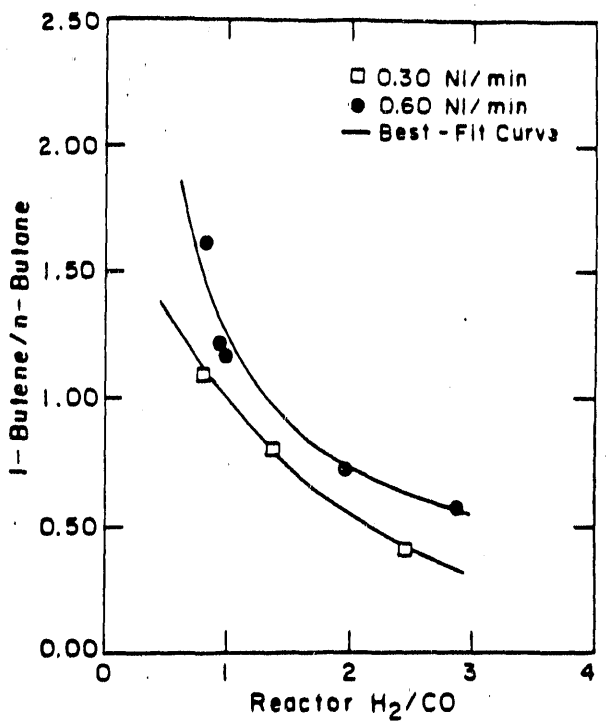

Fig. I-13 The hydrogenation activity was markedly affected by the *in situ* H_2/CO. Standard conditions but with 0.30 or 0.60 Nl/min. feed rate (run H).

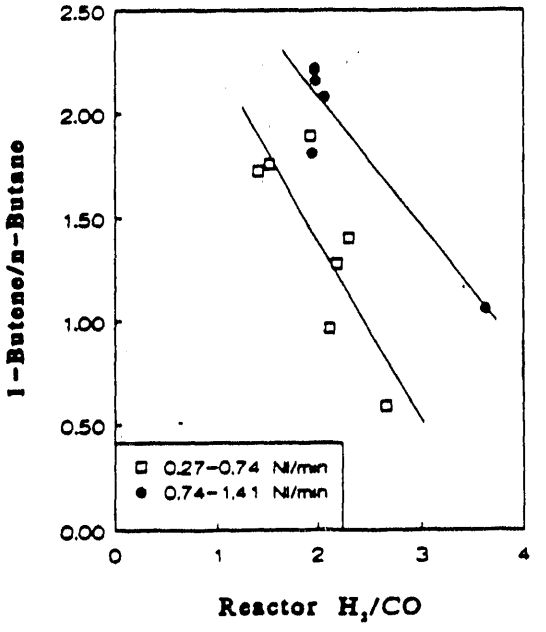

Fig. I-14 The hydrogenation activity of $Co/MgO/SiO_2$ alone increases with increasing *in situ* H_2/CO. (240°C, 0.79 MPa) Data of Yates.[7]

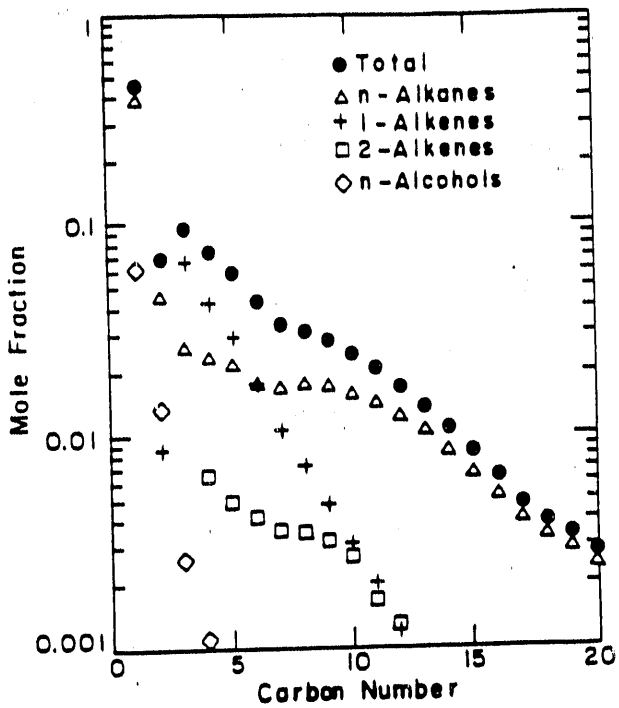

Fig. I-15a A typical component Schulz-Flory diagram from the $Co/MgO/SiO_2$ catalyst operating alone (Yates[7]).

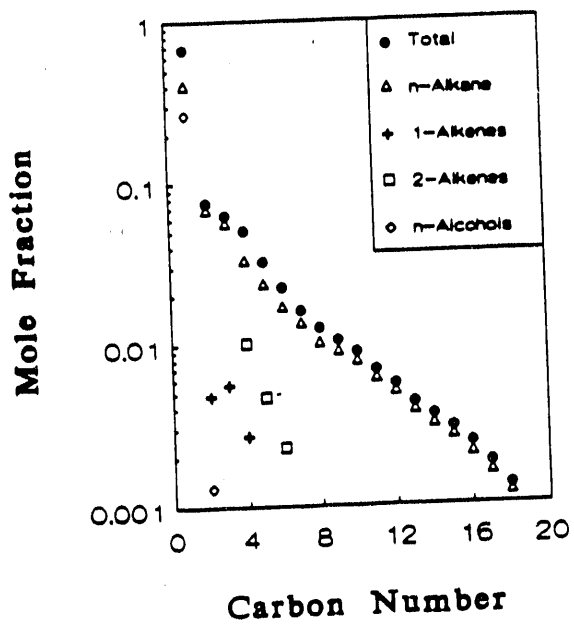

Fig. I-15b A typical component Schulz-Flory diagram from run L. Standard conditions.

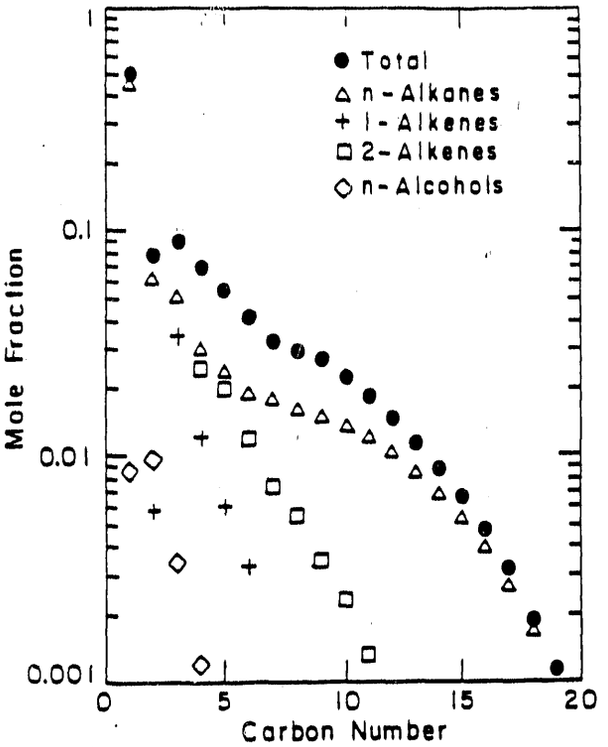

Fig. I-15c A typical component Schulz-Flory diagram from run H. Standard conditions.

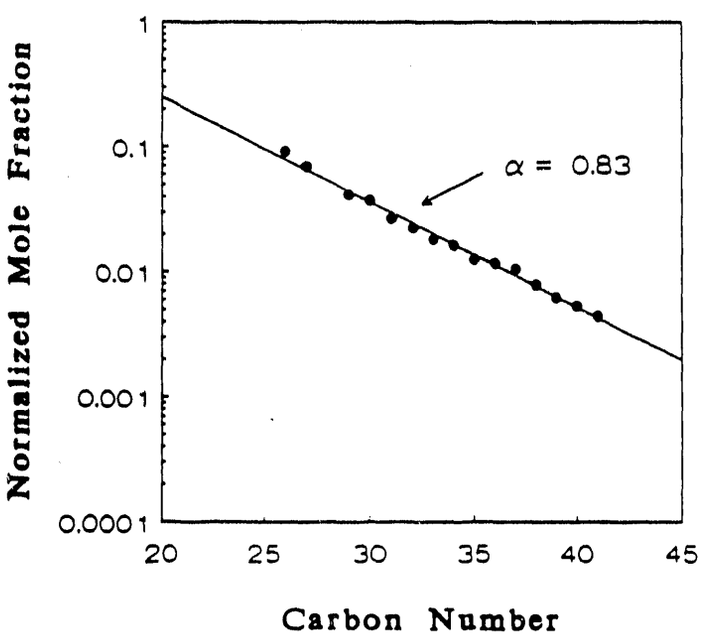

Fig. I-16a Normalized Schulz-Flory diagram from slurry wax sample of run L. Value of $\alpha = 0.83$ determined from linear regression of C_{29}-C_{40}. Standard conditions.

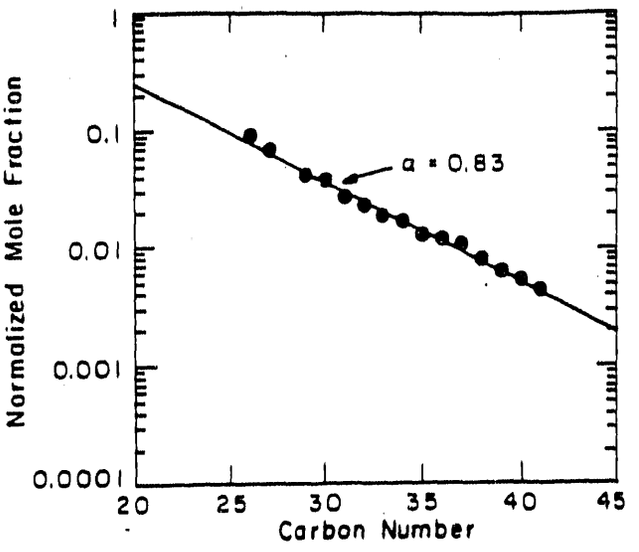

Fig. I-16b Normalized Schulz-Flory diagram from slurry wax sample of run H. Value of $\alpha = 0.83$ determined from linear regression of C_{29}-C_{40}. (240°C, 0.79 MPa, 0.80 ≤ *in situ* H_2/CO ≤ 3.0).

II. THE INTRINSIC KINETICS OF THE FISCHER-TROPSCH SYNTHESIS ON A COBALT CATALYST

Abstract

The rate of synthesis gas consumption over the catalyst was measured at 220 to 240°C, 0.5 to 1.5 MPa, H_2/CO feed ratios of 1.5 to 3.5 and conversions of 6 to 68% of hydrogen and 11 to 73% of carbon monoxide. The inhibiting effect of carbon monoxide was determined quantitatively and a Langmuir-Hinshelwood-type equation of the following form was found to best represent the results:

$$-R_{H_2+CO} = \frac{a\, P_{CO} P_{H_2}}{(1 + b\, P_{CO})^2}$$

The apparent activation energy was 93 to 95 kJ/mol. Data from previous studies on cobalt-based Fischer-Tropsch catalysts are also well correlated with this rate expression.

II. A. Introduction

A number of kinetic studies of the Fisher-Tropsch synthesis over cobalt catalysts have been performed.[1-8] All of the expressions found to fit rate data on these catalysts show that carbon monoxide inhibits the rate of synthesis. However, a wide array of proposed forms for the rate expression exist which is partly a result of the considerable variation in reaction conditions studied. Further, some studies, particularly the earlier work, were performed in fixed-bed reactors. Integral kinetic data from a complex reaction such as the Fischer-Tropsch synthesis cannot be interpreted easily and a fixed-

bed reactor may be difficult to maintain isothermal. In other cases, data are reported only for very low conversions.

Our objective for this part of the study was to develop an intrinsic kinetic expression for the rate of synthesis gas conversion on a cobalt catalyst over a range of industrially-relevant conditions. A mechanically-stirred, one-liter, continuous-flow, slurry reactor was used. The reactor behaves as a CSTR, providing data at uniform temperature and composition which are easy to analyze.

II. B. Background

The Fischer-Tropsch synthesis over cobalt-based catalysts produces mostly n-alkanes and 1-alkenes. The reaction stoichiometry may be approximated as:

$$n\,CO + 2n\,H_2 \longrightarrow (-CH_2-)_n + n\,H_2O \qquad (1)$$

Cobalt is not very active for the water-gas-shift reaction[9]; thus, in contrast to most iron-based Fischer-Tropsch catalysts, only a small fraction of the water produced is subsequently converted to carbon dioxide.

The rate of the Fischer-Tropsch reaction is defined here as the moles of hydrogen plus carbon monoxide converted per time per mass of unreduced catalyst, $-R_{H_2+CO}$. Some previous studies report the rate of conversion of carbon monoxide only, $-R_{CO}$. If the extent of water-gas-shift is negligible, the two rate measures, $-R_{H_2+CO}$ and $-R_{CO}$, are related by a constant, as can be seen from eq 1.

Published intrinsic expressions for the rate of Fischer-Tropsch synthesis over various cobalt catalysts are presented in Table II-1. The rate expressions of Yang et al.[3], Pannell et al.[4], and Wang[6] were all developed by regression of a power-law equation of

the general form:

$$-R = aP_{H_2}{}^{b}P_{CO}{}^{c} \qquad (2)$$

In all of these kinetic expressions, the coefficient b was positive and the coefficient c was negative, suggesting inhibition by adsorbed CO.

Anderson[2] found the equation developed by Brötz[1] to be inadequate for data over a wide range of inlet H_2/CO ratios. From data taken in a fixed-bed at atmospheric pressure over a wide range of H_2/CO ratios and temperatures, Anderson and co-workers at the Bureau of Mines[10] (Storch et al., p.529) developed an equation, eq 4, by postulating that the rate is proportional to the desorption of chains. The concentration of growing chains on the catalyst surface was related empirically to $P_{H_2}{}^{2}P_{CO}$. From samples withdrawn from the beginning of the bed, Anderson[2] (p. 270) and Storch et al. report that eq 4 does not satisfactorily fit the data at high values of $P_{H_2}{}^{2}P_{CO}$. They speculate that this lack-of-fit may be a result of either a hot-spot in the initial part of the bed or a different rate-controlling process being in effect at high values of $P_{H_2}{}^{2}P_{CO}$.

Rautavuoma and van der Baan[5] studied the rate of reaction at atmospheric pressure, 250°C and conversions below 2%. They examined five possible rate determining steps. The expression which fit their data best, eq 7, is consistent with a mechanism in which the reaction proceeds via CO dissociation and formation of a "$-CH_2-$" surface intermediate. The formation of this surface intermediate is the rate determining step. The model also assumes that hydrogen is adsorbed onto the catalyst surface dissociatively, however the authors suggest that the predominant surface species is dissociated CO and therefore do not include a term for dissociated H_2 in the denominator of the rate expression.

In the most recently-published work, Sarup and Wojciechowski[7] describe six different possible mechanisms for the Fischer-Tropsch reaction on cobalt catalysts that are compared to experimental data obtained at 190°C in a Berty internal recycle reactor. The rate of reaction was measured both by the rate of carbon disappearance and by the rate of oxygen appearance as H_2O plus CO_2. A wide range of values of P_{H_2} and P_{CO} were studied, but conversions are not reported.

Four of their proposed expressions presume that dissociated CO participates in the reaction, while two postulate that CO is adsorbed but not dissociated. The development of kinetic expressions from each of their proposed mechanisms is detailed by Sarup and Wojciechowski[7] and reviewed by Wojciechowski[8].

The general form of rate expression which they propose is:

$$-R_{CO} = \frac{k\, P_{CO}^{a} P_{H_2}^{b}}{\left(1 + \sum_i K_i P_{CO}^{c_i} P_{H_2}^{d_i} \right)^2} \qquad (11)$$

In eq 11, k is a kinetic parameter, a and b are the reaction orders of the rate-controlling step, K_i represents an adsorption parameter for the i^{th} adsorption term, and c_i and d_i describe the dependence of surface coverage of the i^{th} adsorption term on the reactant partial pressures. All of the possible reaction mechanisms considered by Sarup and Wojciechowksi involve a bimolecular surface reaction, thus the denominator of eq 11 is squared.

To discriminate among the six models, they regress their data nonlinearly. Because no *a priori* assumptions are made about the relative magnitude of possible inhibition terms, the regression determines all of the model parameters, k and various values of K_i. Three of the models fit the data comparably on the basis of residual sum

of squares, the sum over all the data points of the squared difference of the actual minus the predicted rate. These three models are eq 9 and 10 (Table II-1) and eq 12 (Sarup and Wojciechowksi's models 1, 5, and 6, respectively).

$$-R_{CO} = \frac{aP_{CO}P_{H_2}}{(1 + bP_{CO} + cP_{H_2}^{1/2} + dP_{CO}P_{H_2}^{1/2})^2} \qquad (12)$$

a, b, c, and d in eq 9, 10, and 12 are model-specific, temperature-dependent constants.

Of the three models, eq 12 fits their data best but is rejected by Sarup and Wojciechowski, because one of the adsorption coefficients, either b, c, or d in eq 12, not stated by the authors, is negative, representing a physically-unreasonable situation.

The constant d in eq 9 is reported to be statistically insignificant and they remove it from the model and re-regress the data, making the final form of the equation:

$$-R_{CO} = \frac{a\,P_{CO}^{1/2}P_{H_2}^{1/2}}{(1 + bP_{CO}^{1/2} + cP_{H_2}^{1/2})^2} \qquad (13)$$

The authors state that they are unable to distinguish between eq 10 and 13 on the basis of goodness-of-fit.

II. C. Experimental Section

In this study, the experiments were performed in a continuous, mechanically-stirred, one-liter autoclave. The slurry reactor and ancillary equipment are described in detail elsewhere[11]. The reactor and its contents are well-mixed. Studies with iron-based catalysts of similar particle sizes, catalyst loadings and reaction rates show that the

reactor operated without mass transfer limitations[11,12,13], as indicated by the lack of effect of stirring rate and other variables[12]. Calculations as described by Satterfield[14] further indicate that there are no mass transfer limitations either gas-liquid or within the catalyst particles.

The reactor was initially charged with 400 g of n-octacosane (>99% purity, Humphrey Chemical, Inc.). The n-octacosane had been previously recrystallized in tetrahydrofuran (>99.9% purity, Mallinkrodt, Inc.) to remove a bromine impurity.

The cobalt catalyst used is a Co/MgO on SiO_2. This catalyst was prepared for us by an outside laboratory and is of the approximate composition of the cobalt catalysts used at Ruhrchemie[10]. The nominal composition of the catalyst, as reported to us by its manufacturer, is: 21.4 wt.% Co (as Co), 3.9 wt.% Mg (as Mg), and remainder diatomaceous earth.

Supplied as an extrudate, the catalyst was ground and sieved to 52 to 92 μm (170 to 270 ASTM Mesh). Following sieving, 17 grams of the catalyst were placed in a tubular reduction vessel. The catalyst was held in this reduction unit with 7 μm stainless-steel sintered frits while hydrogen (prepurified, MedTech Gases, Inc.) was brought on-stream at a flow of 1.36 Nl/min (approximately 10,000 V/V/hr). At this flow rate, the pressure in the vessel was 0.79 MPa. The temperature of the reduction tube was increased steadily from 25°C to 330°C over 4 hours while the inlet flow rate was held constant. During this period the pressure in the reduction vessel increased to 0.97 MPa. The reduction unit was held at 330°C for 1.5 hours and then pressured with helium and rapidly cooled. The unit with the catalyst was weighed and comparison with the initial weight indicated that the catalyst lost 18 wt.% during reduction. The reduced catalyst was

added to the one-liter autoclave reactor which was being held under helium.

The reactor was brought on-stream at 0.79 MPa, 187°C, and $H_2/CO=2.0$ at a flow rate of 2.0 Nl/min. The CO used in these experiments was CP grade (Northeast Airgas, Inc.) and the H_2 was prepurified grade (MedTech Gases, Inc.). These gases pass through a 13 X molecular sieve, an activated carbon trap, and a 2 μm filter before entering the base of the reactor. The zeolite and activated carbon remove various potential impurities from the feed gases, including iron carbonyls, water, and sulfur-compounds.

The reactor conditions were held constant for the first 65 hours and then the reactor temperature was increased to 240°C over a period of 7 hours. The reactor was then kept at 0.79 MPa, 240°C, and $H_2/CO=2.0$ at a flow rate of 2.0 Nl/min for 72 hours to allow the catalyst to achieve steady-state activity and to ensure that the overhead products were representative of those being synthesized.

Material balances over a wide range of conditions were performed for periods of 6 to 24 hours, with at least 12 hours allowed between material balances to ensure steady-state operation. When the reactor temperature or pressure was changed, at least 48 hours were allowed between material balances.

Products, liquid hydrocarbons and water, were condensed in two traps, one kept at 85°C and reactor pressure, the other at 1°C and 0.34 MPa. Material balances, including analyses of all condensed and non-condensed products, closed between 97 and 103% on oxygen, which was chosen as the material balance closure criterion because carbon and hydrogen accumulate in the reactor in the form of high molecular weight hydrocarbons[12,15]. Table II-2 shows that returning to a standard set of conditions

periodically verified that the catalyst did not deactivate significantly during the run.

Reactor temperature was set between 220 and 240°C. Pressures were changed from 0.5 to 1.5 MPa and H_2/CO feed ratios from 1.5 to 3.5. Total synthesis gas conversion was varied from 11 to 70% by changing space velocity between 0.085 and 0.008 Nl/min/g of catalyst (unreduced basis).

Products were analyzed with three gas chromatographs, as described by Huff et al.[16]. A Hewlett-Packard 5880 with a dimethyl silicone capillary column and flame ionization detector (FID) was used for hydrocarbon analyses of non-condensable gases and the organic phases from the hot and cold traps. Aqueous liquid samples from the hot and cold traps, and non-condensed water and oxygenated hydrocarbons were analyzed with a Hewlett-Packard 5710 using a glass column packed with 60/80 mesh Tenax and a thermal conductivity detector (TCD). A Carle/Hach refinery gas analyzer Series S AGC 111-H was used for the analysis of non-condensable gases, particularly H_2, CO, and CO_2. Tie components, CO_2, CH_4, and C_2 and C_3 compounds, were used to match the analyses from the three gas chromatographs and provide complete product distributions for each material balance. The partial pressures of H_2 and CO in the reactor were calculated from the molar flow rates of all vapor-phase species present. For the organic products the molar flow rates of each species were calculated by a computer program. There was little change in H_2/CO usage ratio with reaction conditions. This averaged slightly above 2.

II. D. Results and Discussion

The forms of eq 3-13 all have subtle differences in their functional dependence on

P_{H_2} and P_{CO}, so experiments were run over a broad range of H_2/CO ratios in an attempt to avoid a covariance between these two independent variables of regression. Figures II-1 and II-2 are plots of P_{H_2} versus P_{CO} at 220 and 240°C. These figures show no significant correlation between reactant partial pressures.

It was decided that the rate expression should contain only two adjustable parameters, a simplifying approach appropriate for reaction systems with this degree of complexity. In terms of Langmuir-Hinshelwood kinetics, one of these parameters would represent a surface rate constant and the other an adsorption coefficient.

Additional adjustable parameters make the kinetic expression unnecessarily complex. Potential inhibitors of the rate of synthesis are frequently closely related (i.e. co-vary), for example $bP_{CO}^{1/2}$ and dP_{CO} in eq 9. Thus, the addition of numerous inhibition terms in the denominator can rarely be justified statistically. An example of this covariance between inhibition terms for the rate of Fischer-Tropsch synthesis on a reduced fused magnetite catalyst is illustrated by Yates and Satterfield[17]. There, it is shown that the inhibiting effects of H_2O on the synthesis had been incorrectly attributed to CO_2 by previous researchers, as a result of the high degree of correlation between P_{H_2O} and P_{CO_2}.

Eq 4 and eq 7 both contain only two parameters and are thus examined as possible rate expressions without modification. Eq 9, eq 10, and eq 12 contain more than two adjustable parameters. In the case of eq 10 and eq 12, it was assumed that CO was the predominant surface species, which is justified by non-reacting, single-component adsorption data on cobalt surfaces[18]; these data indicate that CO is more strongly adsorbed than H_2. The same simplification is also made by Rautavuoma and van der

Baan in the development of eq 7. In the case of eq 9, which has terms for surface coverage of undissociated CO and dissociated CO, it was assumed that dissociated CO was the predominant surface species. This assumption was implicitly made by Sarup and Wojciechowski[7] when they removed the constant d from eq 9 and re-regressed their data. The following equations represent the simplified, two-parameter forms of eq 9, 10, and 12:

$$-R_{CO} = \frac{aP_{CO}^{1/2}P_{H_2}^{1/2}}{(1 + bP_{CO}^{1/2})^2} \tag{14}$$

$$-R_{CO} = \frac{aP_{CO}P_{H_2}^{1/2}}{(1 + bP_{CO})^2} \tag{15}$$

$$-R_{CO} = \frac{aP_{CO}P_{H_2}}{(1 + bP_{CO})^2} \tag{16}$$

In eq 14-16, a and b are assumed to be temperature dependant constants, a representing a kinetic parameter and b an adsorption coefficient.

Eq 4, 7, 14, 15, and 16 were taken to be the five proposed models. All equations were expressed in terms of the rate of hydrogen plus carbon monoxide consumption. As discussed earlier, in the absence of appreciable water-gas-shift activity, this rate measure is related to the rate of carbon monoxide consumption by a constant.

Three methods were used to determine which expression best fit the data. First, the equations were linearized and plotted to look for outlying data points and general goodness-of-fit. Second, the linearized forms of the expressions were regressed to

quantify goodness-of-fit. Third, the data were regressed nonlinearly with the models and model parameters being tested for statistical significance.

The proposed equations were first linearized as follows:

$$\frac{P_{H_2}^2 P_{CO}}{-R_{H_2+CO}} = \frac{1}{a} + \frac{b\ P_{H_2}^2 P_{CO}}{a} \tag{17}$$

$$\left[\frac{P_{H_2} P_{CO}^{1/2}}{-R_{H_2+CO}}\right]^{1/3} = \frac{1}{a^{1/3}} + \frac{b\ P_{CO}^{1/2}}{a^{1/3}} \tag{18}$$

$$\left[\frac{P_{H_2}^{1/2} P_{CO}^{1/2}}{-R_{H_2+CO}}\right]^{1/2} = \frac{1}{a^{1/2}} + \frac{b\ P_{CO}^{1/2}}{a^{1/2}} \tag{19}$$

$$\left[\frac{P_{H_2}^{1/2} P_{CO}}{-R_{H_2+CO}}\right]^{1/2} = \frac{1}{a^{1/2}} + \frac{b\ P_{CO}}{a^{1/2}} \tag{20}$$

$$\left[\frac{P_{H_2} P_{CO}}{-R_{H_2+CO}}\right]^{1/2} = \frac{1}{a^{1/2}} + \frac{b\ P_{CO}}{a^{1/2}} \tag{21}$$

The majority of the data were collected at 220 and 240°C. The data at 240°C were regarded as more meaningful since they covered a wider range of relative rates. Figures II-3 through II-7 show plots of the data at 240°C according to the five linearized

forms given by eq 17-21. Best-fit linear regression lines are plotted to facilitate visual estimation of goodness-of-fit and scatter. Similar plots were made for the data at 220°C, but are not shown here. Table II-3 gives R-squared values for the fit of the data to the linearized forms of the proposed rate expressions at both 220 and 240°C. The equation which fits the data best is eq 21, the linearized form of eq 16.

Visual examination and regression of linearized rate expressions is a useful tool, but can be misleading because variance in the original data is distorted when the rate expressions are linearized. Table II-4 shows the results of nonlinear regression of the data which confirms that eq 16 fits the data best. Table II-5 presents the parameter values and some related regression information for the fit of eq 16 to the data from this study. The parameters a and b of eq 16 are highly statistically significant at both 220 and 240°C. The substantially higher value of b at 220°C is as would be expected from inhibition by adsorption of CO.

A further test of eq 16 could in principle be obtained by casting a and b into exponential form and calculating the effect of temperature on the exponent. With data from a temperature range of only 20°C, it was not reasonable to do in the present case. However, an apparent activation energy was calculated from rate data for two sets of values of P_{H_2} and P_{CO} that were nearly the same at 220 and 240°C. The apparent activation energies were 92.7 and 94.5 kJ/mol which are very close to apparent activation energies reported previously: 102 kJ/mol calculated by Anderson[2] (p.266) from data of Fischer and Pichler[19], 103 kJ/mol reported by Storch et al.[10] (p.530), 96 kJ/mol calculated by Anderson[2] (p.266) from data of Gibson and Hall[20], and 84 kJ/mol reported by Anderson[2] (p.265). These apparent activation energies were calculated from the slope

of plots of the logarithm of the rate of reaction versus the reciprocal of absolute temperature for data collected at similar pressures, feed rates and feed compositions. Yang et al.[3] report an apparent activation energy of 100 kJ/mol for their constant a in eq 5 which was regressed from their data.

Five of the six studies, including the present one, yield apparent activation energies within the close limits of 93 to 103 kJ/mol. This is perhaps surprising considering the wide range of conditions that were studied.

Figure II-8 shows the fit of eq 16 to the data from this study in the form of a parity plot. Within the scatter in the data, the two-parameter model fits the data well. Data points not included in the regression taken at 230°C are also well predicted by the rate equation, indicating that the estimates of the parameters a and b are reasonably good at both 220 and 240°C.

II. E. Comparison to Literature Data

Data from three of the studies listed in Table II-1 are available in the literature[5,6,8]. Having developed a two-parameter model that was different from any of those recommended by these researchers, we decided to fit their data to eq 16. The linearized form, eq 21, is used to examine goodness-of-fit and to look for outlying data points.

Figure II-9 shows the data of Rautavuoma and van der Baan[5], Figure II-10 the data of Wang[6] (pp.100-101), and Figure II-11 the data of Sarup and Wojiechowski[8]. All three sets of data fit the linear relationship of eq 21 well and have positive slopes and intercepts, as would be expected.

II. F. Conclusions

Data for the rate of synthesis gas consumption on a cobalt catalyst were obtained over a wide range of industrially-relevant conditions. Five different two-parameter rate models were examined for fit to the data by three methods: visual examination of linearized forms of the rate models, regression of these linearized expressions, and nonlinear regression of the expressions. Eq 16 is found to provide the best fit to our data. Data from three previous kinetic studies are also well fit by this kinetic expression. Apparent activation energies for five of six studies, including the present one, all fall within the narrow range of 93 to 103 kJ/mol.

II.G. Nomenclature

a	-temperature-dependent constant, the product of a surface rate constant and adsorption constants (equation specific).
b	-temperature-dependent adsorption constant (equation specific).
c	-temperature-dependent adsorption constant (equation specific).
d	-temperature-dependent adsorption constant (equation specific).
P_i	-partial pressure of component i, MPa.
-R	-rate of disappearance of either hydrogen plus carbon monoxide or carbon monoxide, mmol/min/g of catalyst (unreduced basis).
$-R_{H_2+CO}$	-rate of disappearance of hydrogen plus carbon monoxide, mmol/min/g of catalyst (unreduced basis).
$-R_{CO}$	-rate of disappearance of carbon monoxide, mmol/min/g of catalyst (unreduced basis).

II.H. Literature Cited

(1) Brötz, W. Z. Elektrochem. **1949**, 53, 301.

(2) Anderson, R.B. In Catalysis; Emmett, P.H., Ed., Reinhold: New York, 1959; Vol. IV, pp. 257-283.

(3) Yang, C.-H.; Massoth, F.E.; Oblad, A.G. Adv. Chem. Ser. **1979**, 178, 35.

(4) Pannell, R.B.; Kibby, C.L.; Kobylinski, T.P. Proc. 7th Int. Cong. on Catal. Tokyo, 1980, p. 447.

(5) Rautavuoma, A.O.I.; van der Baan, H.S. Appl. Catal. **1981**, 1, 247.

(6) Wang, J., Ph.D. Thesis, Brigham Young University, Provo, Utah, 1987, p. 99.

(7) Sarup, B.; Wojiechowski, B.W. Can. J. Chem. Eng. **1989**, 67, 62.

(8) Wojiechowski, B.W. Catal. Rev.-Sci. Eng. **1988**, 30, 629.

(9) Newsome, D.S. Catal. Rev.-Sci. Eng. **1980**, 21, 275.

(10) Storch, H.H.; Golumbic, N.; Anderson, R.B. The Fischer-Tropsch and Related Syntheses, Wiley, New York, 1951, p. 529.

(11) Huff, G.A., Jr.; Satterfield, C.N. Ind. Eng. Chem. Fundam. **1982**, 21, 479.

(12) Huff, G.A., Jr., Sc.D. Thesis, M.I.T., Cambridge, Massachusetts, 1982.

(13) Huff, G.A., Jr.; Satterfield, C.N. Ind. Eng. Chem. Process Des. Dev. **1984**, 23, 696.

(14) Satterfield, C.N., Mass Transfer in Heterogeneous Catalysis, reprint edition, Krieger Publishing Company, Inc., Malabar, Florida, 1981.

(15) Donnelly, T.J.; Yates, I.C.; Satterfield, C.N. Energy Fuels **1988**, 2, 734.

(16) Huff, G.A., Jr.; Satterfield, C.N.; Wolf, M.H. Ind. Eng. Chem. Fund. 1983, 22, 258.

(17) Yates, I.C.; Satterfield, C.N. Ind. Eng. Chem. Res., 1989, 28, 9.

(18) Vannice, M.A. Catal. Rev.-Sci. Eng. 1976, 14, 153.

(19) Fischer, F.; Pichler, H. Brennstoff-Chem. 1939, 7, 97.

(20) Gibson, E.J.; Hall, C.C. J. Appl. Chem. 1954, 4, 49.

Table II-1. SUMMARY OF KINETIC STUDIES OF THE FISCHER-TROPSCH SYNTHESIS ON COBALT-BASED CATALYSTS

REFERENCE	CATALYST	REACTOR TYPE	OPERATING CONDITIONS T [°C]	P [MPa]	H_2/CO_{in} [molar]	INTRINSIC KINETIC EXPRESSION [a]	EQ
Brötz [1]	Co/MgO/ThO_2/kies.	Fixed-bed	185-200	0.1	2	$-R_{H_2+CO} = \frac{aP_{H_2}^2}{P_{CO}}$	(3)
Anderson [2]	Co/ThO_2/kies.	Fixed-bed	186-207	0.1	0.9-3.5	$-R_{H_2+CO} = \frac{aP_{H_2}^2 P_{CO}}{(1+bP_{H_2}^2 P_{CO})}$	(4)
Yang et al. [3]	Co/CuO/Al_2O_3	Fixed-bed	235-270	0.17-5.5	1.0-3.0	$-R_{H_2+CO} = aP_{H_2} P_{CO}^{-0.5}$	(5)
Pannell et al. [4]	Co/La_2O_3/Al_2O_3	Berty (low conversion)	215	0.49-0.8	2	$-R_{H_2+CO} = aP_{H_2}^{0.55} P_{CO}^{-0.33}$	(6)
Rautavuoma and van der Baan [5]	Co/Al_2O_3	Fixed-bed (low coversion)	250	0.1	0.2-4.0	$-R_{CO} = \frac{aP_{H_2} P_{CO}^{1/2}}{(1 + bP_{CO}^{1/2})^3}$	(7)
Wang [6]	Co/B/Al_2O_3	Fixed-bed (low conversion)	181	0.1-0.2	0.25-4.0	$-R_{CO} = aP_{H_2}^{0.68} P_{CO}^{-0.5}$	(8)
Sarup and Wojiechowski [7]	Co/kies.	Berty	190	0.2-1.5 [b]	0.5-8.3 [b]	$-R_{CO} = \frac{aP_{CO}^{1/2} P_{H_2}^{1/2}}{(1+bP_{CO}^{1/2}+cP_{H_2}^{1/2}+dP_{CO})^2}$	(9)
and Wojiechowski [8]						$-R_{CO} = \frac{aP_{CO} P_{H_2}^{1/2}}{(1+bP_{CO}+cP_{H_2}^{1/2})^2}$	(10)

[a] a, b, c, and d in these equations are temperature-dependent constants.

[b] These ranges of operating conditions are estimated from their experimental data.

Table II-2.

ACTIVITY FOR REPEATED CONDITIONS OF 240°C, 0.79 MPa, $H_2/CO = 2$, AND SYNTHESIS GAS FEED RATE OF 0.067 Nl/min/g of catalyst†

Time-On-Stream [h]	Oxygen Closure [% molar]	$-R_{H_2+CO}$ [mmol/min/gcat]	P_{H_2} [MPa]	P_{CO} [MPa]
257.5	97.06	0.678	0.48	0.25
617.0	101.23	0.680	0.48	0.24
1073.0†	100.21	0.594	0.45	0.25
2176.5	99.89	0.694	0.47	0.24

† Flow is calculated at standard conditions; grams of catalyst are on an unreduced basis.

† H_2/CO and feed rate were slightly lower for this material balance at 1.95 and 0.066 standard l/min/gcat, respectively.

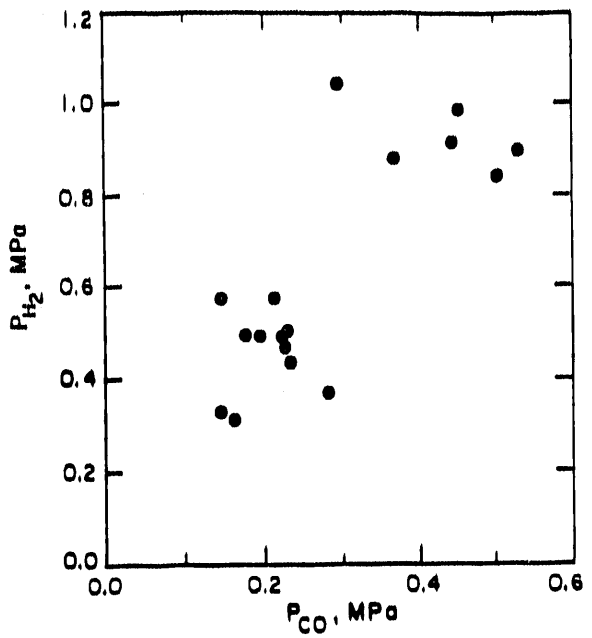

Fig. II-1 Plot showing lack of covariance between P_{H_2} and P_{CO} at 220°C.

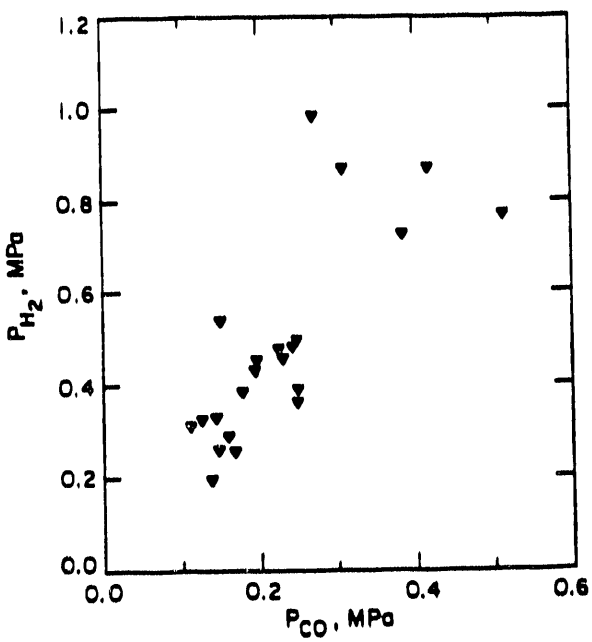

Fig. II-2 Plot showing lack of covariance between P_{H_2} and P_{CO} at 240°C.

Table II-3. R^2 for Linearized Expressions

eq	T, °C	R^2	eq	T, °C	R^2
17	220	0.954	20	220	0.970
	240	0.909		240	0.886
18	220	0.938	21	220	0.968
	240	0.945		240	0.984
19	220	0.927			
	240	0.590			

Table II-4. Nonlinear Regression Statistical Analyses

eq	residuals [sum of squared errors]	F ratio	R^2
4	0.340	42.06	0.663
7	0.072	303.27	0.929
14	0.245	85.82	0.758
15	0.214	101.61	0.788
16	0.062	361.22	0.938

Table II-5. Results of Nonlinear Fit of Data from This Study at 220 and 240 °C to Eq 16

reactor temp, °C	a[a]	std error of a[a]	t value[b] of a	b[c]	std error of b[b]	t value[b] of b
240	75.76	9.20	8.23	11.61	0.97	12.02
220	53.11	1.38	38.63	22.26	3.63	6.62

[a] In mmol/(min·g of catalyst·MPa^2). [b] There were 23 data points collected at 240 °C and 17 at 220 °C. Critical t values for 99% confidence that the parameters are statistically significant are $t_{0.995,21}$ = 2.831 for 240 °C; $t_{0.995,15}$ = 2.947 for 220 °C. t values above these critical values indicate that one can be 99% confident that the parameters are significant. [c] In 1/MPa.

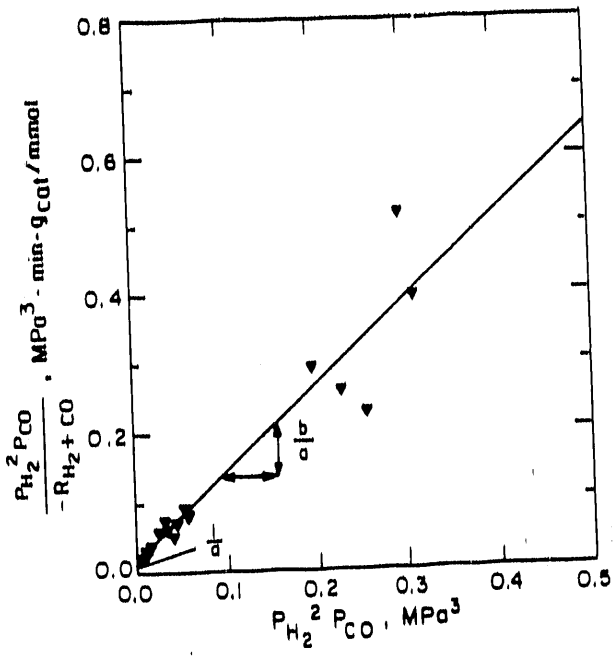

Fig. II-3 Test of eq 17 with experimental results at 240°C. Solid line is best fit linear regression line.

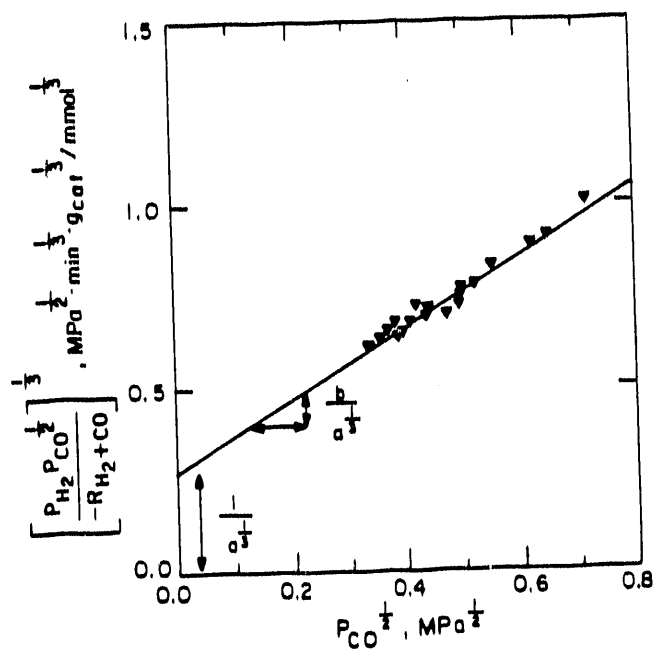

Fig. II-4 Test of eq 18 with experimental results at 240°C. Solid line is best fit linear regression line.

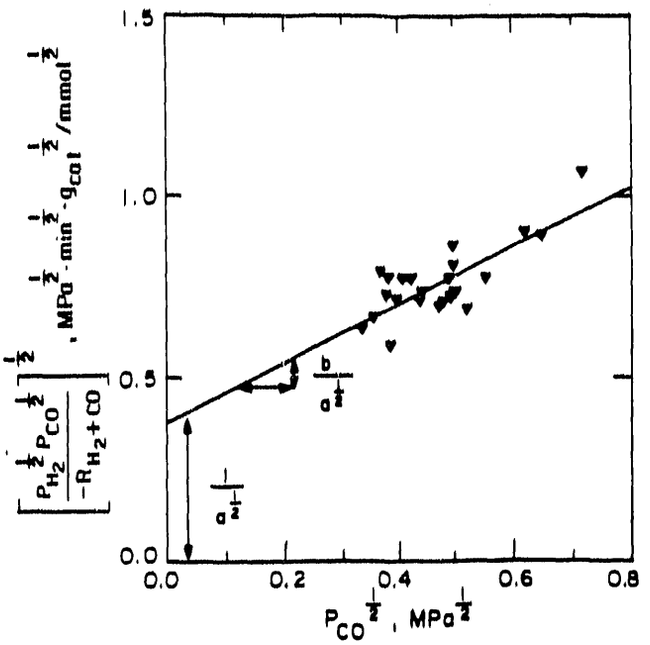

Fig. II-5 Test of eq 19 with experimental results at 240°C. Solid line is best fit linear regression line.

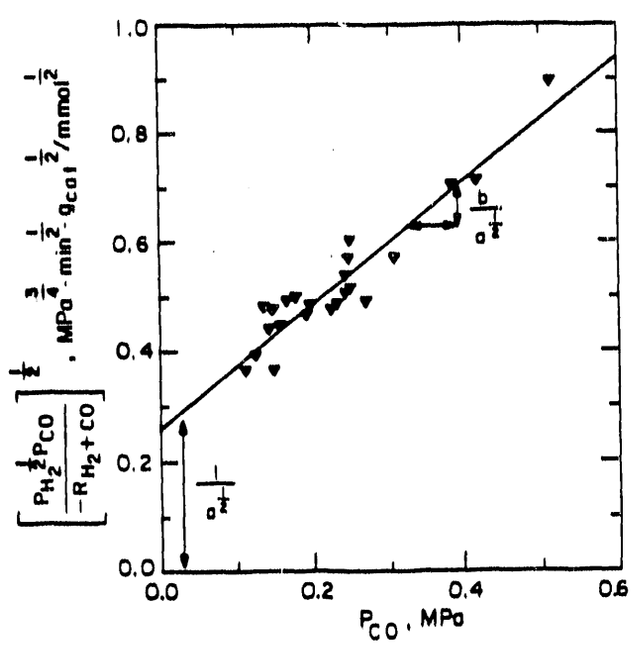

Fig. II-6 Test of eq 20 with experimental results at 240°C. Solid line is best fit linear regression line.

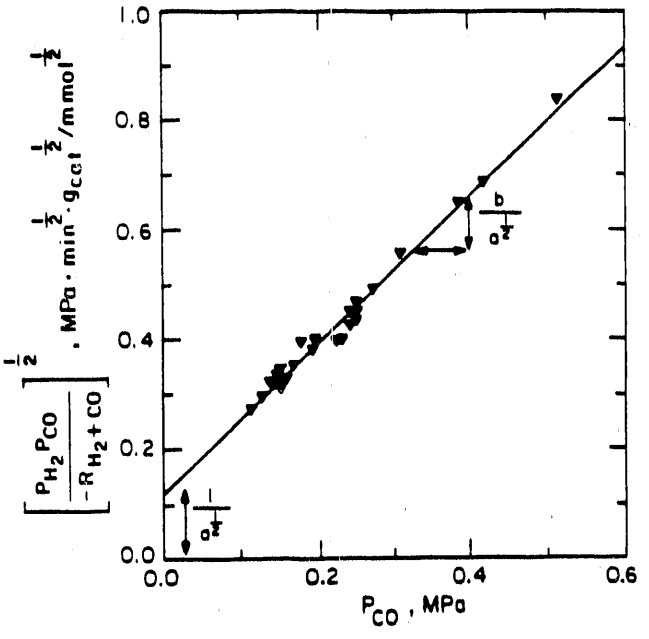

Fig. II-7 Test of eq 21 with experimental results at 240°C. Solid line is best fit linear regression line.

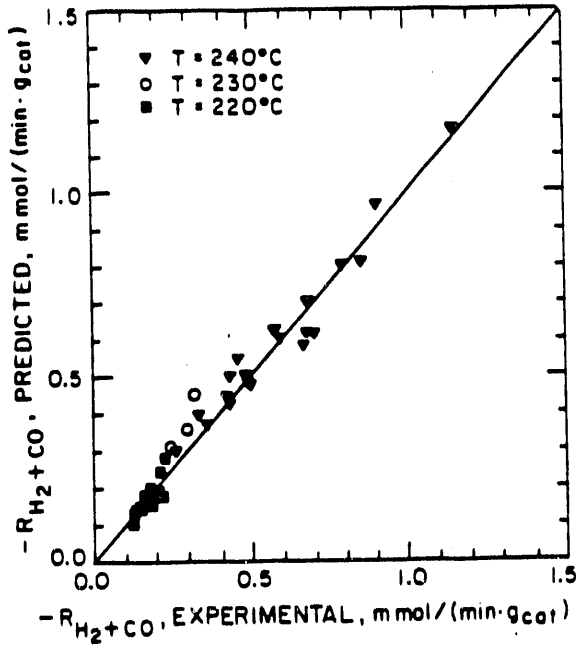

Fig. II-8 Parity plot comparison of data with prediction from eq. 16. Solid line gives predicted values.

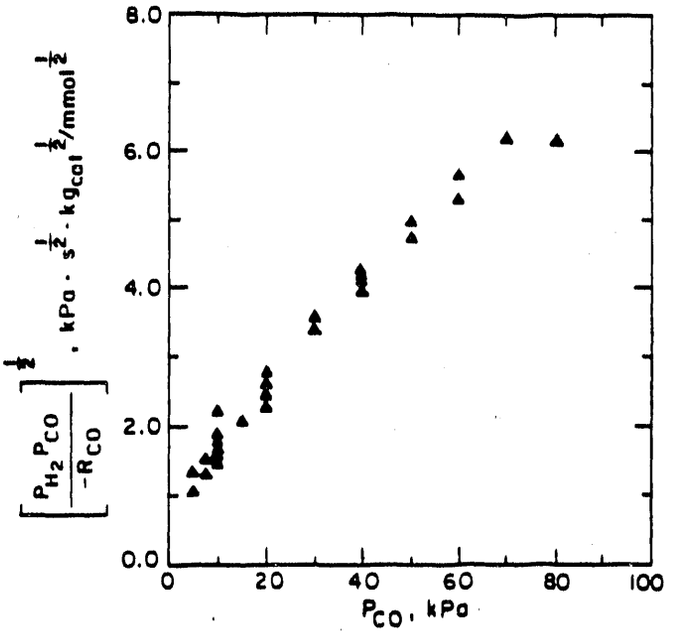

Fig. II-9 Test of eq 21 with data from Rautavuoma and van der Baan.[5]

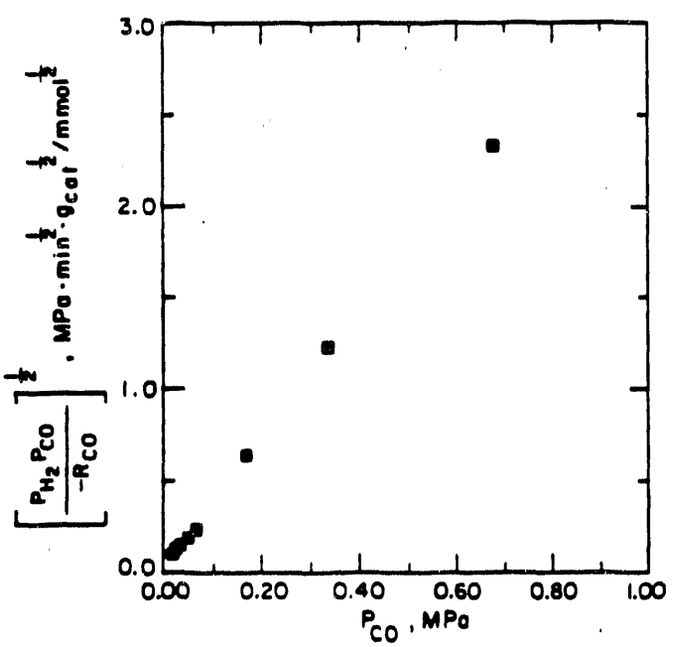

Fig. II-10 Test of eq 21 with data from Wang[6] (pp 100-101).

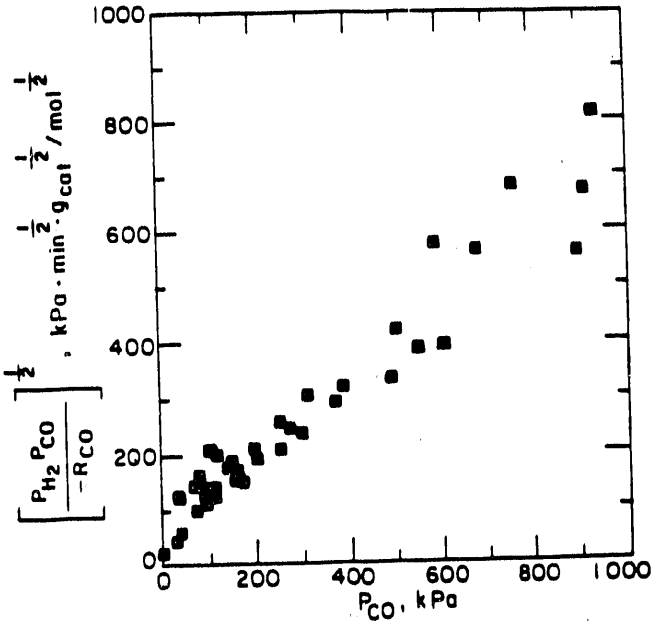

Fig. II-11 Test of eq 21 with data from Sarup and Wojciechowski.[7]

III. The Hydrocarbon Selectivity of Cobalt Fischer-Tropsch Catalysts

Abstract

Increasing space velocity (decreasing conversion) or decreasing reactor H_2/CO ratio decreased the yield of (undesired) C_1 products and increased the yield of (desired) $C_{10}+$ products. Reactor temperature and pressure had little effect on the carbon number distribution. These findings are interpreted in terms of the extent of the readsorption of 1-alkenes into growing chains on the catalyst surface. The relative selectivity to 1-alkenes by the primary synthesis and secondary reaction of l-alkenes to n-alkanes and 2-alkenes depends on reactor H_2/CO ratio and CO concentration.

III. A. Introduction

The chemistry of the Fischer-Tropsch synthesis can be described as the polymerization of single-carbon units on a catalytic site.[1-3] The distribution of products may be characterized by a parameter α, the Schulz-Flory chain growth probability; in its simplest formulation α is the likelihood that a C_n species on the catalyst surface will add another carbon and become a C_{n+1} species, rather than desorb as a product. More than one chain growth probability may exist. The existence of product distributions with two chain growth probabilities, α_1 for low carbon numbers and α_2 for high carbon numbers, has been observed experimentally on iron catalysts by many investigators[4-7] and has been reported also for cobalt in a study by Schulz.[8]

On iron-based Fischer-Tropsch catalysts, a sharp "break" from α_1, with a value usually near 0.6, to α_2, having a higher value, usually near 0.9, occurs on a semi-logarithmic plot of mole fraction versus carbon number, typically at about C_{10}. The double-α and its mathematical development are discussed in detail by Donnelly et al.[3] Data from previous studies indicate that the break from α_1 to α_2 may be less pronounced on cobalt catalysts than on iron catalysts.

The objective of this part of the study was to characterize the hydrocarbon selectivity on a cobalt Fischer-Tropsch catalyst as a function of process variables over a wide range of industrially-relevant conditions. Particular attention was paid to understanding the effects of process variables on the yield of desired high-molecular weight products.

The secondary reactions of 1-alkenes can have a significant effect on the observed product distributions on cobalt. 1-Alkenes can incorporate into growing chains, the

extent of which is affected by competitive reactions, largely alkene hydrogenation and isomerization to the 2-alkene. The effects of 1-alkenes deliberately added during synthesis on the product distribution on cobalt catalysts will be discussed in an accompanying paper,[9] together with relevant literature.

III. B. Literature Review

Reports on hydrocarbon distributions from cobalt catalysts date back to the early days of the Fischer-Tropsch synthesis in Germany, in which cobalt was used in industrial plants during World War II. Results from this early German work and other studies immediately following World War II are summarized by Storch et al.[10] On the $Co/ThO_2/MgO$/kieselguhr catalysts studied, the selectivity to heavy products increased with decreasing H_2/CO ratios, and reportedly went through a maximum with respect to pressure between 0.5 and 0.85 MPa and remained unaffected by conversion. From a considerable number of more recent studies, we comment only on those most closely related to our work. Product distributions can be affected by many variables such as operating pressure, temperature, degree of conversion, H_2/CO ratio, catalyst composition, and nature of reactor, such as integral fixed bed versus a well-mixed flow reactor. Thus some reported results may seem to be contradictory.

Borghard and Bennett[11] studied a 34 wt.% Co/SiO_2 catalyst at 2.03 MPa and 250°C with a H_2/CO feed ratio of 2 in a fixed bed reactor and compared the product distribution with that from several iron catalysts. In differential reactor studies performed at 250°C, atmospheric pressure, and conversions below 2% on a Co/Al_2O_3 catalyst, Rautavuoma and van der Baan[12] report data on the C_1-C_7 hydrocarbon

distribution. Values of α varied from 0.49 to 0.82. Beuther et al.[13] describe Fischer-Tropsch synthesis on 100 Co:18ThO_2:200Al_2O_3 and 21.9% Co: 0.5% Ru: 2.2% ThO_2: 74.5% Al_2O_3 catalysts. The data are somewhat difficult to interpret, but the selectivity to higher hydrocarbons can be inferred to decrease with increasing temperature.

The most extensive results are from a variety of studies by Schulz and co-workers. Some of these appear in rather inaccessible sources and frequently work with cobalt is discussed in conjunction with more extensive studies on iron. The most extensive studies were apparently obtained by Schulz[8] on five different cobalt compositions, all containing ThO_2 and a silica gel support. Three also contained MgO. Reaction conditions were varied from 0.1 to 3.3 MPa, 175 to 210°C and H_2/CO ratios usually of 1.8 to 2.0, utilizing a fixed bed reactor. A double α product distribution is reported, breaking at about C_{10}, attributed to incorporation of olefinic primary products. The carbon number distribution of products varied substantially with operating conditions.

From this study and a later report summarizing much of his work, Schulz et al.[14] drew a number of generalizations. The ratio of alkenes to alkanes decreased with increasing carbon number, increased with increasing pressure and decreased with increasing space velocity (lower conversion). These are basically trends in alkene hydrogenation. Higher molecular weight alkenes are postulated to be more strongly adsorbed, the reduction in hydrogenation at higher pressures is attributed to inhibition of alkene adsorption by increased adsorption of CO. At high space velocities (low conversion) increased hydrogenation is attributed to higher hydrogen pressure. Hydrogenation increased with increasing temperature, which can also be interpreted in terms of competitive adsorption of CO, that would be expected to decrease at higher

temperatures. Methane selectivity was reported to be in the range of 7 to 14 carbon% (% of total C in hydrocarbon products, qualitatively very similar to wt.%) and increased with increasing temperature. The formation of 2-alkenes was lower at low conversions, and decreased with increasing pressure and temperature. The isomerization of 1-alkenes to 2-alkenes increased with increasing carbon numbers, possibly as a result of longer residence times of higher-molecular weight 1-alkenes.

Operating with a Berty reactor at 250°C, Sarup and Wojciechowski[15] examined the effect of H_2/CO ratio on product distribution over a Co/SiO_2 catalyst Products from C_1 to C_{30} were identified as predominantly linear alkanes, monomethyl isomers and some 1- and 2-alkenes. The C_3+ products were reported to follow a single-α Schulz-Flory distribution. However, graphs of the data taken after a significant time-on-stream show a possible second α beginning in the C_{10} range. The chain growth probability decreased with increasing H_2/CO ratio.

Fu et al.[16] studied 10 and 15 wt.% Co on Al_2O_3 at 0.1 MPa in a differential reactor. Temperature was varied from 200°C to 235°C, H_2/CO ratios from 0.5 to 3, and a four-fold range of space velocities was examined. Selectivities are reported in terms of C-number ranges, the highest being $C_{12}+$. The resulting α_1 values varied from about 0.6 to 0.8. Chain growth probability decreased with increasing inlet H_2/CO ratio and increasing temperature.

III. C. Hydrocarbon Carbon Number Distributions

Cobalt catalysts form mostly straight chain hydrocarbons. In the range of C_{10} to C_{20}, such products are of value as diesel and jet fuels. Heavier waxy products in the

C_{20}+ range can be hydrocracked back to lower molecular weight fuels. The results presented here focus on the effects of process variables on the hydrocarbon product distributions of the synthesis. Particular attention was paid to the selectivity to the desired C_{10}+ fraction and the undesired C_1 fraction. Because incorporation or secondary reactions of alkenes may be responsible for the sensitivity of the product distributions to operating conditions, the secondary reactions of synthesized 1-alkenes were also examined.

III. C. 1. Representative Product Distributions. Figures III-1 and III-2 show representative Schulz-Flory diagrams of products volatilized from the reactor. The C_3+ data are well described by a double-α Schulz-Flory model. The solid line in Figures III-1 and III-2 is the best-fit nonlinear regression of a double-α model as developed by Donnelly et al.[3] Above about C_{15}-C_{20}, the overhead product distribution deviates increasingly from that actually formed because of retention of heavy products in the reactor.

This model was used as a basis for comparison of the data from this study with data from previous studies on iron catalysts. For the two material balances shown, α_1 is calculated to be about 0.54 and α_2 near 0.89. The "break" carbon number, the carbon number at which the contributions of both α_1 and α_2 are equal, is near 5, which is lower than is typically observed on iron catalysts.[20,21,22] For a description of this two-site interpretation of the double-α, see [4,20,22].

Figure III-3 shows a Schulz-Flory diagram of a wax sample taken from the reactor slurry at the end of the run. The value of α_2 estimated by linear regression of the data

between C_{30} and C_{53} was 0.87. Although this sample represents the sum of all product distributions from the entire run, note that this value of α_2 is close to that calculated by the nonlinear regression from the overhead products. The asymptotic linear relationship holds over a wide range of carbon numbers, indicating that chain growth probability reaches a constant value at high carbon numbers.

III. C. 2. The Effect of Operating Parameters. A useful method of reporting results on product distributions is to report α_1, α_2, and either Ω, the breakpoint between the two distributions, or x_1, the product fraction formed by the α_1 distribution. In addition, we determine respective 95% confidence intervals or standard deviation of parameter estimate. However, Ω or x_1 is difficult to estimate precisely from regression of experimental data and therefore, an additional method of reporting selectivity data is useful. Because of low volatility, products at higher carbon numbers tend to remain in the slurry liquid. Therefore, to develop a complete distribution of the products being synthesized, the mole fractions above C_{15} must be estimated.

The recommended method used here is as follows. First, the data from C_3 to C_{11} are fit and estimates of α_1, α_2, and Ω made. Second, the mole fractions from C_N to C_{100} are extrapolated and used to generate estimates of the "data" in terms of weight fractions. Assuming that all products above C_N have the molecular weight of alkanes is generally reasonable; however, if more precise estimates about the within-carbon-number selectivity are known, these can be included also. Third, the actual weight of products produced at C_1 and C_2 are included and the data are then expressed in terms of weight classes. Weight classes which are industrially-relevant are C_1, C_2-C_4 (light gas), C_5-C_9

(gasoline), and C_{10}+ (diesel and wax). Finally, to check that the estimate of the weight classes is reasonable, the closure on carbon, including the extrapolated hydrocarbons, is estimated and required to fall between 95 and 105%.

By expressing the data in terms of these weight classes, minor differences in the nonlinear regression results will have less tendency to mislead interpretation of the data and selectivity correlation. For example, in some analyses α_2 may seem slightly high, while Ω may be also be high; thus, it is impossible to determine which conditions are better by examining the effect of process conditions on α_2 only. To simplify presentation of the results here, only C_1 and C_{10}+ products are reported. These two product classes are representative of undesirable and desirable products, respectively.

III. C. 3. Space Velocity. Figure III-4 shows the effect of space velocity on the yield of products at 0.79 MPa, 240°C, and H_2/CO feed ratio of 2. This H_2/CO feed ratio is near the usage ratio of cobalt and therefore varying space velocity has little effect on reactor H_2/CO. Increasing space velocity (decreasing conversion) increases the fraction of C_{10}+, while decreasing the yield of C_1 products.

One possible interpretation is that at higher conversions, a product, such as water, might readsorb onto the surface of the catalyst and increase chain termination. However, the effect seems to be related rather to the extent of chain incorporation of 1-alkenes relative to being hydrogenated or isomerized to 2-alkenes. At higher space velocity (lower residence time), 1-alkenes are hydrogenated or isomerized less than at lower space velocities because of the decrease in residence time of the 1-alkenes.

III. C. 4. Pressure. Figure III-5 shows that, at 220°C and 0.017-0.018 Nl/min/gcat (unreduced basis) of $H_2/CO=2$ synthesis gas, the selectivity to C_1 and $C_{10}+$ products remained constant over a range of total reactor pressure of 0.5 to 1.5 MPa. In a study at 175°C, and pressures of 0.12 to 3.3 MPa, using a (H_2/CO) inlet ratio of 1.8, Schulz[8] reported that methane selectivity decreased with increasing pressure. The $C_{10}+$ product distribution scattered considerably with pressure. The (H_2/CO) exit ratio was nearly constant, in the range of 1.6 to 1.7.

III. C. 5. Temperature. Figure III-6 shows the dependence of the weight fractions of C_1 and $C_{10}+$ for total synthesis gas conversions between 31 and 33% at 220 and 240°C. Data are presented at comparable conversion, rather than equivalent space velocities, because the ratio of product to reactant concentration appears to have a marked effect. No trend is observed over this limited temperature range. In a study at 1.7 MPa and 170 to 190°C, using a (H_2/CO) inlet ratio of 1.0, Schulz[8] reported that methane formation increased with temperature but there was little effect of temperature on the $C_{10}+$ distribution. However the exit (H_2/CO) ratio varied substantially through the reactor. The exit value decreased from 0.65 at 170°C to 0.24 at 190°C.

III. C. 6. Reactor H_2/CO Ratio. Figure III-7 shows the effect of reactor H_2/CO ratio on the relative yield of C_1 products at 220°C. Similar plots were generated showing the analogous trends at 230 and 240°C[23] but are not shown here. Increasing reactor H_2/CO ratios increases the relative weight fraction of C_1 at all temperatures, although the trend is more apparent at lower temperatures. Methane may be formed by a mechanism separate from chain growth, which may have a positive dependence on the

P_{H_2}/P_{CO} ratio, as is examined below.

Figure III-8 shows the effect of reactor H_2/CO ratio on the fractional yield of products in the $C_{10}+$ range at 220°C. Again, similar plots were generated showing the analogous trends at 230 and 240°C,[23] but are not shown here. Increasing reactor H_2/CO ratio decreases the yield of high-molecular weight products relative to total hydrocarbons synthesized. This decrease can be primarily attributed to the increase in rate of production of low-molecular weight products, particularly methane. This general trend has also been reported by others.[8,11,16]

III. D. Selectivity to Various Product Classes

Figures III-9 and III-10 show component Schulz-Flory diagrams including the distribution of three major product classes, n-alkanes, 1-alkenes, and n-alcohols. Three other components were observed in much lower concentrations than these at each carbon number; in order of relative abundance, they were 2-alkenes, branched alkanes, and aldehydes (only at C_2 and C_3 and in very low concentrations). Methane lies above the line that would be predicted by a double-α Schulz-Flory mechanism, while C_2 products lie below, as is characteristic of most Schulz-Flory diagrams of hydrocarbon products.[3] The observed C_2 concentration on cobalt is generally less than on iron.[8]

Both the n-alkanes and n-alcohols exhibit a double-α type distribution; that is, at low carbon numbers, the mole fraction of products drops off quickly, while, at higher carbon numbers, the mole fraction drops off more slowly. Above C_3, the fraction of synthesized products which are hydrogenated increases with increasing carbon number.

In contrast to n-alkanes and n-alcohols, 1-alkenes appear to follow a single-α type

distribution in Figures III-9 and III-10. The extent to which observed products represent primary synthesis versus secondary reactions varies depending on reactor conditions. 1-alkenes, presumed to be the primary product of the synthesis by Schulz et al.,[14] may be hydrogenated to n-alkanes or isomerized to 2-alkenes. The ratio of 1-alkene/n-alkane and 1-alkene/2-alkene both decrease with increasing carbon number, as was also observed by Schulz[8] and Rautavuoma and van der Baan.[12] As shown below, a large fraction of n-alkanes appear to be produced by the hydrogenation of 1-alkenes. Therefore, assuming independent mechanisms for the production of 1-alkenes and alkanes, based on differences in component Schulz-Flory diagrams, may be incorrect.

Since the formation of C_1 products appeared markedly different from the formation of other components, we examined the fit of the rate expression developed elsewhere for the consumption of synthesis gas to the formation of C_1 and C_2+ products as two separate groups. The expression is[24]:

$$-R_{H_2+CO} = \frac{aP_{CO}P_{H_2}}{(1 + bP_{CO})^2} \qquad (22)$$

Figure III-11 shows that the rate of C_1 formation is well fit by the linearized form of equation 1. Figure III-12 shows that the rate of C_2+ formation is also well fit by equation 1. Thus, the decrease in yield of higher molecular weight products with increasing H_2/CO does not seem to result from competing rate mechanisms for formation of C_1 versus C_2+ products.

III. E. Secondary Reactions of 1-Alkenes

In characterizing secondary reactions, the rate of formation of ethane, n-butane, and 2-butene were studied. Ethane represents hydrogenation only; the behavior of the C_4 compounds is taken as representative of that of the C_3+ products. As discussed by Hanlon and Satterfield,[25] and Donnelly and Satterfield,[7] C_4 products are the highest molecular weight products which do not split between vapor and liquid phases in our traps and therefore are the least subject to experimental error.

III. E. 1. Rate of Ethane Formation from Ethene. Figure 13 shows the dependence of the rate of formation of ethane on the ratio of $P_{C_2H_4}P_{H_2}/P_{CO}$ in the reactor; data at 220°C are shown as representative. This assumes that ethane formation is a simple hydrogenation process inhibited by adsorbed CO. While the data scatter somewhat, much of the variation in the rate of ethane formation can be explained by such a simple model. The vertical axis intercept of this figure represents the amount of ethane produced as primary product. Over most of the range of operating variables studied, the amount of ethane produced by primary synthesis is less than half of the total amount synthesized.

III. E. 2. Rate of n-Butane Formation from 1-Butene. Figures 14 shows the dependence of the rate of formation of n-butane on the ratio of $P_{C_4H_8}P_{H_2}/P_{CO}$ in the reactor; data at 220°C are shown as representative. Again, a simple hydrogenation process inhibited by adsorbed CO is assumed. While there is considerable scatter in the data in Figure 14, the rate of n-butane formation clearly increases with increasing $P_{C_4H_8}P_{H_2}/P_{CO}$. The vertical axis intercept of this figure is related to the amount of n-

butane produced in the primary synthesis; over the range of operating variables studied, the amount of n-butane produced by primary synthesis is generally less than half of the total amount synthesized.

The behavior of these two simple hydrogenation models is consistent with the observations of Schulz[8,14] and Rautavuoma and van der Baan[12] on cobalt and Donnelly and Satterfield[7] on iron that increasing hydrogen to carbon monoxide ratio decreases the 1-alkene/n-alkane ratio.

III. E. 3. Rate of 2-Butene Formation from 1-Butene. 2-alkenes are not considered to be a primary product, but are assumed to be produced solely by isomerization of 1-alkenes.[14] Thus a model was developed which accounts for all of the production of 2-butene in terms of 1-butene isomerization. A Langmuir-Hinshelwood-type relationship of the following form is proposed:

$$R_{2\text{-butene}} = \frac{kP_{1\text{-butene}}}{(1 + K_{CO}P_{CO})} \qquad (2)$$

Equation 2 assumes that the rate of 2-butene formation is simply proportional to the concentration of 1-butene and inhibited by carbon monoxide. Equation 2 can be linearized, yielding

$$\frac{P_{1\text{-butene}}}{R_{2\text{-butene}}} = \frac{1}{k} + \frac{K_{CO}P_{CO}}{k} \qquad (3)$$

Following the relationship of equation 3, Figures III-15a and III-15b depict the dependence of the rate of formation of $P_{1\text{-butene}}/R_{2\text{-butene}}$ on P_{CO} at 220 and 240°C respectively. Both figures show that increasing P_{CO} will decrease the rate of 1-butene isomerization. Data from two temperatures are shown here in order to justify the added complexity of the proposed two-parameter 2-alkene production model.

The conclusion of Schulz et al.[14] that the ratio of 1-alkenes/total alkenes increases with increasing total pressure is consistent with equation 2 since the range of values of (H_2/CO) through his fixed bed reactor was within the range of 1.8 to 1.6 throughout his wide range of pressure.

III. E. 4. Summary. Three interesting conclusions can be drawn. First, a large fraction of the alkanes and all 2-alkenes appear to be produced by secondary reactions. Second, increasing the reactor H_2/CO ratio increases the ratio of alkane to 1-alkene at each carbon number. If 1-alkenes readsorb onto the catalyst surface and incorporate into growing chains, then the decrease in 1-alkene concentration, relative to n-alkane concentration, at increased P_{H_2}/P_{CO} may explain the decrease in high-molecular weight products at high P_{H_2}/P_{CO}. Finally, increasing the concentration of carbon monoxide may decrease the amount of 2-alkene formation. If 1-alkene incorporation plays a role in hydrocarbon production, then again the decrease in 1-alkene concentration, relative to 2-alkene concentration, at low values of P_{CO} may explain the decrease in high-molecular weight products at high values of P_{H_2}/P_{CO}. Studies of the extent to which 1-alkene incorporation is affected by process variables such as temperature and total pressure may

provide fundamental insight into the effects of process variables on the selectivity of the synthesis.

III. F. Conclusions

The relative production of $C_{10}+$ on a weight basis increased with increasing space velocity and decreasing reactor H_2/CO, but was independent of reactor pressure or temperature. Conversely, the relative yield C_1 on a weight basis decreased with increasing space velocity and decreasing reactor H_2/CO, and was also relatively insensitive to reactor pressure or temperature.

Above C_3, the 1-alkene/n-alkane ratio decreased with increasing carbon number. Hydrogenation modelling indicates that a large fraction of the n-alkanes were synthesized by hydrogenation of 1-alkenes, a primary synthesis product. Increasing the reactor H_2/CO ratio decreased the 1-alkene/n-alkane ratio, while increased concentrations of CO in the reactor inhibited the isomerization of 1-alkenes to 2-alkenes.

III. G. Literature Cited

(1) Herington, E.F.G. Chemistry and Industry **1946**, 65, 346.

(2) Anderson, R.B. The Fischer-Tropsch Synthesis; Harcourt, Brace & Jovanovich: New York, 1984.

(3) Donnelly, T.J.; Yates, I.C.; Satterfield, C.N. Energy & Fuels **1988**, 2, 734.

(4) König, L.; Gaube, J. Chem.-Ing. Tech. **1983**, 55, 14.

(5) Huff, G.A., Jr.; Satterfield, C.N. J. Catal. **1984**, 85, 370.

(6) Dictor, R.A.; Bell, A.T. J. Catal. **1986**, 97, 121.

(7) Donnelly, T.J.; Satterfield, C.N. Appl. Catal. **1989**, 52, 93.

(8) Schulz, H. Report to the Bundesministerium für Forschung und Technologie, "Katalysatoren und Selektivitätslenkung bei der Fischer-Tropsch-Synthese," BMFT-FB-T 80-124, Nov., 1980.

(9) Yates, I.C.; Satterfield, C.N. to be submitted.

(10) Storch, H.H.; Golumbic, N.; Anderson, R.B. The Fischer-Tropsch and Related Syntheses; John Wiley and Sons: New York, 1951.

(11) Borghard, W.G.; Bennett, C.O. Ind. Eng. Chem. Process Res. and Dev., **1979**, 18, 18.

(12) Rautavuoma, A.O.I.; van der Baan, H.S. Appl. Cat., **1981**, 1, 247.

(13) Beuther, H.; Kibby, C.L.; Kobylinski, T.P.; Pannell, R.B. United States Patent 4,399,234, August 16, 1983.

(14) Schulz, H.; Rosch, S.; Gokcebay, H. Proceedings 64th CIC Coal Symposium-A.M. Al Taweel, ed., C.S.Ch.E., Ottawa (1982).

(15) Sarup, B.; Wojciechowski, B.W. Can. J. Chem. Eng., **1984**, 62, 249.

(16) Fu, L.; Rankin, J.L.; Bartholomew, C.H. C1 Mol. Chem., 1986, 1, 369.

(17) Huff, G.A., Jr.; Satterfield, C.N. Ind. Eng. Chem. Fund., 1982, 21, 479.

(18) Donnelly, T.J.; Satterfield, C.N. Appl. Catal. 1989, 56, 231.

(19) Huff, G.A., Jr.; Satterfield, C.N. Ind. Eng. Chem. Process Des. Dev., 1984, 23, 696.

(20) Huff, G.A., Jr. Fischer-Tropsch Synthesis in a Slurry Reactor, Sc.D. Thesis, Massachusetts Institute of Technology, Cambridge, Massachusetts, 1982.

(20a) Huff, G.A., Jr.; Satterfield, C.N.; M.H. Wolf, Ind. Eng. Chem. Fund., 1983, 22, 258.

(21) Matsumoto, D.K., The Effects of Selected Process Variables on the Performance of an Iron Fischer-Tropsch Catalyst, Sc.D. Thesis, Massachusetts Institute of Technology, Cambridge, Massachusetts, 1987.

(22) Donnelly, T.J., Product Distributions of the Fischer-Tropsch Synthesis, Ph.D. Thesis, Massachusetts Institute of Technology, Cambridge, Mass., 1989.

(23) Yates, I.C., The Slurry-Phase Fischer-Tropsch Synthesis, Ph.D. Thesis, Massachusetts Institute of Technology, Cambridge, Massachusetts, 1990.

(24) Yates, I.C.; Satterfield, C.N. Energy & Fuels, 1991, 5, 168.

(25) Hanlon, R.T.; and Satterfield, C.N. Energy & Fuels, 1988, 2, 196.

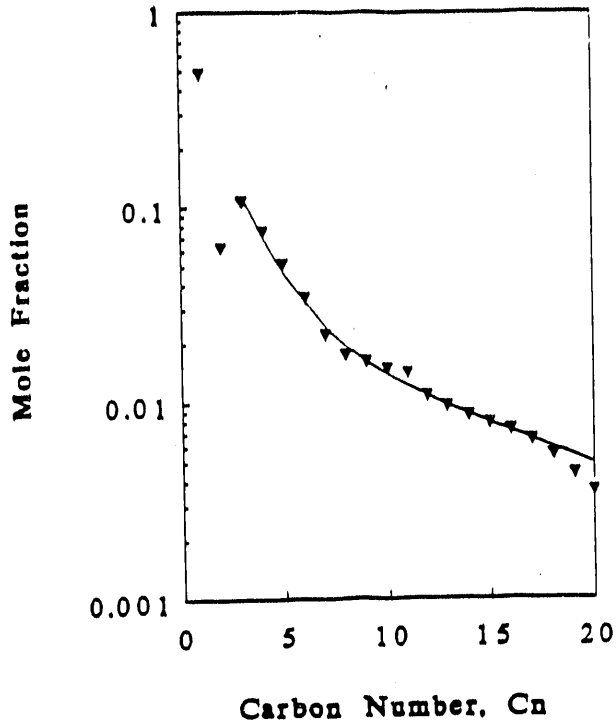

Fig.III-1 Representative Schulz-Flory Diagram showing a double-α-type distribution (220°C, 1.48 MPa, feed rate = 0.032 Nl/min/gcat). $(H_2/CO)_{in} = 1.64$. (H_2/CO) in reactor = 1.65. $\alpha_1 = 0.54$, $\alpha_2 = 0.91$, and $\Omega = 5.4$.

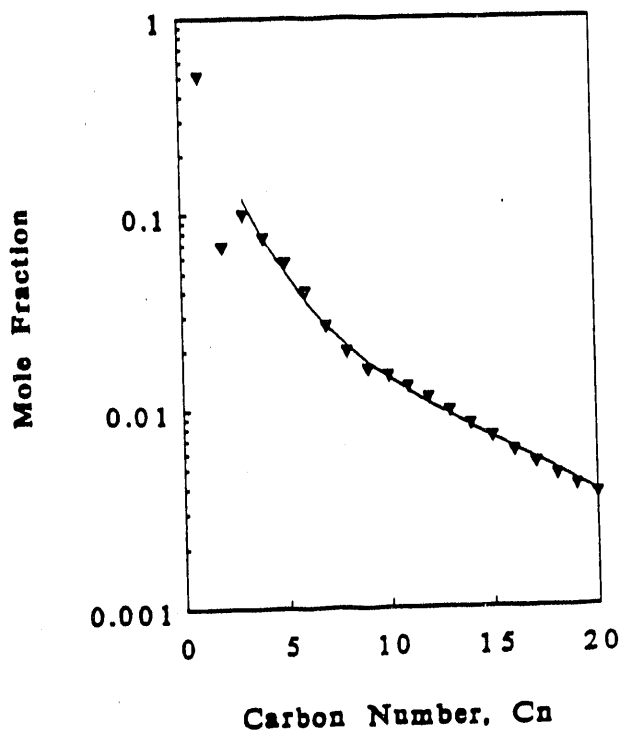

Fig. III-2 Representative Schulz-Flory Diagram showing a double-α-type distribution (230°C, 0.79 MPa, feed rate = 0.020 Nl/min/gcat). (H_2/CO) in reactor = 1.39. $(H_2/CO)_{in} = 1.55$. $\alpha_1 = 0.54$, $\alpha_2 = 0.88$, and $\Omega = 5$.

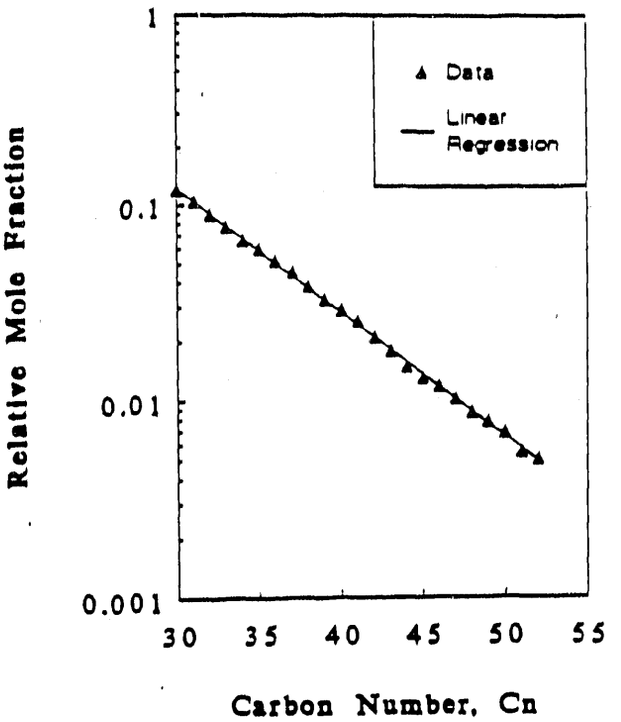

Fig. III-3 Schulz-Flory diagram for reactor liquid at completion of run. $\alpha_2 = 0.87$.

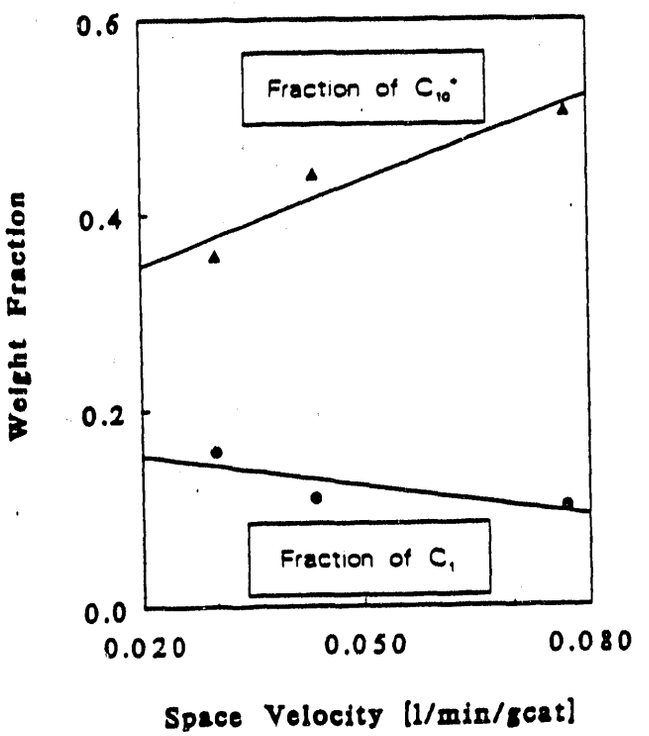

Fig. III-4 The C_{10}+ yield is greater at higher space velocities. Data at 240°C, 0.79 MPa, and $(H_2/CO)_{in} = 2$.

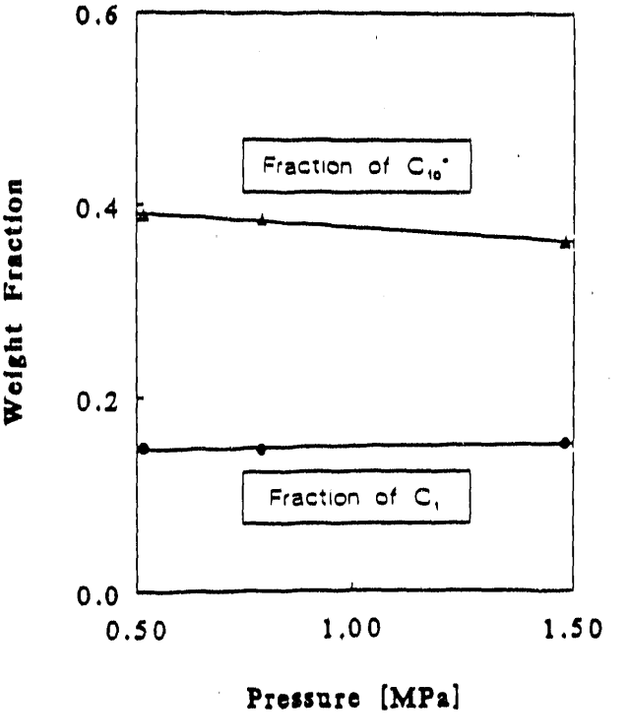

Fig. III-5 Pressure has no noticeable effect on product distribution. Data at 220°C and feed rate of 0.017-0.018 Nl/min/gcat. $(H_2/CO)_{in}=2$.

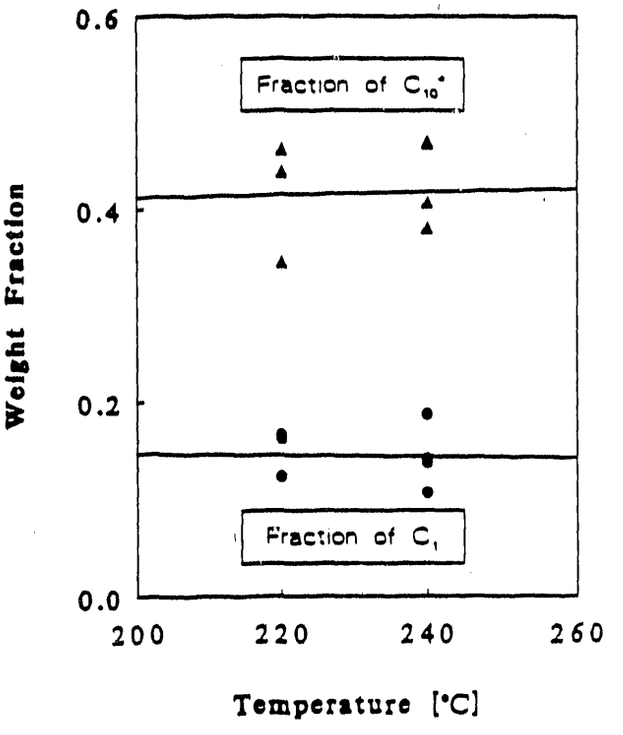

Fig. III-6 Temperature has no effect on product distributions. Total synthesis gas conversions are between 31 and 33%, allowing comparison of similar product to reactant ratios.

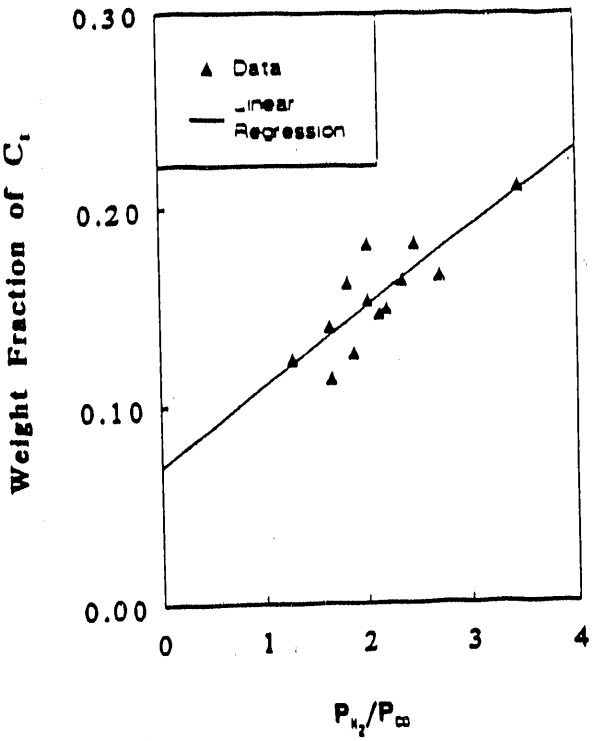

Fig. III-7 Weight fraction of C_1 increases with increasing H_2/CO, 220°C.

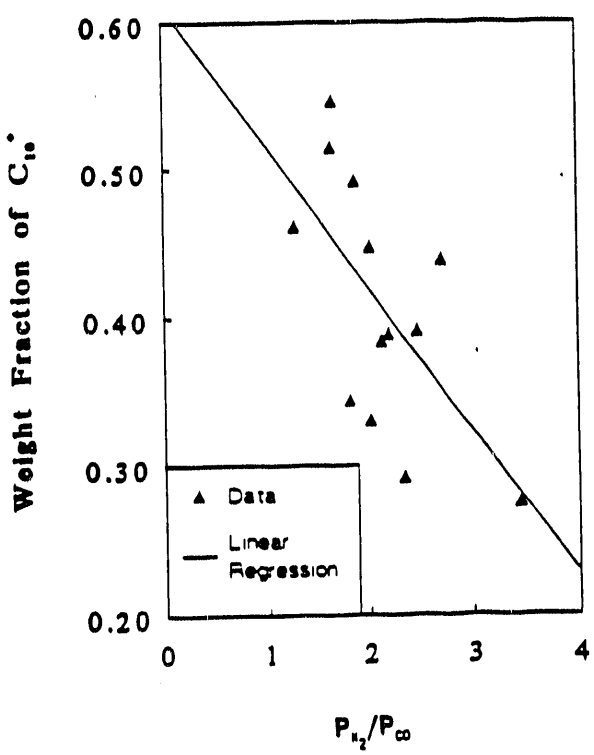

Fig. III-8 Weight fraction of $C_{10}+$ decreases with increasing H_2/CO, 220°C.

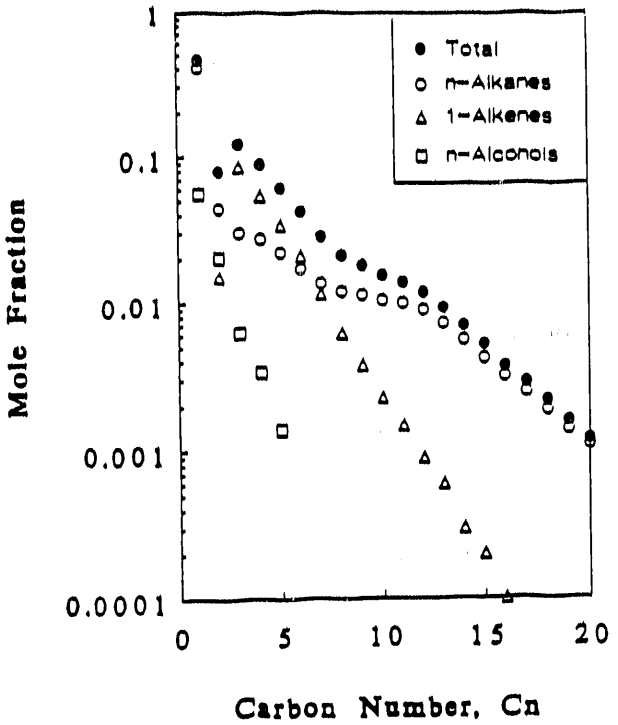

Fig. III-9 Component product distribution showing primary products, n-alkanes, 1-alkenes, and n-alcohols (220°C, 1.48 MPa, and feed rate of 0.015 Nl/min/gcat). $(H_2/CO)_{in} = 1.66$.

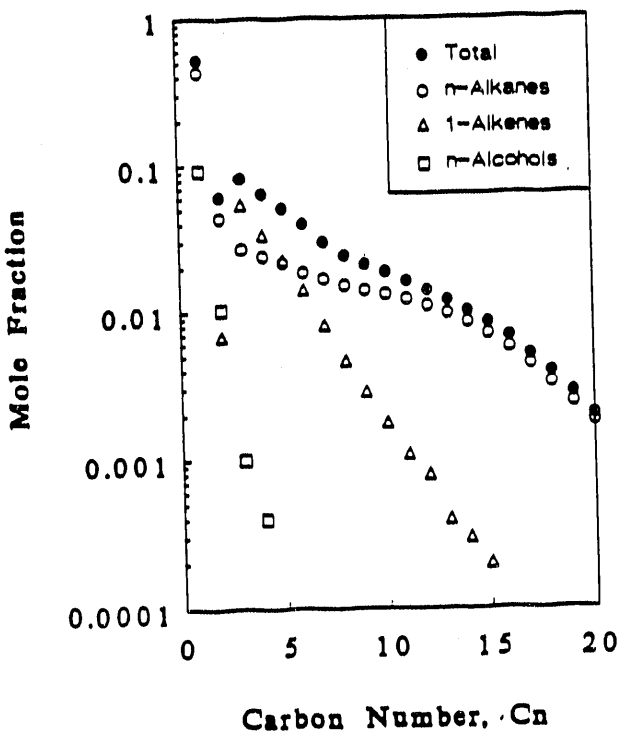

Fig. III-10 Component product distribution showing primary products, n-alkanes, 1-alkenes, and n-alcohol (240°C, 0.79 MPa, and feed rate of 0.035 Nl/min/gcat). $(H_2/CO)_{in} = 2.15$.

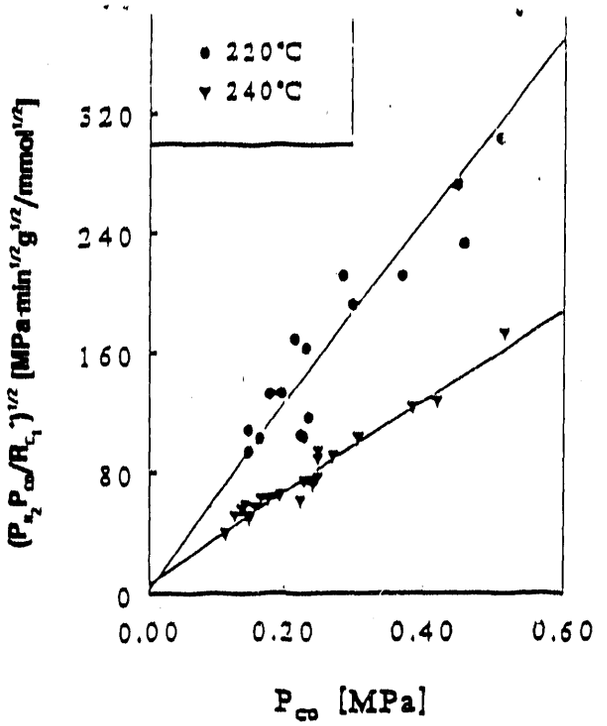

Fig. III-11 The rate of methane plus methanol formation is well fitted by equation 1.

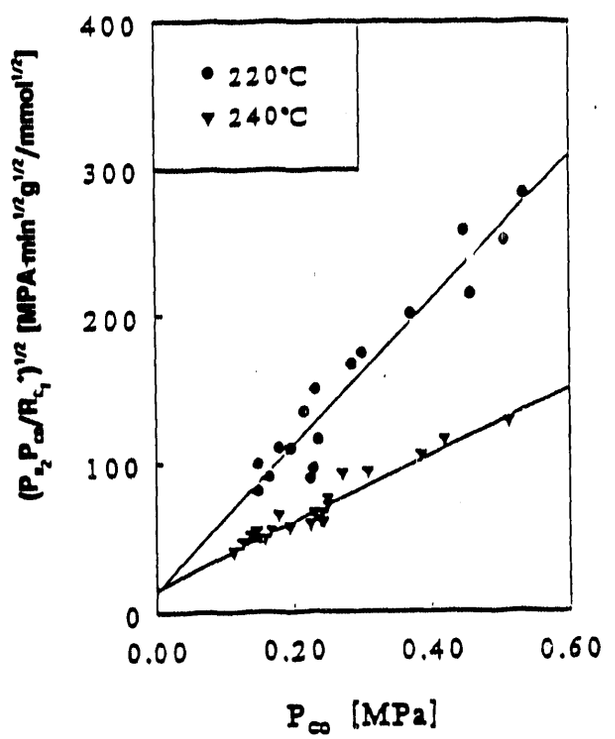

Fig. III-12 Rate of formation of C_2+ compounds is well fitted by equation 1.

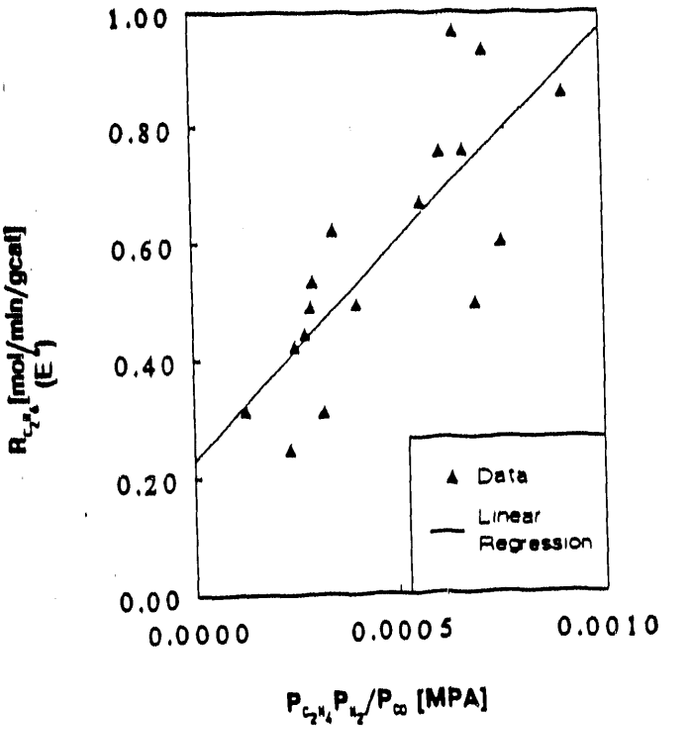

Fig. III-13 Most ethane is produced from ethene, according to a simple hydrogenation model, data at 220°C.

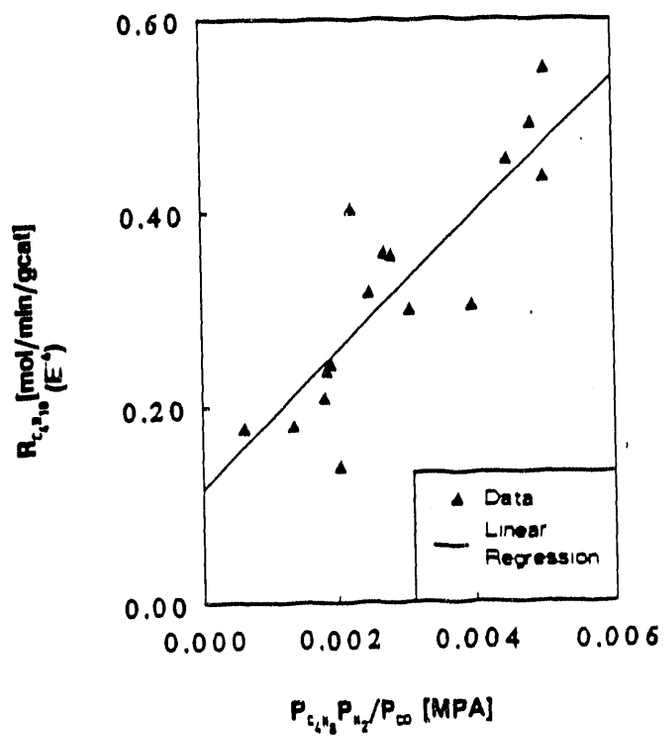

Fig. III-14 Most n-butane is produced from 1-butene, according to a simple hydrogenation model, data at 220°C.

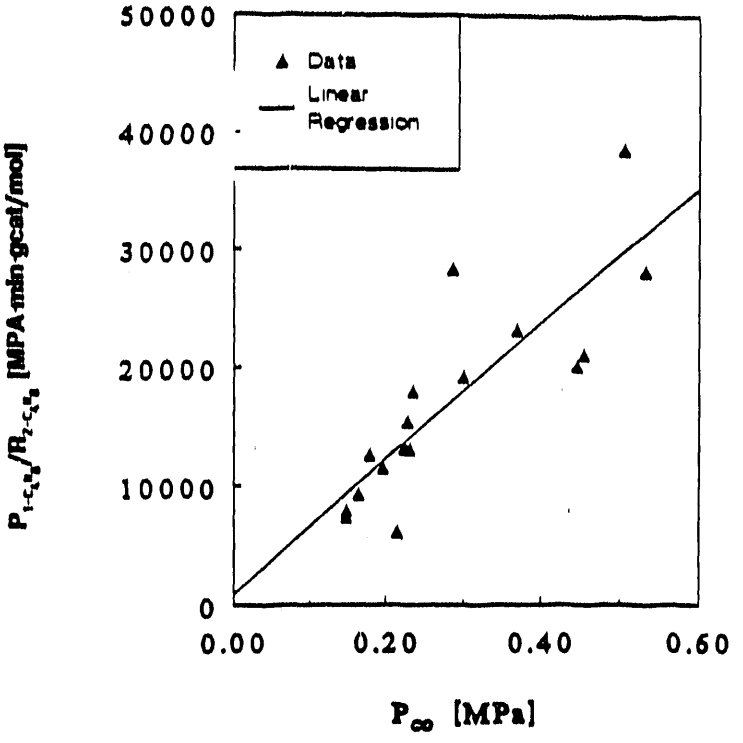

Fig. III-15a Most 2-butene is produced from 1-butene, according to simple isomerization model (see equation 2), 220°C.

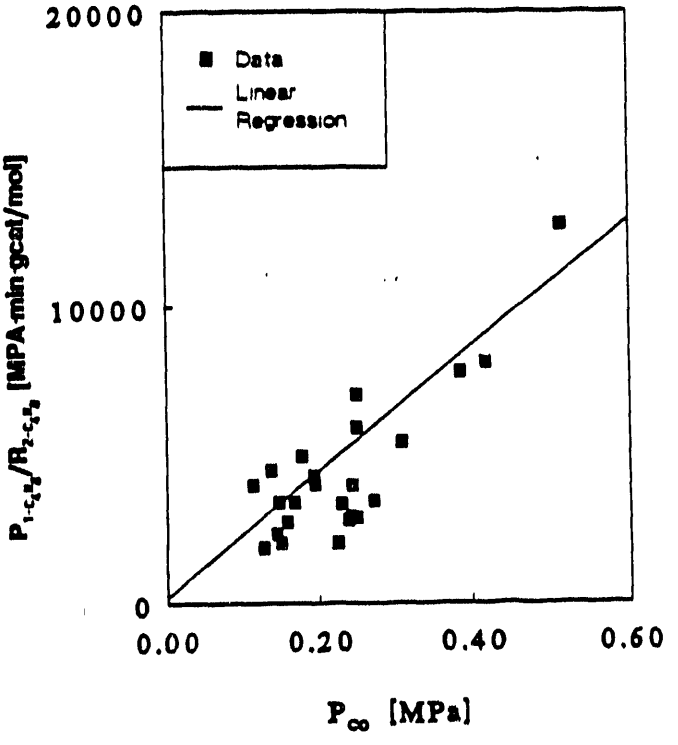

Fig. III-15b Most 2-butene is produced from 1-butene, according to simple isomerization model (see equation 2), 240°C.

IV. The Effect of 1-Alkene Addition on Hydrocarbon Product Distribution on a Cobalt Catalyst

Abstract

The cobalt-catalyzed reactions of C_2H_4, C_3H_6, or 1-C_4H_8 added to synthesis gas in concentrations ranging from 0.5 to 1.2 mol.% of total feed were studied at 220°C, and 0.45 to 1.48 MPa. H_2/CO feed ratios were varied between 1.45 to 2.25 and H_2 + CO conversions between 5 and 30% were observed.

1-Alkenes incorporate into growing chains on the catalyst surface, probably by initiating and/or terminating the chain growth process. Only ethene may propagate chain growth significantly. The propensity of the 1-alkenes to incorporate decreases with increasing carbon number of the 1-alkene and is affected by the extent of competitive reactions, notably hydrogenation to the alkene and isomerization to the 2-alkene. Incorporation is most evident in products above about C_{10}+.

The double-α behavior exhibited by most Fischer-Tropsch catalysts can be interpreted as the sum of two growth processes, one a stepwise single-carbon growth process and the other a 1-alkene incorporation process. Many of the effects of process variables on the hydrocarbon selectivity of Fischer-Tropsch catalysts are consistent with this theory.

IV. A. Introduction

Section III describes the effect of process variables on the product composition and carbon number distribution of a cobalt catalyst. The sensitivity of the hydrocarbon distribution to process variables seems to be greater than that encountered with iron catalysts. Therefore, secondary reactions of 1-alkenes formed by the primary synthesis may be important in determining the final product composition. These reactions are primarily chain incorporation, hydrogenation, and isomerization of a 1-alkene to the 2-alkene. The objective of this part of the study was to develop a more fundamental understanding of the role of 1-alkenes in the hydrocarbon chain growth process on Fischer-Tropsch catalysts.

A large number of studies have been published on the effects observed upon addition of 1-alkenes to synthesis gas in contact with iron catalysts, but relatively little on effects observed on cobalt. Summaries of the literature, focussing on iron, have been published recently.[2-5] In most cases, with either iron or cobalt catalysts, the possibility of chain incorporation has been examined with respect to light hydrocarbon products. There is general agreement that ethene is much more reactive than propylene or butene, but the extent of incorporation is dependent on many variables. Incorporation into light products on iron typically appears to be minor.

Our two previous studies with reduced fused magnetite catalysts in which we added light l-alkenes to synthesis gas indicated that chain incorporation could be observed but was minor in amount. Then we were focussing on carbon products mostly of C_{10} and less. A new feature from our present study is the observation that effects are much more noticeable for higher molecular weight products. In agreement with earlier

work, we conclude that incorporation occurs more readily on cobalt than on iron catalysts. The following summarizes the literature on cobalt.

In early work, Gibson and Clarke[6] fed 5.1 mol.% labelled ^{14}CO, 49.1 mol.% C_2H_4, and 45.8 mol.% H_2 to a 100Co:5ThO_2:8MgO:200kieselguhr catalyst. Operating conditions of their fixed-bed reactor were 185°C, 0.1 MPa, and they achieved about 50% C_2H_4 conversion. The average radioactivity at each carbon atom within the C_6 and C_7 1-alkenes was determined. Because the radioactivity was significantly lower nearer the end of the C_6 and C_7 chains, they concluded that ethene both initiates and terminates the chain growth process. They were unable to determine if ethene propagates chain growth.

Schulz et al.[7] performed the most complete study of the effects of adding selected labelled compounds during synthesis on cobalt. They added ethene (^{14}C), propene (1-^{14}C and 2-^{14}C), butane (1-^{14}C), 2-methylpentadecane (15-^{14}C), and 1-hexadecene (1-^{14}C) at concentrations ranging from 0.10 to 0.78 vol.% of total synthesis gas feed. They ran their fixed-bed reactor at 185-190°C, 0.1 MPa, with $H_2/CO=2$ synthesis gas at a space velocity of 75 Nl/min/liter of catalyst (unreduced basis). For the 1-alkenes studied, hydrogenation to alkanes was the predominant reaction, with 67 mol.% of the added ethene hydrogenated, 51 mol.% of the propene, and 79 mol.% of the 1-hexadecene. Of the added 1-alkene which was not hydrogenated, they found that 88 mol.% of the ethene was incorporated into growing chains, 63 mol.% of the propene, and 31 mol.% of the 1-hexadecene, thus producing higher molecular weight products.

Schulz and coworkers also examined the radioactivity of products at carbon numbers greater than the added component and noted two different behaviors, one for ethene and one for both propene and 1-hexadecene. Adding ethene, products at even

carbon numbers had higher radioactivity than those at odd carbon numbers, indicating that ethene can propagate growing hydrocarbon chains; the levels of radioactivity at odd carbon numbers were consistent with the hypothesis that ethene can terminate and/or initiate growing chains. In contrast, propene was found to propagate growing chains only slightly, producing monomethyl branched compounds. Schulz and coworkers conclude that C_3+ 1-alkenes must be involved predominantly in chain termination and initiation. The added alkanes underwent negligible reaction at the process conditions studied. No data on the effect of process variables on the rate of incorporation were presented.

In a report to the German government, Schulz[7a] reported the results of extensive studies on five cobalt catalysts, all containing ThO_2 on aerosil (a silica gel). Three contained MgO in addition. Reaction conditions were 175 to 185°C and 9 bar. The compositions containing MgO showed a much more pronounced double α than those without and gave a considerably higher fraction of C_{10}+. In the presence of MgO, the C_2H_4 in the product was substantially less than when MgO was absent. Although this was not commented on by the author, this seems to be additional evidence that C_2H_4 was being incorporated into C_{10}+ product and by a mechanism influenced by MgO.

Kibby et al.[8] co-fed ethene or propene at 10 vol.% with a $(H_2/CO)_{in}$ of 1 and 2 to a reduced 30 wt.% Co, 5 wt.% ThO_2, on 65 wt.% Al_2O_3 catalyst in an internal recycle reactor operated at 195°C and 0.79 MPa. To calculate yields to various product classes, Kibby et al. measured the composition of the light gases (C_1-C_4) and determined the yield to C_5+ as the difference between the CO consumption and the C_1-C_4 yield. Present analysis of their data at $(H_2/CO)_{in}$=2 indicates that the wt.% of C_5+ hydrocarbons increased to 62.5 wt.% with ethene addition and 54.7 wt.% with propene

addition, as compared with 44.6 wt.% with no added 1-alkenes. With ethene addition the wt.% of C_5+ hydrocarbons increased to 85.4 wt.% at $(H_2/CO)_{in}=1$ from 62.5 wt.% at $(H_2/CO)_{in}=2$. This effect of decreasing incorporation with increasing H_2/CO ratio is consistent with a set of reaction pathways for alkenes in which hydrogenation and incorporation both consume alkenes competitively; thus, at higher H_2/CO, more alkenes are hydrogenated and consequently less are incorporated in growing chains. In separate experiments at feed conditions similar to Gibson and Clarke,[7] Kibby et al. also observed "hydropolymerization" of ethene, propene, and 1-butene.

Most alkene addition studies on cobalt by various researchers were performed in conjunction with a more extensive study of feed additions to iron catalysts; as a result, cobalt catalysts were studied at only a few different process conditions. Although 1-alkenes appear to be incorporated into growing chains on cobalt, there is little agreement as to the extent to which incorporation affects the product distribution; further, no studies exist which cover a wide range of process conditions, for example only Kibby and co-workers performed experiments at above atmospheric pressure.

IV. B. Experimental Procedure

Catalyst composition, reduction procedure and experimental methods are described in previous sections. After reduction, the catalyst was allowed to achieve stable activity and selectivity. Process variables were then manipulated to provide data over a broad operating range, during the course of a single run that lasted over several hundred hours. Data were obtained at 220°C, 0.45 to 1.48 MPa and synthesis gas flow rate between 0.015 and 0.030 Nl/gcat/min with inlet H_2/CO ratios of 1.45 to 2.25 yielding H_2 + CO conversions between 5 and 30%.

The 1-alkenes were co-fed with the synthesis gas feed in about 2 mol.% of a single 1-alkene in CP Grade CO (Matheson and MedTech Gases, Inc.); each of three 1-alkenes, C_2H_4, C_3H_6, and 1-C_4H_8, were added in quantities to comprise from 0.5 to 1.2 mol.% of total feed. At these feed rates, the added 1-alkenes are present in concentrations ranging from 2 to 10 times those observed during normal synthesis. These light 1-alkenes were chosen because they are not condensed to any significant extent in either our hot or cold traps[10,11] and, therefore, analysis of these light 1-alkenes is less subject to error. 15 material balances were performed adding C_2H_4, six adding C_3H_6, and eight adding C_4H_8.

For each material balance in which 1-alkenes were added, a material balance was performed at similar process conditions without 1-alkenes added, so that comparison of hydrocarbon selectivity with and without alkene addition could be made directly.

IV. C. Evidence for Incorporation on Cobalt

Figures IV-1a, IV-1b, and IV-1c show Schulz-Flory diagrams comparing ethene, propene, and 1-butene additions to material balances at similar process conditions without added alkenes. To avoid presenting dilution effects in these results, data are normalized to remove the "added" carbon number, according to equation 1:

$$\text{Normalized}(M_n) = \frac{\text{Observed}(M_n)}{(1-\text{Observed}(M_{added}))} \qquad (1)$$

In equation 1, Observed(M_n) are the actual mole fraction data and the Observed(M_{added}) is the mole fraction at the carbon number added. Thus, for Figure IV-1a, the actual mole fraction data are divided by (1-M_2); the normalized M_2 are removed from the plot

and thus the normalized data, the first 20 carbon numbers of which are shown on the plot, sum to unity. The figures show that 1-alkenes incorporate into growing chains on the catalyst surface, as evidenced by the increase in products at higher carbon numbers. This increase in products predominantly in the α_2 region of the Schulz-Flory plot will be discussed in detail below.

A measure of the extent to which the C_n added alkene incorporated was determined by comparing the C_{n+1}/C_{n-1} of the material balance with added alkene to the base case material balance. If C_n alkene incorporates, then the C_{n+1} hydrocarbon is affected most dramatically, while the C_{n-1} hydrocarbon yield remains unchanged, assuming negligible cracking. Thus, the higher this C_{n+1}/C_{n-1} ratio is relative to the base case, the more the C_n alkene can be inferred to incorporate.

Figures IV-2a through IV-2c show the ratio of C_{n+1}/C_{n-1} for the C_n addition material balance divided by the C_{n+1}/C_{n-1} for the base case versus P_{H_2}/P_{CO} for ethene, propene, and 1-butene additions respectively. Although the data scatter, ethene can be inferred to incorporate more than propene, which incorporates more than 1-butene. Similar trends upon co-feeding 1-alkenes with synthesis gas were reported on cobalt[7,8] and on iron.[7] Increasing H_2/CO ratio decreases incorporation, seen most readily in Fig. IV-2a. This is consistent with the observation that the rate of hydrogenation of alkenes is approximately proportional to the H_2/CO ratio.[1] In using the C_{n+1}/C_{n-1} criterion with respect to ethylene addition, it should be recalled that methane formation occurs by a mechanism that does not involve a carbon species polymerization.

In most previous studies with olefin addition, either radioactive tracers were used or relatively high concentrations of olefin were added, e.g., 5 to 10 mol% of the synthesis

gas feed, to magnify reaction effects and make possible overall material balances to search for the fate of the added olefin. The approach here was to use much lower added olefin concentrations that were closer to those formed by the normal synthesis, so that the results might be more representative of ordinary practice. This gain was purchased at the loss of being able to make useful material balances on the added component.

To verify that added alkenes were not undergoing cracking to any significant extent, Figure IV-3 shows that the rate expression for the rate of production of methane[9] fits the data collected here, even when alkenes are added to the feed. There are reports from studies on iron that added ethene may have an inhibiting effect on methanation, but these seem to have occurred only with much higher ethene concentrations. Adesima et al.[5] in a study on a cobalt catalyst at 0.11 MPa and 200°C report that methane production rates were unchanged upon addition of 1 to 2% ethene. Figure IV-4 shows a Schulz-Flory diagram for two material balances performed without added alkene and 1850 hours-on-stream apart. Within the scatter of the data, the hydrocarbon selectivity is unchanged with time.

IV. D. Mathematical Modelling of Incorporation

To develop a fundamental understanding of the effect of incorporation on product distributions, mathematical models for incorporation were developed. These models are complex, but their mathematical behavior closely parallels that of a single-α distribution. The double-α is postulated to be the sum of two growth processes, one a stepwise single-carbon growth process, represented by α_1, and the other a 1-alkene incorporation process, represented by α_2.

Alkene incorporation adds mathematical complexity to the mathematical models of the chain growth process and introduces a number of adjustable parameters. Alkenes can be assumed to either initiate and terminate hydrocarbon chains only or initiate, terminate, and propagate chains. These two behaviors are treated separately below.

All formulations for alkene incorporation are somewhat complex, have a large number of parameters, and require knowledge of relative rates of surface reaction that cannot be measured directly. To develop a useful model, the limiting behavior of these different models is shown to match that of a most probable, single-α distribution, except at very low carbon numbers. This single-α chain growth probability is therefore essentially a lumped parameter which accounts for contributions to the chain growth process from the incorporation reactions of the entire series of alkenes.

IV. D. 1. Initiation and Termination by 1-Alkenes. If 1-alkenes initiate and terminate growing chains, then the mole fraction of products observed at a given carbon number (M_n) depends not only on the mole fraction one carbon number before it (M_{n-1}), but also on the mole fractions of all the carbon numbers before it, (M_{n-2}, M_{n-3}, etc.).

Equation 2 shows how the simple, no-incorporation chain growth process represents the dependence of mole fraction at carbon number n on the mole fraction at carbon number n-1, as

$$M_n = p_1 M_{(n-1)} \tag{2}$$

In equation 2, p_1 is analogous to a Schulz-Flory chain growth probability, α.

To develop an equation for 1-alkene incorporation, only ethene and propene are assumed to initiate and terminate alkenes, for the purposes of illustration. This analysis can be easily extended by analogy to include initiation or termination by any number of alkenes; however, for simplicity, only this model is presented.

If ethene and propene can initiate or terminate growing chains, then the mole fraction for C_4+ is given by:

$$M_{n>3} = p_1 M_{(n-1)} + p_2 M_{(n-2)} + p_3 M_{(n-3)} \tag{3}$$

In equation 3, p_1 is the probability of C_1 addition, p_2 is the probability of C_2 initiation or termination, and p_3 is the probability of C_3 initiation or termination.

To develop a closed-form expression for the mole fraction at all carbon numbers, it is noted that, since only initiation or termination can occur, a C_n can only be formed by either all C_1 growth (like equation 2), all C_1 growth except for having incorporated one C_2, or all C_1 growth except for having incorporated one C_3. Thus, the mole fractions of all components can be expressed in terms of an arbitrary constant, M_o. M_o can be thought of as the hypothetical mole fraction at carbon number zero. Equations 4-7 show the mole fraction in terms of this arbitrary constant, M_o.

In equation 7, the first term is the stepwise growth process adding C_1 units one-at-a-time,

$$M_1 = p_1(1-p_1)\ M_o \tag{4}$$

$$M_2 = p_1^2(1-p_1)\ M_o \tag{5}$$

$$M_3 = p_1^3(1-p_1)\ M_o + p_2p_1(1-p_1)M_o$$

$$M_{n>3} = p_1^n(1-p_1)\ M_o + p_2p_1^{(n-2)}(1-p_1)M_o + p_3p_1^{(n-3)}(1-p_1)M_o \tag{7}$$

the second term accounts for C_2 initiation or termination, and the last term accounts for C_3 initiation or termination.

To remove the arbitrary constant, the mole fractions are summed from n=1 to ∞ and equated to 1. Thus, the constant is found to be,

$$M_o = \frac{1}{p_1\left(1 + p_2 + p_3\right)} \tag{8}$$

Substituting equation 8 into equations 4-7, the complete distribution can be described in terms of p_1, p_2, and p_3, by the following equations:

$$M_1 = \frac{(1 - p_1)}{(1 + p_2 + p_3)} \tag{9}$$

$$M_2 = \frac{p_1(1 - p_1)}{(1 + p_2 + p_3)} \tag{10}$$

$$M_3 = \frac{\left(p_1^2(1 - p_1) + p_2(1 - p_1)\right)}{(1 + p_2 + p_3)} \tag{11}$$

$$M_{n>3} = \frac{\left(p_1^{(n-1)}(1-p_1) + p_2p_1^{(n-3)}(1-p_1) + p_3p_1^{(n-4)}(1-p_1)\right)}{(1 + p_2 + p_3)} \qquad (12)$$

Figure IV-5 shows a theoretical product distribution for $p_1=0.7$, $p_2=0.3$, and $p_3= 0.1$. $p_2 > p_3$ matches the experimental evidence, presented in Figures IV-2a through IV-2c, which show that ethene incorporates more than propene. The multiparameter initiation and termination model appears to be very similar to a single-α model at carbon numbers above 3. C_2 and C_3 hydrocarbons are produced in lower quantities than would be observed by a Schulz-Flory mechanism; this behavior of C_2 lying below the line predicted by Schulz-Flory mathematics has been observed previously on a number of catalysts operated over a wide range of conditions.[12]

IV. D. 2. Initiation, Termination, and Propagation by 1-Alkenes. The above model for the hydrocarbon products of the Fischer-Tropsch synthesis describes the product distribution if only initiation or termination by alkenes occurs; however, on cobalt catalysts, Schulz et al.[7] have observed propagation by ethene and, to a lesser extent, propene.

Novak et al.[13] developed a model to predict carbon number distribution by C_1 chain growth combined with independent C_2 addition. Their model has four parameters, α (a stepwise chain growth probability), Γ (a reactivity ratio of C_2 to C_1 addition processes), Θ_1 (the mole fraction of C_1), and Θ_2 (the mole fraction of C_2). The product distribution is derived to be:

$$M_{n>2} = \frac{\left((\Theta_2 - \Theta_1 f_2) f_1^{(n-1)} + (\Theta_1 f_1 - \Theta_2) f_2^{(n-1)}\right)}{(f_1 - f_2)} \qquad (13)$$

$$\text{where } f_{1,2} = \frac{\alpha}{2(1+\Gamma\alpha)} \pm \left[\left(\frac{\alpha}{2(1+\Gamma\alpha)}\right)^2 + \frac{\Gamma\alpha}{(1+\Gamma\alpha)}\right]^{1/2} \qquad (14)$$

$f_{1,2}$ are the roots of the quadratic equation; M_1 is the same as Θ_1, and M_2 is the same as Θ_2.

Equation 13 appears qualitatively similar to the double-α formulation typically used to describe Fischer-Tropsch product distributions; however, f_2 in equation 13 is negative (see equation 14), causing oscillation of the product distribution. Schulz et al.[7] present data from ethene additions to cobalt which show oscillating levels of radioactivity, with even carbon numbers higher than odd carbon numbers; such behavior is consistent with this type of formulation.

Oscillations are not observed in experimental carbon number distributions for at least two reasons. First, if the ratio of C_2 propagation to C_1 is low (i.e. Γ is almost zero), then the oscillations are observed at only very low carbon numbers. Second, there can be a great deal of "scatter" in experimentally-obtained hydrocarbon distributions which causes subtleties, such as minor oscillations, to be masked.

Figure IV-6 shows a theoretical product distribution based on ethene both initiating, terminating, and propagating chains on the catalyst surface, for $\Theta_1 = 0.5$, $\Theta_2 = 0.1$, $\alpha = 0.62$, and $\Gamma = 0.2$. As with the model which accounts for only initiation and termination, the model is similar to a single-α distribution at high carbon numbers.

Thus, in summary, both multiparameter incorporation behaviors can be well represented by a lumped parameter, single-α chain growth process, shown in equation 2.

This lumped parameter is the probability that a C_n hydrocarbon will become a C_{n+1} hydrocarbon by any alkene incorporation process and, therefore, represents the sum of all alkene incorporation processes.

Using sophisticated models that account for a large number of surface processes is inappropriate, because experimentally-obtained hydrocarbon data do not provide the resolution necessary to determine these models' parameters accurately. For example, accounting for C_1, C_2, and C_3 initiation and termination and C_1 and C_2 propagation, all of which have been observed experimentally, requires a model with at least seven adjustable parameters; this many adjustable parameters should not be estimated from Fischer-Tropsch product distribution data.

IV. E. A Model for the Double-α Distribution

A double-α model has been developed to describe the mole fraction of products at carbon number n for the C_3+ products.[12] This can be expressed as[9,14]:

$$M_n = x_1(1-\alpha_1)\alpha_1^{(n-1)} + (1-x_1)(1-\alpha_2)\alpha_2^{(n-1)} \qquad (15)$$

In equation 15, x_1 can be visualized as the mole fraction of products synthesized by the "α_1" mechanism; therefore, $(1-x_1)$ is the mole fraction of products synthesized by the "α_2" mechanism.

In Figures IV-1a through IV-1c, the difference in the Schulz-Flory diagrams between alkene addition runs and base case runs is most notable at higher carbon numbers. Based on this observation, the "α_1" site is postulated to be the site on which normal stepwise addition of C_1 units occurs and the "α_2" process is assumed to be the site which accounts for the incorporation processes. As discussed above, the sum of all

incorporation processes can be approximated by a single chain growth probability, in this case α_2. In this theory, x_1 represents the mole fraction of products synthesized by the simple stepwise growth process of C_1 units and $(1-x_1)$ is the mole fraction of products synthesized by the sum of all incorporation processes.

This model is not catalyst-specific, and the results of the alkene addition experiments can be well interpreted in its terms. When alkenes are added to the feed, only the mole fraction of products synthesized by alkene incorporation should change relative to the base case material balance without alkenes added; thus, adding alkenes should decrease x_1, while α_1 and α_2 should remain constant.

Figure IV-7 shows the Schulz-Flory diagrams of the ethene addition and base case material balances. The solid line is the fit of the double-α model to the base-case data. To fit the data from the ethene addition studies, the values of α_1 and α_2 are retained, and only the value of x_1 is changed. The resulting fit is shown as the dashed line. More heavy products are produced by alkene incorporation processes when alkenes are added to the feed; thus, the value of x_1 decreases.

Figure IV-8 shows the ratio of products with ethene addition to the ratio of products from base case material balances. The change in the normalized mole fractions is well predicted by the model.

IV. F. Explanations of Selectivity Trends

IV. F. 1. Cobalt. Process variable effects observed during normal synthesis[1] can be explained by the effects of the process variables on the concentration of 1-alkenes and

thus on the rate of incorporation. Table IV-1 shows the observed process variable effect on selectivity and the postulated explanation, based on incorporation being an important mechanism for chain growth. Figure IV-9 shows the effect of space velocity on the yield of C_1 (undesired) and $C_{10}+$ (desired). Data labels show the *in situ* ethene to ethane ratio. At higher space velocities (lower total conversions) less hydrogenation of alkenes occurs, as indicated by the increase in ethene to ethane ratio; thus, more high molecular weight products are synthesized via the "α_2" mechanism. Figure IV-10 shows the effect of *in situ* H_2/CO on the yield of $C_{10}+$. Data labels show the *in situ* ethene to ethane ratio. At higher H_2/CO ratios, a greater fraction of ethene is hydrogenated, reducing the fraction of products synthesized by the "α_2" mechanism. Figures IV-9 and IV-10 provide experimental evidence that the theory is consistent with actual behavior of a cobalt catalyst.

IV. F. 2. Iron. Many of the effects of process variables on the product distribution on iron catalysts can be interpreted in terms of their effects on the concentration of 1-alkenes and their degree of adsorption onto the catalyst, and thus on the degree of their incorporation into the product. Thus increased potassium loading increases the yield of heavy products, but it also decreases secondary hydrogenation and isomerization, thereby increasing 1-alkene concentration and the probability of chain incorporation. Increasing the H_2/CO ratio decreases the yield of heavy products by increasing the hydrogenation of 1-alkenes and thereby decreasing incorporation.

Sorting out these and other effects in detail is complex since most data available are from fixed bed reactors in which composition varies with position. For example, competitive adsorption between 1-alkenes and CO can cause markedly different effects at low and high degrees of conversion with H_2-rich gas, and these effects are integrated in the exit product. Further, pressure and temperature can affect competing reactions differently.

IV. G. Conclusions

The cobalt-catalyzed reactions of light 1-alkenes added to synthesis gas feed have been studied. Reaction conditions were 220°C, 0.45 to 1.48 MPa utilizing a synthesis gas flow rate between 0.015 and 0.030 Nl/gcat/min, with H_2/CO ratios of 1.45 to 2.25. C_2H_4, C_3H_6, and 1-C_4H_8 were added to the synthesis gas feed in concentrations ranging from 0.5 to 1.2 mol.% of total feed. For each material balance in which 1-alkenes were added, a "base case" material balance was performed at similar process conditions without 1-alkenes added. Material balances without added 1-alkenes were also repeated

to verify catalyst selectivity stability.

1-Alkenes are found to incorporate into growing chains on the catalyst surface and are thought to initiate and terminate the chain growth process. The relative reactivity of the 1-alkenes decreases with increasing carbon number. On the basis of data in the literature, only ethene is believed to propagate chain growth.

A theory is presented which postulates that the double-α is the sum of two growth processes, one a stepwise single-carbon growth process (the α_1 mechanism) and the other the sum of the 1-alkene incorporation processes (the α_2 mechanism). Many of the effects of process variables on the hydrocarbon selectivity of Fischer-Tropsch catalysts are consistent with this model.

IV.H. Nomenclature

$f_{1,2}$ - parametric constants for ethene propagation model.

M_{added} - mole fraction of products at carbon number of added alkene.

M_o - constant, the mole fraction of products at carbon number "zero".

M_n - mole fraction of products at carbon number n.

n - carbon number.

Normalized(M_n) - normalized mole fraction, with M_{added} removed.

Observed(M_n) - mole fraction data, observed experimentally.

p_1 - the probability of C_1 addition.

p_2 - the probability of C_2 initiation or termination.

p_3 - the probability of C_3 initiation or termination.

x_1 - mole fraction of products produced by α_1 mechanism.

Greek

α - single chain growth probability.

α_1 - chain growth probability for stepwise addition of C_1.

α_2 - chain growth probability for incorporation of alkenes.

Γ - ratio of reactivity of C_2/C_1.

Θ_1 - mole fraction of C_1.

Θ_2 - mole fraction of C_2.

IV.I. Literature Cited

(1) Yates, I.C.; Satterfield, C.N. "Hydrocarbon Selectivity of Cobalt Fischer-Tropsch Catalysts," Energy & Fuels, submitted.

(2) Snel, R.; Espinoza, R.L. J. Mol. Cat. **1987**, 43, 237.

(3) Boelee, J.H.; Cüsters, J.M.G.; van der Wiele, K. Appl. Catal. **1989**, 53, 1.

(4) Tau, L-M.; Dabbagh, H.A.; Davis, B.H. Energy & Fuels, **1990**, 4, 94.

(5) Adesima, A.A.; Hudgins, R.R.; Silveston, P.L. Appl. Catal. **1990**, 62, 295.

(6) Gibson, E.J.; Clarke, R.W. J. Appl. Chem. **1961**, 11, 293.

(7) Schulz, H.; Rao, B.R.; Elstner, M. Erdol und Kohle **1970**, 23, 651.

(7a) Schulz, H. Report to the Bundesministerium für Forschung und Technologie, "Katalysatoren und Selektivitätslenkung bei der Fischer-Tropsch Synthese," BMFT-FB-T80-124, November 1980.

(8) Kibby, C.L.; Pannell, R.B.; Kobylinski, T.P. A.C.S. Pet. Chem. Preprints **1984**, 29(4), 1113.

(9) Yates, I.C. The Slurry-Phase Fischer-Tropsch Synthesis, Ph.D. Thesis, Massachusetts Institute of Technology, Cambridge, Massachusetts, 1990.

(10) Hanlon, R.T.: Satterfield, C.N. Energy & Fuels, **1988**, 2, 196.

(10a) Chanenchuk, C.A.; Yates, I.C.; Satterfield, C.N. Energy & Fuels, submitted.

(11) Matsumoto, D.K., The Effects of Selected Process Variables on the Performance of an Iron Fischer-Tropsch Catalyst, Sc.D. Thesis, Massachusetts Institute of Technology, Cambridge, Mass., 1987.

(12) Donnelly, T.J.; Yates, I.C.; Satterfield, C.N. Energy & Fuels **1988**, 2, 734.

(13) Novak, S.; Madon, R.T.; Suhl, H. J. Chem. Phys., **1981**, 74, 6083.

(14) Huff, G.A., Jr., Fischer-Tropsch Synthesis in a Slurry Reactor, Sc.D. Thesis, Massachusetts Institute of Technology, Cambridge, Mass., 1982.

TABLE IV-1

INTERPRETATION OF OBSERVED PROCESS VARIABLE EFFECTS ON COBALT

Process variable	Effect on yield to desired products	Postulated explanation based on incorporation of 1-alkenes
Decreasing space velocity (increasing conversion)	Decreases yield of desired heavy products	At low space velocities, 1-alkenes are converted to n-alkanes and 2-alkenes more readily.
Increasing H_2/CO ratio	Decreases yield of desired heavy products	At high H_2/CO ratio, 1-alkenes are more readily hydrogenated and therefore less are incorporated.
Pressure	No effect	1-alkene reactions are affected predominantly by the ratio of reactant pressures, not total pressure.
Temperature	No effect	The rate of incorporation and of competing reactions such as hydrogenation and isomerization are affected by temperature similarly.

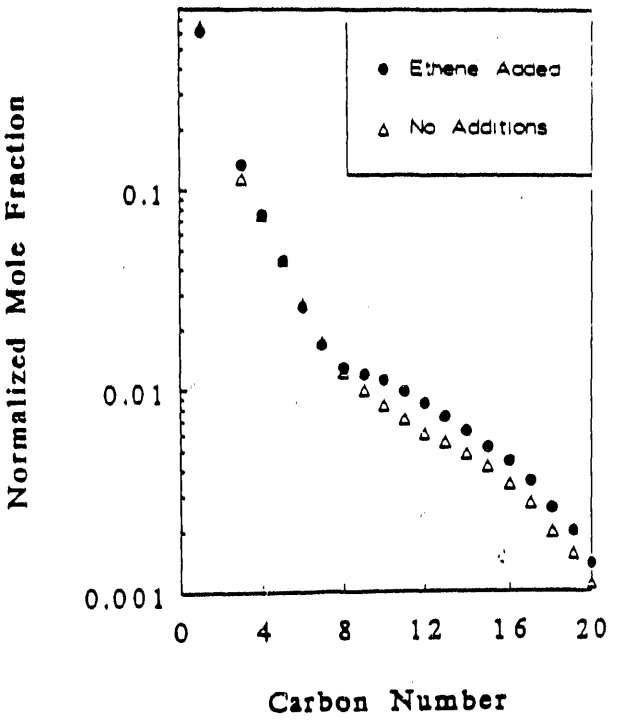

Fig. IV-1a Ethene incorporates into growing chains on cobalt. Ethene added to comprise 0.64 mol.% of feed (220°C, 1.48 MPa. Entering H_2/CO = 2.15, (H_2/CO) in reactor ~ 2.2. Feed rate = 0.030 Nl/min/gcat (unreduced basis)).

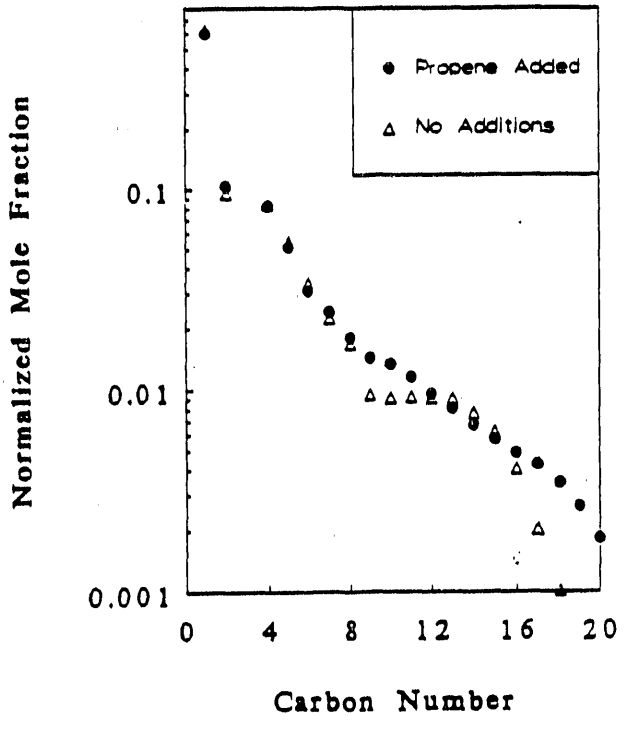

Fig. IV-1b Propene incorporates into growing chains on cobalt. Propene added to comprise 0.70 mol.% of feed (220°C, 1.48 MPa. Entering (H_2/CO) = 1.61, (H_2/CO) in reactor ~ 1.59. Feed rate = 0.029 Nl/min/gcat (unreduced basis)).

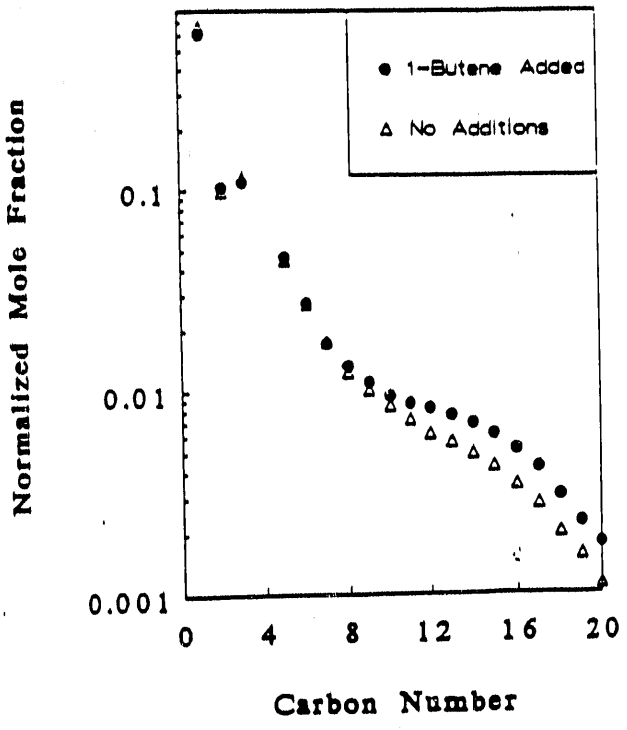

Fig. IV-1c 1-butene incorporates into growing chains on cobalt. 1-butene added to comprise 0.64 mol.% of feed (220°C, 1.48 MPa. Entering (H_2/CO) = 2.15, (H_2/CO) in reactor ~ 2.17. Feed rate = 0.030 Nl/min/gcat (unreduced basis)).

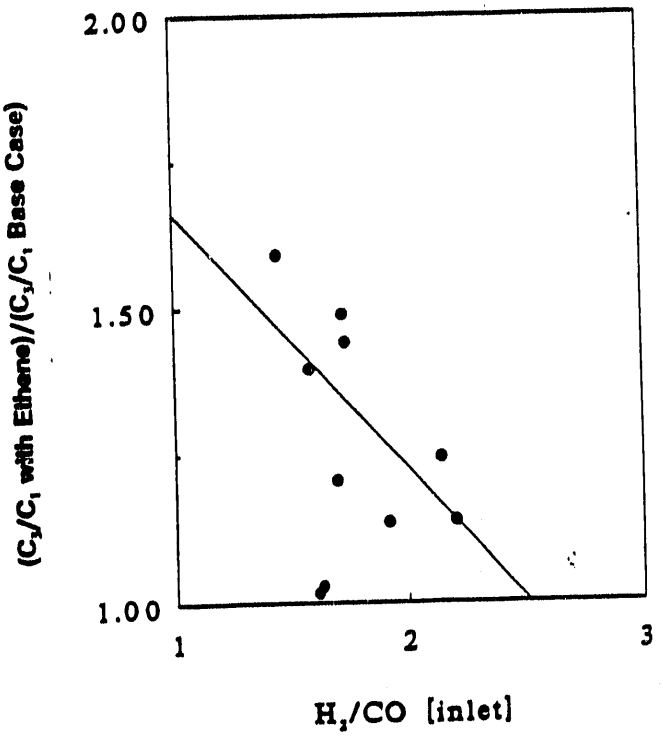

Fig. IV-2a Hydrogenation decreases incorporation of ethene. Comparing the vertical axis values for this plot with Figures 2b and 2c indicates that ethene incorporates more than propene or 1-butene.

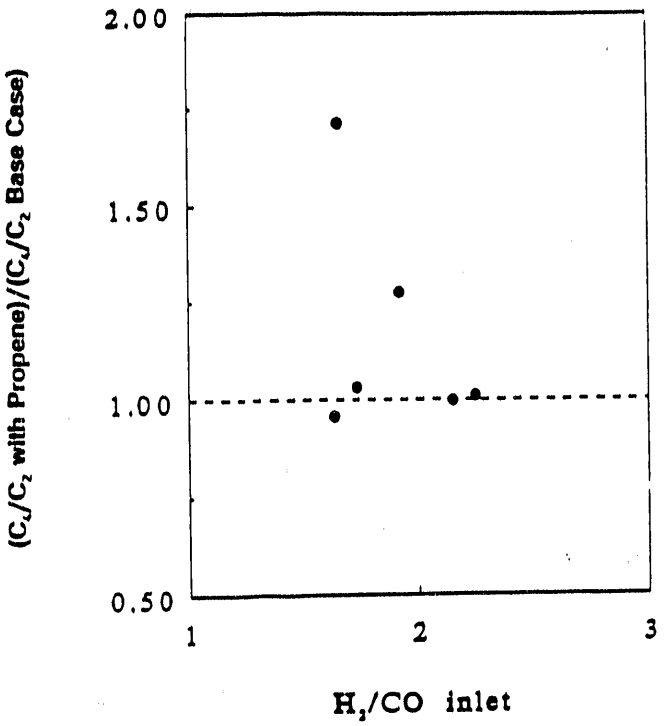

Fig. IV-2b Propene incorporates into growing chains. Propene incorporates less than ethene, but more than 1-butene (see Figure 2a and 2c).

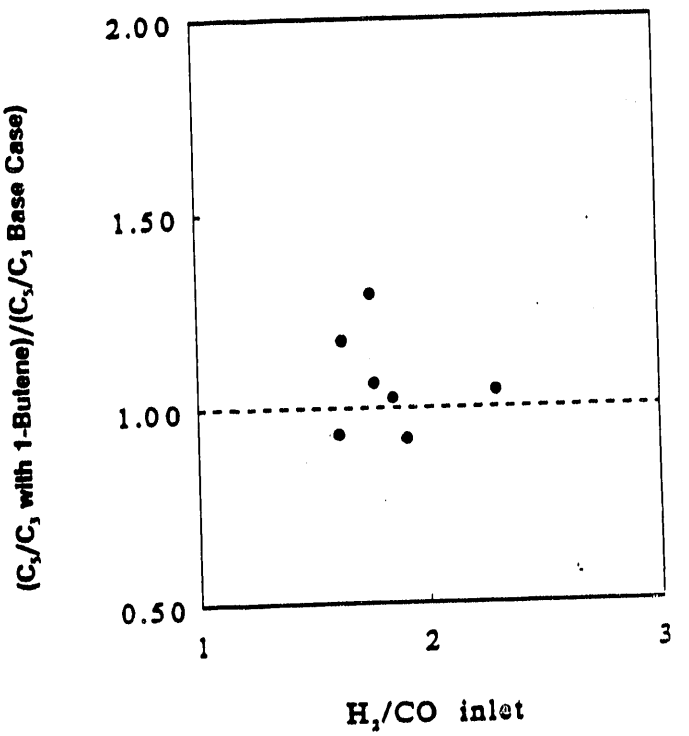

Fig. IV-2c 1-butene incorporates into growing chains. 1-butene incorporates less than either ethene or propene (see Figure 2a and 2b).

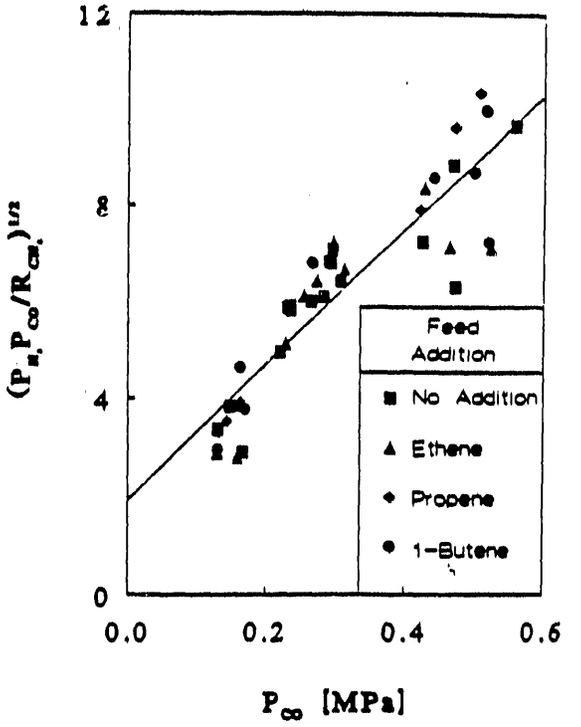

Fig. IV-3 Methanation rate is unaffected by alkene additions. (220°C, 0.5 to 1.5 MPa.)

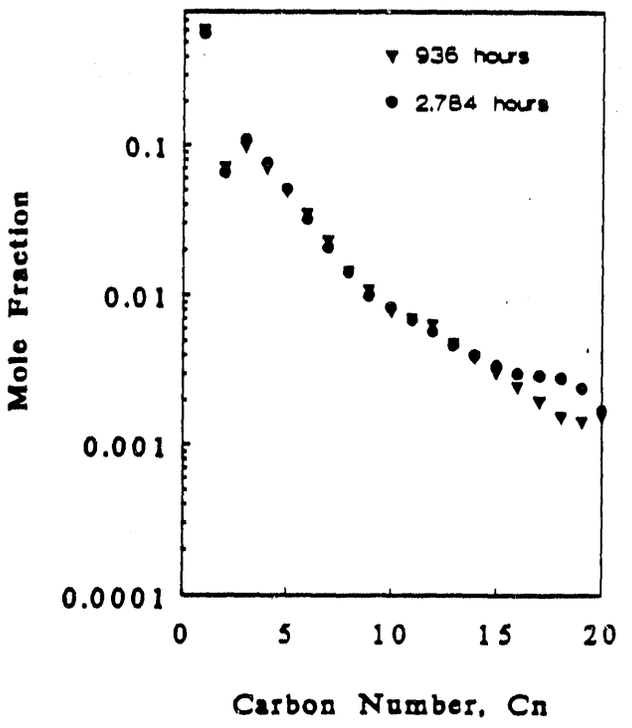

Fig. IV-4 Hydrocarbon selectivity was stable throughout alkene addition experiments (220°C, 0.79 MPa. Entering $(H_2/CO) = 1.62$, (H_2/CO) in reactor = 1.65. Feed rate = 0.017 Nl/min/gcat (unreduced basis)).

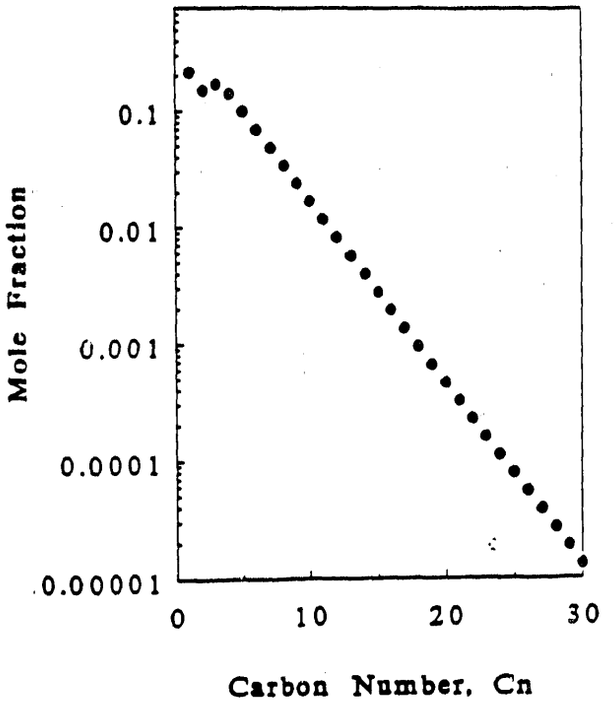

Fig. IV-5 Model accounting for initiation and termination by C_2 and C_3 alkenes appears similar to single-α model, except at low carbon numbers ($p_1 = 0.7$, $p_2 = 0.3$, and $p_3 = 0.1$).

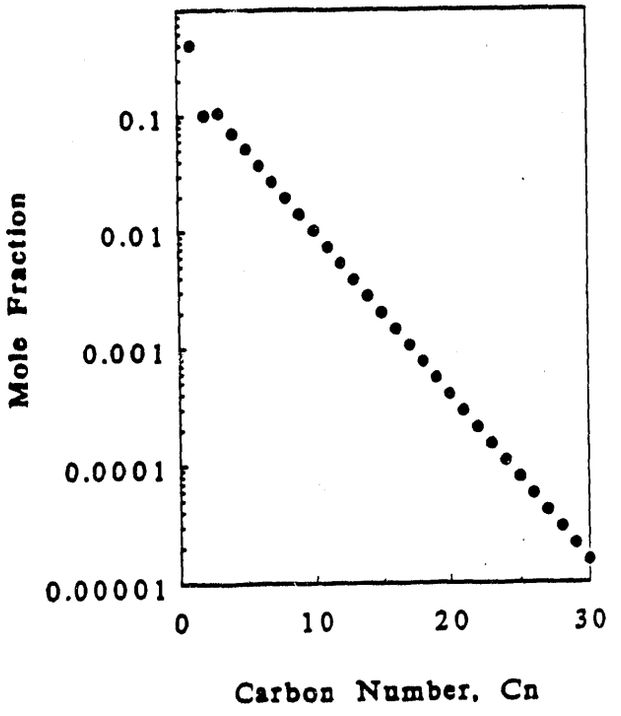

Fig. IV-6 Model accounting for initiation, termination, and propagation by ethene appears similar to single-α model, except at low carbon numbers ($\Theta_1 = 0.5$, $\Theta_2 = 0.1$, $\alpha = 0.62$, and $\Gamma = 0.2$).

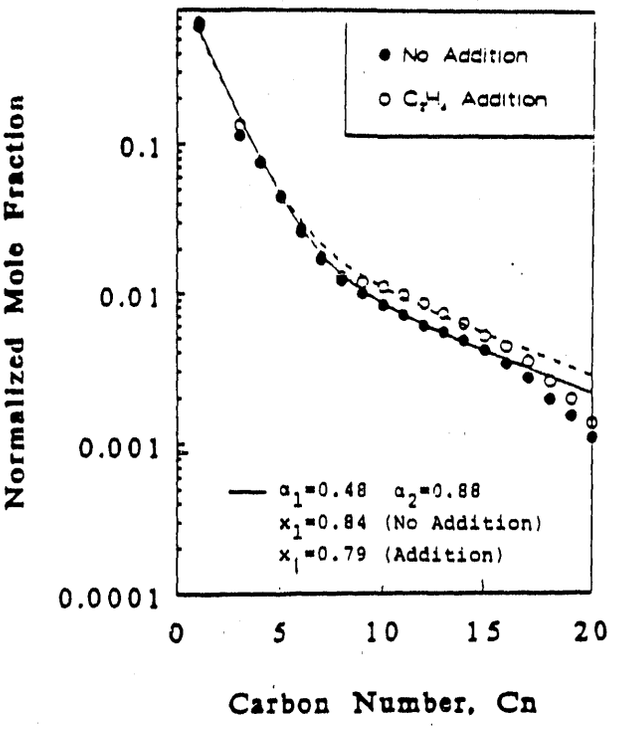

Fig. IV-7 Fitting of ethene addition results to a model which accounts for separate contributions by a stepwise growth process and a 1-alkene incoproration process. (Same data as Figure 1a).

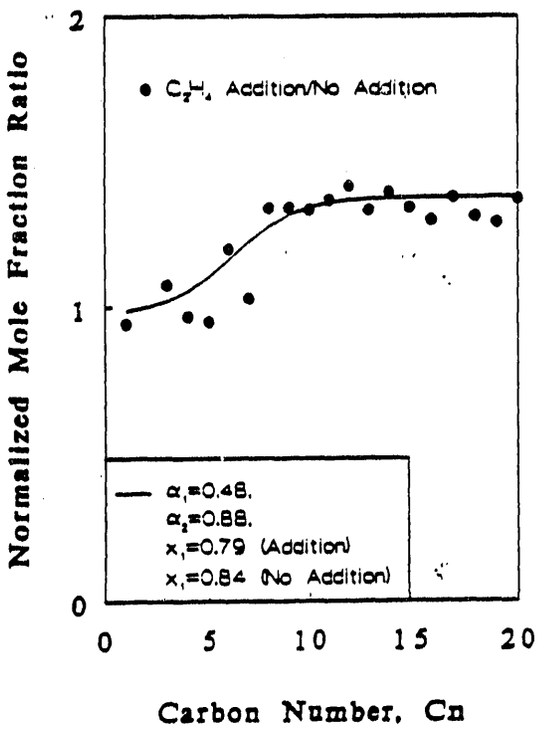

Fig. IV-8 Alkene addition data can be interpreted by a model which accounts for separate contributions by a stepwise growth process and a 1-alkene incorporation process. (Same data as Figure 1a).

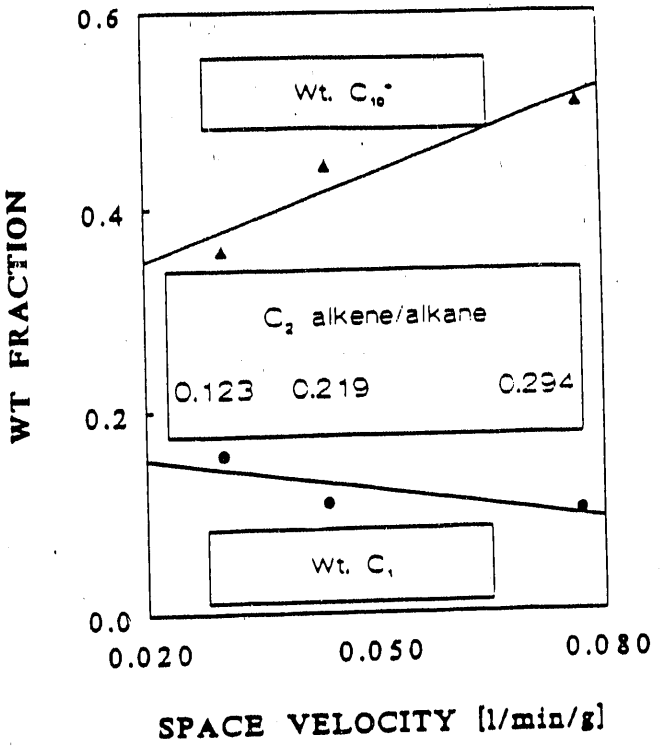

Fig. IV-9 Space velocity affects the yield of C_1 (undesired) and $C_{10}+$ (desired). Data labels show the *in situ* ethene to ethane ratio.

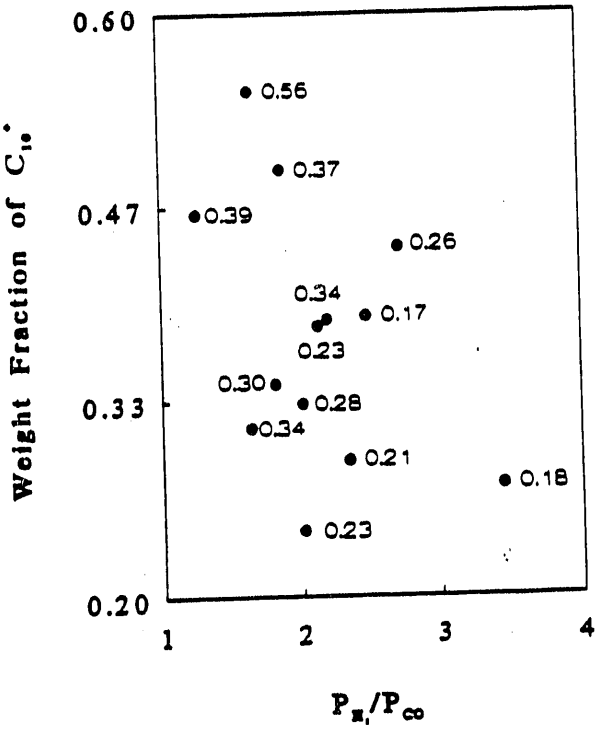

Fig. IV-10 (H_2/CO) ratio affects the yield of desired $C_{10}+$. Data labels show the *in situ* ethene to ethane ratio. Effect is consistent with hypothesis that α_2 is caused by incorporation processes.

END

DATE
FILMED
6/1/92